

Crystallisation of Semiconductive Oxides from Borate Glasses

Dissertation

zur Erlangung des akademischen Grades doctor rerum naturalium
(Dr. rer. nat.)

vorgelegt dem Rat der Chemisch-Geowissenschaftlichen Fakultät der
Friedrich-Schiller-Universität Jena

von Dipl.-Chem. Ing. Ralitsa Peteva Rosenow
geboren am 22.03.1977 in Sofia, Bulgarien

Gutachter:

1. Prof. Dr. Dr. C. Rüssel, Otto-Schott-Institut, Friedrich-Schilleruniversität Jena
2. Prof. Dr. D. Stachel, Otto-Schott-Institut, Friedrich-Schilleruniversität Jena

Tag der öffentlichen Verteidigung: 27.04.2005

„I am singing a song of admiration on the merits
not of rubies, not of gold but of glass....“

M. V. Lomonosov

For my husband Torsten
and my parents

Contents

1 Zusammenfassung.....	1
1.1 Zusammenfassung für In_2O_3 und $\text{In}_2\text{O}_3\text{:SnO}_2$ (ITO).....	3
1.2 Zusammenfassung für SnO_2 and $\text{SnO}_2\text{:Sb}_2\text{O}_3$ (ATO).....	5
2 Introduction.....	7
2.1 Aim of the work.....	8
3 Background Theory and Literature Review.....	9
3.1 Indium oxide (In_2O_3).....	9
3.1.1 In_2O_3 thin films.....	11
3.1.2 In_2O_3 nano-crystals.....	12
3.2 Indium tin oxide (ITO).....	13
3.2.1 ITO- thin films.....	13
3.2.2 $\text{In}_2\text{O}_3\text{: SnO}_2$ (ITO)-nano-powders.....	16
3.3 Tin oxide (SnO_2).....	17
3.3.1 SnO_2 thin films.....	18
3.3.2 SnO_2 nano-crystals.....	18
3.4 Antimony doped SnO_2 ($\text{SnO}_2\text{: Sb}_2\text{O}_3$ or ATO).....	19
3.4.1 ATO thin films.....	19
3.4.2 ATO nano-crystals.....	22
3.5 In- and Sn-containing glasses.....	22
3.6 Crystallisation of melts.....	25
3.6.1 Nano-crystallisation from glasses.....	26
3.6.2 Pendulum effect theory.....	27
4 Experimental part.....	28

4.1 Methods for analysis.....	28
4.1.1 X-ray diffraction (XRD).....	28
4.1.2 Scanning Electron Microscopy (SEM).	29
4.1.3 Transmission Electron Microscopy (TEM).....	29
4.1.4 Energy Dispersive X-ray analysis (EDX).....	30
4.1.5 Differential Thermal Analyse (DTA).....	34
4.1.6 UV-VIS-NIR-spectrometry.....	34
4.1.7 Fourier-Transform-Infrared Spectrometry (FTIR).....	34
4.2 Procedure for preparation of In_2O_3 -, $\text{In}_2\text{O}_3\text{:SnO}_2$ -, SnO_2 - and $\text{SnO}_2\text{:Sb}_2\text{O}_3$ - nano-powders from glasses.....	32
5 Results	34
5.1 Synthesis and optical properties of In_2O_3 -nano-powder.....	34
5.1.1 Choice of the glass system.....	34
5.2 Melting and thermal treatment of glasses.....	37
5.3 Dissolution of the glass matrix and of non In- containing phases.....	45
5.4 Separation of In_2O_3 nano-particles.....	47
5.5 Optical properties of the In_2O_3 nano-particles.....	54
5.5.1 Heat treatment in air.....	54
5.5.2 Influence of the heat treatment atmosphere.....	55
5.6 Synthesis, characterisation and optical properties of $\text{In}_2\text{O}_3\text{:SnO}_2$ nano-powder.....	56
5.7 Synthesis of SnO_2 nano-powder.....	64
5.7.1 Choice of the glass system.....	64
5.7.2 Melting procedure.....	66
5.7.2.1 SnO_2 raw material.....	66
5.7.2.2 Complete dissolution of SnO_2 in the melt.....	67
5.7.3 Glass samples thermal treatment.....	70

5.7.4 Dissolution of the matrix.....	76
5.7.5 Separation of the SnO ₂ nano-crystals.....	77
5.7.6 Characterisation of SnO ₂ nano-crystals.....	78
5.8 Synthesis and optical properties of SnO ₂ : Sb ₂ O ₃ nano-powder.....	84
6 Discussion.....	88
6.1 Discussion for In ₂ O ₃ and In ₂ O ₃ :SnO ₂ -containing glasses, glass-ceramics and nano-powders.....	88
6.2 Discussion for SnO ₂ and SnO ₂ :Sb ₂ O ₃ -containing glasses, glass-ceramics and nano-powders.....	90
7 Summary.....	93
7.1 Summary for In ₂ O ₃ and In ₂ O ₃ :SnO ₂ (ITO).....	93
7.2 Summary for SnO ₂ and SnO ₂ :Sb ₂ O ₃ (ATO).....	95
8 Bibliography.....	97
9 List of Figures.....	103

1 Zusammenfassung

Halbleitende Nanokristalle aus Indiumoxid (INO), SnO_2 dotiertem Indiumoxid (ITO), Zinnoxid (TO) oder Sb_2O_3 dotiertem Zinnoxid (ATO) werden hauptsächlich als Beschichtungsmaterial für elektrisch leitende und transparente Schichten (z.B. als Elektrodenmaterial in Flüssig-Kristall-Monitore (Liquid Crystal Displays) und in OLED-Geräten (Organic Light Emitting Diodes) benutzt. Die ITO- und ATO- Nanopartikel auf der anderen Seite zeigen gleichzeitig eine Undurchlässigkeit in NIR- und hohe Transparenz in sichtbaren optischen Bereich. Deswegen finden sie u.a. Anwendung in IR reflektierende und VIS-transparente Schichten auf Gläsern (z.B. Wärmeschutzgläser).

Die optischen und die elektrischen Eigenschaften dieser Nanoteilchen werden hauptsächlich von den Defekten in der Kristallstruktur (Sauerstoffmangel) bestimmt. Es gibt drei Möglichkeiten, um diesen Sauerstoffmangel zu beeinflussen: Bildung der Kristalle bei hohen Temperaturen (z.B. bei CVD (Chemical Vapour Deposition) und PLD (Pulsed Laser Deposition), Kristallisation unter reduzierenden Bedingungen z.B. in Formiergas (5% H_2 +95% Ar) und/oder Dotierung von SnO_2 (für In_2O_3) bzw. Sb_2O_3 (für SnO_2).

Um Transparenz im sichtbaren Bereich zu bekommen, ist es notwendig, dass die Kristalle kleiner als 100 nm sind, ansonsten kommt es zur Streuung. Zusätzlich sollen entsprechenden Nanokristalle mit einer schmalen Korngrößenverteilung hergestellt werden, da schon durch eine kleine Konzentration größerer Teilchen Streuung und Undurchlässigkeit im sichtbaren Bereich resultieren.

Bei einem Glaskristallisationsverfahren ist die Möglichkeit defekte Strukturen in den Kristallen zu erhalten sehr hoch. Durch dieser Methode können durch Variation der Temper-Temperatur und -Zeit nano-skalige Teilchen mit vorgegebene Kristallgrößen hergestellt werden. Die Glaskristallisation hat als weiteren Vorteil gegenüber anderen

Methoden, dass diese für die Herstellung von Kristallen mit schmaler Kristallgrößenverteilung prädestiniert ist.

So können Nanokristalle mit defekten Strukturen bei hohen Temperaturen hergestellt und diese in eine Polymermatrix eingefügt werden. Die anderen Techniken zur Herstellung von dünnen Schichten aus ITO und ATO (wie CVD und PLD) benötigen hohe Temperaturen bei der Beschichtung und können deshalb nicht für Polymersubstrate angewendet werden. Durch die Nutzung von Polymersubstraten mit infrarot undurchlässigen und gleichzeitig im sichtbaren Bereich transparenten Nanopartikeln können transparente Wärmeschutz Nano-Polymerkomposite hergestellt werden.

Hauptziel dieser Arbeit ist es auf der Basis der Glaskristallisationstechnik ein Herstellungsverfahren für kristalline Nanopulver aus In_2O_3 , SnO_2 , $\text{In}_2\text{O}_3:\text{SnO}_2$ (ITO) und $\text{SnO}_2:\text{Sb}_2\text{O}_3$ (ATO) zu entwickeln.

Ein weiteres Ziel dieser Arbeit ist es halbleitende Nanopulver mit einer Undurchlässigkeit im NIR- (Nahes Infrarot) und Transparenz im sichtbaren Bereich des optischen Spektrums zu erhalten.

Um eine möglichst große Menge von Nano-Kristallen zu erhalten, müssen transparente und Röntgenamorphe Gläser mit einem möglichst hohen Anteil an In_2O_3 oder SnO_2 hergestellt werden. Die Nanokristalle sollen durch gesteuerte Glaskristallisation erhalten werden. Die mittlere Kristallgröße soll durch die Variation der Glaszusammensetzung und Kristallisationsbedingungen (Temperatur und Zeit) gesteuert werden. Die Kristalle sollen kleiner als 100 nm sein und auch eine schmale Kristallgrößenverteilung aufweisen. Die gewünschte Nano-Kristallphase soll durch Auflösung der Matrix separiert werden. Deshalb muss ein Glassystem gewählt werden, welches eine geringere chemische Beständigkeit in Wasser, Lauge oder Säure aufweist als die der In_2O_3 -, $\text{In}_2\text{O}_3:\text{SnO}_2$ -, SnO_2 - oder $\text{SnO}_2:\text{Sb}_2\text{O}_3$ -Kristallphasen. Nach Auflösung der Matrix, sollen die Nanokristalle getrennt werden. Somit werden reine In_2O_3 -, ITO-, SnO_2 - oder ATO-Nanopulver hergestellt.

1.1 Zusammenfassung für In_2O_3 und $\text{In}_2\text{O}_3\text{:SnO}_2$ (ITO)

In den Gläsern des Systems $\text{Na}_2\text{O}/\text{B}_2\text{O}_3/\text{Al}_2\text{O}_3/\text{In}_2\text{O}_3$ wurde durch thermische Behandlung im Temperaturbereich von 500-700 °C die Bildung von Kristallphasen untersucht. Die gewünschten In_2O_3 -Kristalle wurden bei einem molaren Verhältnis (MV) $[\text{Na}_2\text{O}]/[\text{B}_2\text{O}_3] = 1,1$ gebildet. Für ein Verhältnis von $[\text{Na}_2\text{O}]/[\text{B}_2\text{O}_3] = 1,4$ wurden NaInO_2 -Kristalle beobachtet und in den Gläsern mit $[\text{Na}_2\text{O}]/[\text{B}_2\text{O}_3] \leq 0,7$ wurden keine indiumhaltigen Kristallphasen mehr gebildet.

Ein weiterer wichtiger Faktor für die Entstehung von In_2O_3 -Kristallen ist die Konzentration an Al_2O_3 . Ohne Al_2O_3 in der Zusammensetzung ist eine gesteuerte In_2O_3 -Kristallisation nicht möglich. Es kommt unter diesen Bedingungen zu einer spontanen Kristallisation von NaInO_2 (bei $\text{MV} = 1,4$), von In_2O_3 ($\text{MV} = 1,1$) oder es entstehen keine indiumhaltigen Kristallphasen ($\text{MV} \leq 0,7$).

Die Zugabe von Al_2O_3 zu den Zusammensetzungen erweitert generell den Glasbildungsbereich. Al_2O_3 -Konzentrationen im Bereich von 5 bis 12 mol% ($\text{MV} = 1,1$) ermöglichten die gesteuerte Kristallisation von In_2O_3 mittels Temperaturbehandlung. Als günstigste Glaszusammensetzung in Bezug auf die Bildung von In_2O_3 erwies sich dabei (in mol%) 45 Na_2O ·40 B_2O_3 ·10 Al_2O_3 ·5 In_2O_3 . Mit einer ausreichend hohen Konzentration von 5 mol% In_2O_3 , einem Gehalt von 10 mol% Al_2O_3 und einem $\text{MV} = 1,1$ wurde diese Zusammensetzung als Ausgangsglas für die weiteren Untersuchungen gewählt.

Da bei der Temperaturbehandlung der Gläser neben den gewünschten In_2O_3 -Nanokristallen als Kristallphasen auch NaBO_2 und/oder $\text{Na}_2\text{Al}_2\text{B}_2\text{O}_7$ entstehen, werden diese ebenso wie die Glasmatrix von den In_2O_3 -Nanokristallen separiert. Dies erfolgt durch die Auflösung aller nicht indiumhaltigen Phasen in 0,6 N Essigsäure. Das bei der Auflösung der Glasmatrix in Essigsäure und nach anschließendem Trocknen entstandene Natriumacetat (CH_3COONa) konnte durch ein Dialyseverfahren abgetrennt werden. Bei der Dialyse handelt es sich um ein häufig angewandtes Verfahren zur Abtrennung von organischen Makromolekülen. Dabei diffundieren die gelösten Substanzen durch eine selektiv permeable Membran entlang des Konzentrationsgradientens, von der hohen zu niedrigen Konzentrationen. Im Vergleich zu dem bisher üblichen Verfahren zur Trennung von

Nanokristallen, der Zentrifugation mit CCl_4 , werden bei dieser Methode keine toxischen Substanzen eingesetzt und die In_2O_3 -Nanopartikel können vollständig von den während der Auflösung der Matrix gebildeten Salzen abgetrennt werden. Unseren Wissens nach wurde die Dialyse bis jetzt noch nie als Trennungsmethode für Nanokristalle aus aufgelösten Gläsern angewendet.

Die durchschnittliche Größen der In_2O_3 -Nanokristalle in Abhängigkeit von Temperatur und -Zeit liegen im Bereich von 13 bis 53 nm (kalkuliert mit der "Scherrer-Gleichung"). Die Auswertung von TEM-Aufnahmen erbrachte mit Kristallgrößen von 19 nm (Temper-Temperatur 580 °C), 25 nm (Temper-Temperatur 630 °C) und 42 nm (Temper-Temperatur 700 °C) Werte die im selben Größenbereich liegen. Unberücksichtigt bleibt im Rahmen dieser Arbeit das mögliche Auftreten aggregierter Nanopartikel nach der Auflösung der Glasmatrix. Da durch die gesteuerte Kristallisation auch eine enge Kristallgrößenverteilung eingehalten werden konnte, können die Ziele hinsichtlich Größe und Größenverteilung der In_2O_3 -Nanokristalle als weitgehend erfüllt angesehen werden..

Eine weitere Vorgabe war es, Nanopartikel zu erhalten, die im sichtbaren Wellenlängenbereich transparent aber undurchlässig für den NIR-Bereich sind.

Die Auswertung der UV-VIS-NIR-Spektren für die In_2O_3 -Nanokristalle zeigte aber sowohl für die in Luft als auch für die in Formiergas getemperten Proben Transparenz im VIS- und NIR-Bereich.

Um die Transparenz im NIR-Bereich zu unterdrücken (abhängig vom Sauerstoffmangel in der In_2O_3 Kristallstruktur) wurde das Glas mit 1 mol% SnO_2 dotiert und die Herstellung der Nanokristalle mit folgender Glaszusammensetzung durchgeführt (in mol%) 44,5 Na_2O · 39,6 B_2O_3 · 10 Al_2O_3 · 5 In_2O_3 · 1 SnO_2 . Das erhaltene transparente Glas wurde im Bereich von 500 bis 700 °C für 1 bis 6 h in Luft und Formiergas getempert. Nach Separation wurden kubische $\text{In}_2\text{O}_3\text{:SnO}_2$ –Nanokristalle (ITO) mit einer durchschnittlichen Größe von ca. 25 nm erhalten. Die Untersuchung der optischen Eigenschaften der unter Formiergas getemperten Proben ergab eine Transparenz von etwa 90 % im sichtbaren Wellenlängenbereich und die gewünschte Undurchlässigkeit im NIR-Bereich.

Die so hergestellten $\text{In}_2\text{O}_3\text{:SnO}_2$ –Nanokristalle erfüllen somit die in der Zielstellung genannten Anforderungen sowohl hinsichtlich der Kristallgröße als auch deren optischen Eigenschaften.

1.2 Zusammenfassung für SnO_2 und $\text{SnO}_2\text{:Sb}_2\text{O}_3$ (ATO)

Die für die Darstellung von SnO_2 bzw. $\text{SnO}_2\text{:Sb}_2\text{O}_3$ (ATO)-Nanokristallen untersuchten Zusammensetzungen, wurden analog zu denen für die In_2O_3 - und ITO-Systeme verwendeten ausgewählt: $\text{Na}_2\text{O}/\text{B}_2\text{O}_3/\text{Al}_2\text{O}_3/\text{SnO}_2$ und $\text{Na}_2\text{O}/\text{B}_2\text{O}_3/\text{Al}_2\text{O}_3/\text{SnO}_2/\text{Sb}_2\text{O}_3$.

Transparente Gläser konnten hierbei nur mit einer speziellen Auflösungsprozedur des SnO_2 in der Borat-Schmelze erreicht werden. Dazu wurde als Rohstoff ein feindisperses SnO_2 eingesetzt, das über eine nasschemische Methode hergestellt wurde. Das Einschmelzen erfolgte in zwei Schritten. Im ersten Schritt wurde die Viskosität der Vorschmelze kontrolliert, in dem diese bei relativ niedrigen Temperaturen (von 850 bis 950 °C) über längere Zeit (bis 24 h) gehalten wurde. Im zweiten Schritt wurde bei höheren Temperaturen (von 1250 bis 1350 °C) für 30 Minuten geschmolzen. Dadurch konnte sich das SnO_2 besser in der Schmelze lösen und transparente Gläser mit bis zu 10 mol% SnO_2 hergestellt werden. Anschließend wurden die Gläser zwischen 500 und 820 °C thermisch behandelt.

Der Einfluss der Zusammensetzung wurde ausgehend von der schon für die Herstellung der In_2O_3 -Nanokristalle günstigen Glaszusammensetzung (in mol%) 45 Na_2O 40 B_2O_3 10 Al_2O_3 5 SnO_2 hinsichtlich ihrer Eignung untersucht. Dabei zeigten die Zusammensetzungen mit relativ hohen Na_2O -Konzentrationen bei molaren Verhältnissen von $[\text{Na}_2\text{O}]/[\text{B}_2\text{O}_3] \geq 1,1$ eine bevorzugte Kristallisation von Na_2SnO_3 oder $\text{Na}_2\text{Sn}_2\text{O}_5$. Das molare Verhältnis von $[\text{Na}_2\text{O}]/[\text{B}_2\text{O}_3] = 1,1$ scheint dabei die Grenze zwischen der Entstehung von SnO_2 - und $\text{Na}_2\text{Sn}_2\text{O}_5$ -Kristallen zu bilden. Um die Bildung des Natriumstannates zu unterdrücken wurden eine große Anzahl von Zusammensetzungen mit verschiedenen molaren Verhältnissen untersucht. In Zusammensetzungen der molaren Verhältnisse $[\text{Na}_2\text{O}]/[\text{B}_2\text{O}_3] < 0,3$ trat eine unerwünschte spontane Kristallisation des SnO_2 auf. Darum ergab sich als bevorzugter Bereich für die SnO_2 -Kristallisation molare Verhältnisse zwischen 0,5 und 1,0.

Der Einfluss der Al_2O_3 -Konzentration ist für die SnO_2 -Kristallisation im Vergleich zu der In_2O_3 -Kristallisation wesentlich geringer ausgeprägt. So wird sowohl in Gläsern mit als auch ohne Al_2O_3 die Bildung von SnO_2 -Kristallen beobachtet.

Generell erwies sich die schon für die Herstellung von In_2O_3 - und ITO-Nanokristallen entwickelte Methode auch für die entsprechenden SnO_2 - und ATO-Nanokristalle als geeignet. So wurde die gleiche Technik der Glaskristallisation eingesetzt, mit anschließender Separierung der Glasmatrix und der anderen kristallinen Phasen wie z.B. NaBO_2 und $\text{Na}_2\text{Al}_2\text{B}_2\text{O}_7$ durch Auflösen in Essigsäure. Durch die abschließende Dialyse wurden die dabei gebildeten Salze von den SnO_2 - oder $\text{SnO}_2\text{:Sb}_2\text{O}_3$ -Nanokristallen abgetrennt.

Für die Zusammensetzung mit 5 mol% SnO_2 wurden nach Temperung für 4 h bei 600 °C, nadelförmige Nanokristalle mit einer Dicke von 4 bis 7 nm und einer Länge von 25 bis 100 nm erhalten. Bei einer höheren Temperatur von 700 °C wuchsen sowohl die Kristalldicke auf 250 nm als auch die Länge auf 1,2 bis 2 µm.

Ein Wechsel der Morphologie der SnO_2 -Kristalle wurde für die Zusammensetzung mit 5 mol% SnO_2 bei einer Temperaturerhöhung auf 820°C beobachtet. Dabei wurden die anfänglich dünnen und langen Kristalle mit zunehmender Temper-Zeit (0,5-16 h) dicker und kürzer. Dieses Ergebnis bestätigt die "Kristallisations-Pendel-Theorie", bei der das "Kristallisations-Pendel" ein Typ der intergranularen Ostwald-Reifung ist.

Sb_2O_3 -dotierte SnO_2 -Kristalle konnten für das System $\text{Na}_2\text{O}/\text{B}_2\text{O}_3/\text{Al}_2\text{O}_3/\text{SnO}_2\text{:Sb}_2\text{O}_3$ erhalten werden. Aus den transparenten und röntgenamorphen Gläsern mit 5 mol% SnO_2 und 0,4-1 mol% Sb_2O_3 wurden über eine zweistufige Temperaturbehandlung nadelförmige Nanokristalle mit einer Dicke von etwa 50 nm und Längen im Bereich von 300 bis 600 nm erhalten.

Die SnO_2 und $\text{SnO}_2\text{:Sb}_2\text{O}_3$ Nanokristalle besitzen eine Transparenz im VIS- und NIR-Bereich. Die gewünschte Undurchlässigkeit in NIR-Bereich wurde bis jetzt nur für SnO_2 dotierte In_2O_3 -Nanokristalle erreicht. Die Optimierung der Dotierungskonzentration (Sb_2O_3) und der thermischen Behandlung könnte dazu führen, NIR- undurchlässiges und VIS-transparentes ATO-Nanopulver zu erhalten.

2 Introduction

Nanomaterials are a significant part of the contemporary science with fundamental and potential technological importance [Ali 96], [Wel 93], [Sch 94]. These materials often show different promising properties such as electrical, optical, chemical and magnetical as their bulk materials [Mül 99a], [Rez 94].

In the past, the crystallization of semiconductive phases from glasses has predominantly been utilized to produce optical filters with sharp absorption edges. The attributed wavelength can be adjusted by the variation of the band gap, i. e. the chemical composition. Here, the system Cd (S, Se) is of special importance [Bor 87], [Pot 88], [Yan 89], [Wog 91a], [Wog 91b], [Goe 94], [Ban 95]. In the past few years, such materials have gained interest, because of their potential applications as semiconductor lasers [Gie 96], optical limiters [Bin 96] and saturable absorbers [Sar 90].

The crystallization of semiconducting phases has also been reported for other chalcogenide phases, such as zinc- and lead sulfide as well as for small quantities of elementary silicon. In analogy to cadmium chalcogenides, only small concentrations (~ 1 wt %) can be precipitated from a glass. The crystallization of semiconductive oxides has only been reported for TiO_2 , SnO_2 [Ris 93] and recently for In_2O_3 [Lös 01a]. The latter is of special potential because of the large solubility of In_2O_3 in convenient silicate and borate melts. By contrast, the solubility of SnO_2 is restricted to few percent and furthermore, the dissolution rate in glass melts is extremely low [Xia 76], [Ben 03], [Kum 69].

At the moment, semiconductive nano-crystallites from indium oxide (INO), Sn doped indium oxide (ITO), tin oxide or Sb doped tin oxide (ATO) are predominantly used as coating materials for transparent electric conductors [Läs 01b], [Tah 97] (e. g. as electrode material in liquid crystals displays (LCD) and in OLED-devices (organic light emitting diodes)). They are used as well as infrared reflective material [Fra 60], [Val 96], [Moh 03], [Cho 83], [Vas 92] or coatings for glasses with IR-protection [Cho 83], [Ham 86].

These coatings on glassy substrates can be produced using a large variety of techniques, such as sputtering or sol-gel. By contrast, these methods can hardly be used for polymer substrates. Here, the favourite possibility to achieve non-transparency in the near infrared range should be the incorporation of nano-crystalline semiconductive and IR-reflecting powders into a polymer matrix. To achieve transparency in the visible range, the crystallites should be smaller than half of the wavelength of the visible light. Otherwise, light scattering will occur. Additionally, a narrow particle size distribution is required, because small concentrations of large particles will lead to light scattering and to non transparency in the visible range. One of the most favourite methods to prepare such particles is the glass crystallization technique, up to now predominantly used for ferromagnetic or ferroelectric phases [Kom 84], [Mül 99b], [Wol 04] or ferroelectric nano-crystallites with narrow particle size distribution.

2.1 Aim of the work

The aim of the recent work is to develop a preparation method for obtaining nano-powders of In_2O_3 , SnO_2 , $\text{In}_2\text{O}_3:\text{SnO}_2$ (ITO) and $\text{SnO}_2:\text{Sb}_2\text{O}_3$ (ATO), based on the glass crystallisation technique.

To achieve non transparency in the near infrared (NIR) and transparency in the visible region of the optical spectra, by using the semiconducting nano-powders is also an aim of the research work. Colourless glasses should be prepared, which contain a relatively large amount of In_2O_3 , $\text{In}_2\text{O}_3:\text{SnO}_2$, SnO_2 or $\text{SnO}_2:\text{Sb}_2\text{O}_3$. The nano-powders should be obtained by controlled glass crystallisation. The mean crystallite size can hereby be adjusted by the tempering conditions. The nano-particles should be much smaller than the wavelengths of the visible light, because otherwise light scattering will occur. Therefore, also a narrow crystal size distributions is required. The obtained nano-crystals should be isolated from the glass matrix. For this purpose the chosen glass matrix should have low solubility in H_2O , acids or bases in comparison to the desired crystalline phase. After dissolution of the matrix, the nano-crystals should be separated and so the preparation of pure In_2O_3 -, ITO-, SnO_2 - or ATO- nano-powders is enabled.

3 Background Theory and Literature Review

3.1 Indium oxide (In_2O_3)

Crystalline indium oxide has a cubic centred structure with two non-equivalent In sites (see Fig. 3.1.1) [Cho 83], [Qua 98]. In_2O_3 has a melting point of 2000 °C, a density of 7180 kg m⁻³ and possesses yellow colour at room temperature [Ren 32]. It could exist in two forms: stoichiometric and non stoichiometric. The non-stoichiometry form differs in electrical and optical properties from the stoichiometry one, depending on the extend oxygen deficiency [Xirouchaki 98].

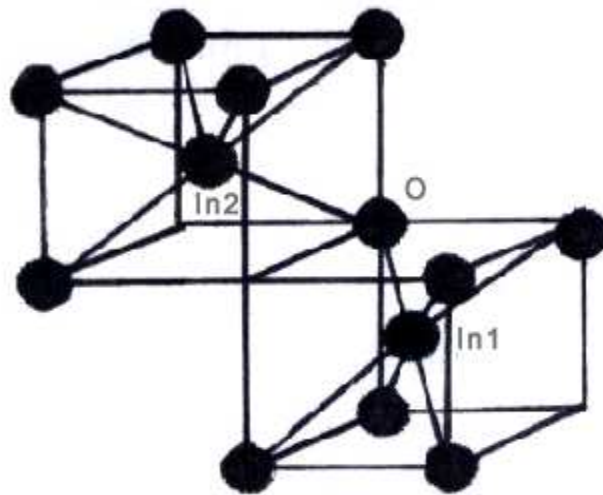


Fig. 3.1.1 Crystal structure of In_2O_3 [Qua 98]

The non-stoichiometric indium oxide, $\text{In}_2\text{O}_{3-x}$, possesses oxygen vacancies and is a material with relatively high electrical conductivity and optical transmittance in the visible range. It is used as targets for the preparation of transparent electrodes for liquid crystal display systems [Cas 98], [McMee 00].

Another possibility to increase the free electron concentration in In_2O_3 is to dope it with donors such as Sn^{4+} or F^- . These ions introduce donor energy levels within the band-gap near the conduction band (Fig. 3.1.2 a). In the case of Sn doped In_2O_3 thin films, the formula could be expressed as $\text{In}_{2-x}\text{Sn}_x\text{O}_{3-2x}$ [Bas 98]. The introduction of an acceptor energy level near the valence band is also possible by the substitution of the In^{3+} with lower valency cations such as Zn^{2+} or Cu^{2+} [Moh 03] Fig. 3.1.2 b.

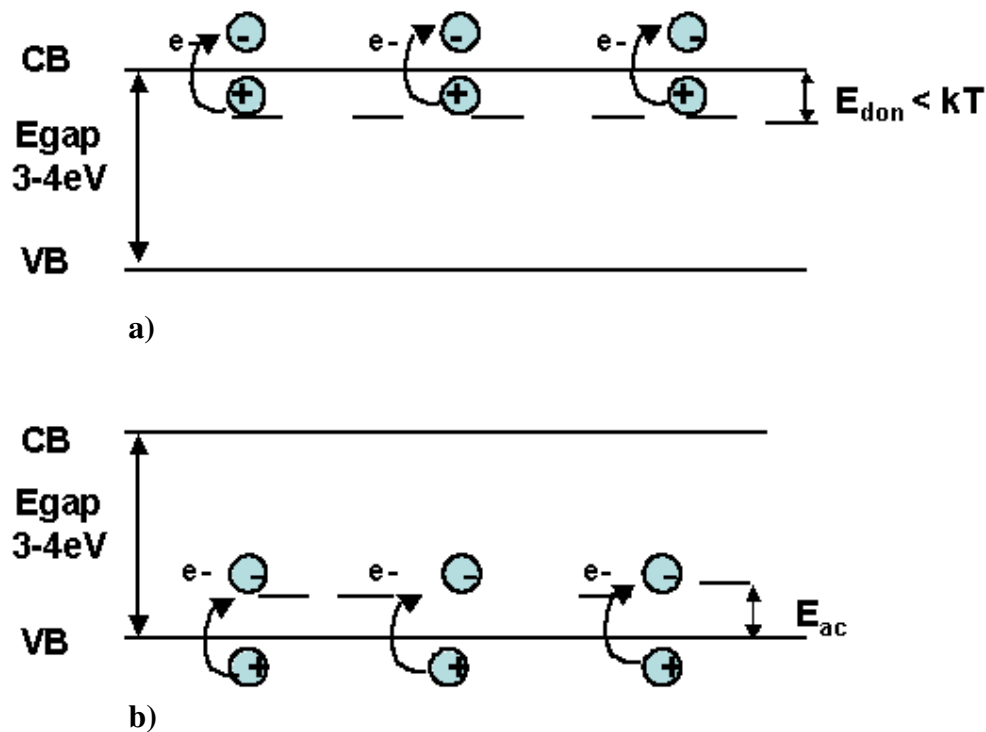


Fig 3.1.2 Scheme of additional energy level in the Energy band gap:
a) donor levels, b) acceptor levels VB = valence band; CB = conductive band; Egap = energy band gap

3.1.1 In₂O₃ thin films

In₂O₃ nano-particles are predominantly used for the preparation of thin films since the most literature data are concerning their properties, there are numerous reviews in the literature.

The structure of In₂O₃ thin film can be polycrystalline or amorphous, depending on the deposition technique. The grain size is usually from 100 Å to 400 Å, in dependence of the film preparation conditions, such as deposition technique, substrate temperature, doping level and subsequent heat treatment. Appropriate film preparation and post-heat-treatment enables to increase the electrical conductivity [Cho 83].

Pulse laser deposition (PLD) method in pure inert background gas is used for the deposition of In₂O₃ thin films on an unheated glass substrate. The optical properties (transmittance), electrical properties (resistivity) and the crystalline structure of the films are characterized in relation to the background gas pressures (He gas). The films deposited at He pressures below 0.5 Torr have transmittances of nearly 0 % at a wavelength of 550 nm. A transmittance of 80 % at the same wavelength has been reported in films deposited at He pressures of about 1.0 Torr.

In pure He gas, the films deposited below 0.5 Torr show volume resistivity of around 10⁻³ Ωcm. By comparison, films deposited at 0.5 Torr in He/O₂ gas mixture show a resistivity of 1.53x10⁻³ Ωcm. Stoichiometric crystalline In₂O₃ films have been obtained in the case of high He pressure without the introduction of oxygen [Yamada 99]. PLD method is used also to produce indium oxide thin-films for holographic recorders [Gri 97].

Cathode sputtering is another method used to produce In₂O₃ films [Wei 66]. The optical absorption of In₂O₃ is analysed and quantitatively interpreted in relation to the energy band structure. The direct allowed transitions observed in indium oxide at room temperature correspond to an energy gap of 3.75 eV. Indirect transitions are indicated at about 2.75 eV.

An optical band gap of 3.65 eV is observed also from Krishna et al. [Kri 00]. In this work indium oxide thin films have been deposited on glass substrates at 373-673 K by reactive evaporation of indium in an oxygen partial pressure of 2x10⁻⁴ mbar. The electrical resistivity of the films formed at 373 K is 3.7x10⁻¹ Ω cm due to their partly amorphous

structure. By contrast, the films formed at 673 K have been fully crystallized (In_2O_3 crystal phase). In this case the electrical resistivity is decreased to $4.2 \times 10^{-3} \Omega \text{ cm}$. The Hall mobility in these films increased from $2 \text{ cm}^2/\text{V sec}$ to $10 \text{ cm}^2/\text{Vsec}$ with the increase of substrate temperature from 423 to 673 K. The Hall mobility measurements indicated that the films are n-type semiconductors. The carrier concentration is also increased from $8.3 \times 10^{19} \text{ cm}^{-3}$ to $1.5 \times 10^{20} \text{ cm}^{-3}$ with an increase of substrate temperature (from 423 to 673 K).

Dc magnetron sputtering have been used to obtain indium oxide films with a mean crystalline size of 21 nm and thicknesses between 100 and 1600 nm. The films have been obtained onto glass substrate in oxygen-argon atmosphere at room temperatures. The conductivity of the films change about six orders of magnitude between an insulating and a very high conductive state. The reason is an irradiation of the films with ultraviolet light ($h\nu \geq 3.5 \text{ eV}$) in vacuum. The mechanism responsible for the changes in the conductivity have been supposed to be the UV-induced production of oxygen vacancies. [Xir 98].

3.1.2 In_2O_3 nano-crystals

Indium oxides nano-crystals have been synthesized within pores of mesoporous silica, annealed at temperatures from 500 to 850 °C [Zho 99]. Photo luminescence at about 350 nm (UV region) is observed by excitation at 275 nm at the samples annealed at 500 °C. In contrast the aggregates of indium oxide nano-particles have exhibited no luminescence. The luminescence in the In_2O_3 nano-particles dispersed in SiO_2 differs from that of indium oxide films and from the photo luminescence of ITO film (peak at 637 nm) [Lee 96].

3.2 Indium tin oxide (ITO)

The indium tin oxide ($\text{In}_2\text{O}_3:\text{SnO}_2$) has cubic bixbyite crystalline structure as In_2O_3 . Indium tin oxide is formed by substitutional doping of In_2O_3 with Sn which replaces the In^{3+} atoms from the cubic bixbyite structure of indium oxide (see Fig. 3.1.1). The lattice constants and bond lengths in the In_2O_3 lattice are a function of the Sn-dopant concentration [McMee 00].

3.2.1 ITO-thin films

Tin doped indium oxide (ITO) thin films are of great importance due to their transmittance of 95 % in the visible range and an electric conductivity as high as $10^4 \Omega^{-1}\text{cm}^{-1}$. It finds applications as transparent conducting electrodes for liquid crystal displays (LCD) [Yamada 00], [McMee 00], [Bas 98], [Yoo 04], [Goeb 00], [Hir 98]. ITO thin films are also used as transparent heat mirrors for buildings and cars or for saving energy, because of their non-transparency in IR and a part of NIR region [Moh 03], [Cho 83], [Vas 92].

ITO thin films have been obtained by electron beam evaporation [Cas 98]. Hot pressed powder mixtures of 87 wt% In_2O_3 and 3 wt% SnO_2 (99.999 % purity) have been used as a target. The films have been deposited on glass substrates with substrate temperatures in the range from 120 to 400 °C. The films were mainly built by long whiskers, 0.5-1 μm in length with diameters in the range from 450 to 2000 Å.

$\text{In}(\text{NO}_3)_3$ dissolved in ethanol and $\text{SnCl}_2 \cdot 2\text{H}_2\text{O}$ have been used for the preparation of ITO films on glass substrates [Lös 01a]. Spray and dip coating methods were used. The composition of the ITO films was 88.5 $\text{In}_2\text{O}_3 \cdot 11.5 \text{SnO}_2$. Thermal treatment (500 °C, 2 h) of the coated substrates have been carried out, and a crystallisation of In_2O_3 was observed. A mean crystalline size of 10 nm was calculated. The thickness of the coatings was 136 ± 4 nm. The spray-coated ITO samples with a thickness of 110 and 136 nm, possess

resistances of 3.3 and 3.7 k Ω/\square , respectively. The dip-coated films (102 and 173 nm thick) have resistances of 7.9 and 5.6 k Ω/\square .

Anti-reflective and electromagnetic shielding double-layered ITO coatings have been prepared for cathode ray tubes (CRTs) by wet chemical processes [Abe 03]. ITO particles have been used in the inner layer in order to lower the sheet resistance and to attain electromagnetic shielding properties. The transmittance of the film in the near-infrared region (NIR) was measured. When the curing condition of coating became more reductive, the film transmittance in NIR (Fig. 3.2.1) and the surface resistance of the films decreases.

It has been reported that the non transparency in the NIR region depends on the plasma frequency of the ITO particles. The plasma frequency could be expressed with the following equation:

$$\omega_p^2 = nq^2 / (\epsilon \cdot m_e), \quad \text{Equation 3.2.1.1}$$

where ω_p is the frequency, which corresponds to plasma oscillation, n , q , ϵ and m_e are the carrier concentration, the electric charge of the carrier, the dielectric constant and the effective mass of an electron, respectively. Equation 3.2.1.1 shows that the reflective wavelength of the film, which is proportional to the reciprocal plasma frequency is shifted toward the visible region as a result of an increase in carrier concentration of the films [Abe 03].

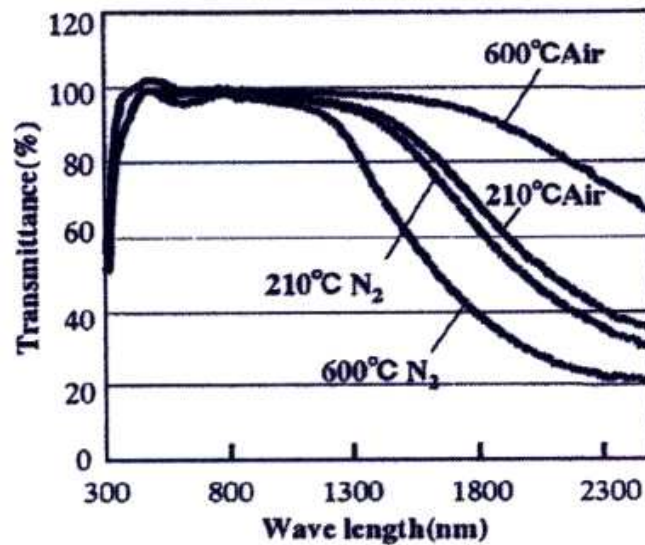


Fig.3.2.1 Spectral transmittance of double layered (inner layer ITO) coating films quoted from Ref. [Abe 03]

ITO thin films have been produced by spin coating of a dispersion of ITO nano-particles (16 nm) on glass substrates [Ede 03]. The films have a resistivity as low as $2 \times 10^{-4} \Omega\text{cm}$, comparable to the resistivity of dense high quality ITO films. The films have been heat treated in reducing atmosphere at different temperatures. An increase in the absorption and a shift of the absorption peak towards shorter wavelengths, upon annealing is seen in Fig. 3.2.2. It is reported that the carrier concentration, n_e , is increased upon annealing in a reduction atmosphere as a result of the increased number of oxygen vacancies. The oxygen vacancies are supposed to be created close to the particle surface. The analysed films are porous and hence a large internal sample surface is in contact with the reducing atmosphere. The increase of n_e , leads to a shift of the plasma frequency towards shorter wavelengths [Ede 03].

ITO nano-powders dispersed in alcohol have been used for the preparation of low resistivity ITO films [Goeb 00]. Single layers with thicknesses up to 400 nm have been fabricated with this method. The sheet resistance of the coatings was decreased with the sintering temperature. The lowest resistivity was $\rho = 2 \times 10^{-2} \Omega\text{cm}$, after sintering at 900 °C.

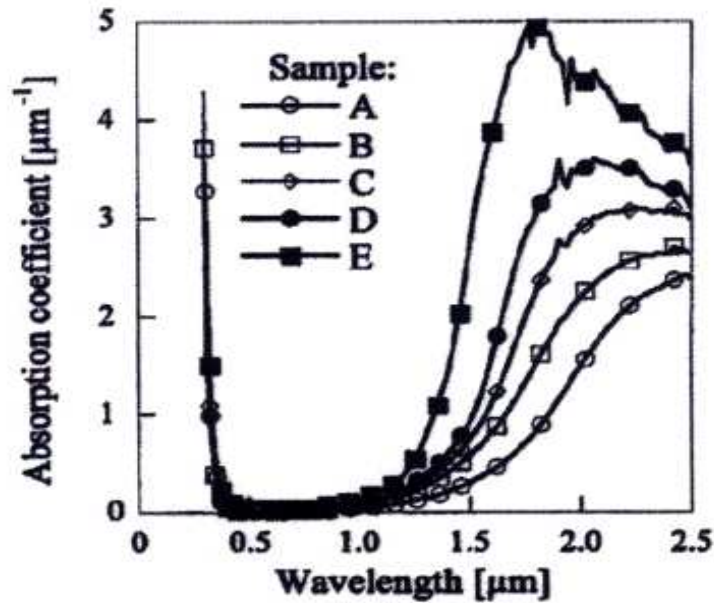


Fig.3.2.2 Spectral absorption coefficient from samples annealed for 1 h in air and 1 h in N_2 at different temperatures: sample A (300 °C), B (400 °C), C (500 °C), D (650 °C) and E (800 °C) [Ede 03]

Low resistant ITO films have also been obtained by DC-magnetron sputtering [McMee 00]. A high density ITO target (7080 kg.m^{-3}) has been used and resistivity of $1.49 \times 10^{-4} \Omega \text{ cm}$ at 200 °C was achieved. ITO films prepared without using high density targets, led to a resistivity of $2 \times 10^{-4} \Omega \text{ cm}$ at 200 °C [McMee 00].

3.2.2 $\text{In}_2\text{O}_3\text{:SnO}_2$ (ITO)-nano-powders

Indium tin oxide nano powders with different compositions (In:Sn = 90:10; 70:30, 50:50) have been prepared by heat treatment (300 - 450 °C) of mixed hydroxides prepared from In (NO_3)₃ and SnCl_4 [Nim 02]. Crystalline phase SnO_2 (cassiterite) is detected with XRD, in the case of In:Sn=50:50. Cubic phase of In_2O_3 was observed in the case of doping with up to 30 % of Sn. The bulk material with the composition In:Sn= 90:10 possesses a resistivity of around $0.6 \Omega \text{ cm}$. An mean crystalline size of 11 to 23 nm was calculated by Scherrer's

equation. Particles with sizes in the range from 150 to 170 nm were observed by SEM, which is probably a result from an agglomeration of the nano-particles [Nim 02].

ITO powder have also been obtained by heat treatment of ITO films (400-700 °C, 1 h) [Lim 04]. The powder was consisting of nanorods with diameters of ~ 75-145 nm. A bulk resistivity of ~5 Ωcm was measured.

3.3 Tin oxide (SnO₂)

The SnO₂ is another representative of the transparent conducting oxides (TCOs). In comparison to In₂O₃ it is much cheaper and in some extend less toxic. It is used for production of ITO thin films transparent electrodes for flat-panel displays and polymer based electronics [Xio 01], [Cho 83]. Tin dioxide is as well a widely used component for sensors since it is an n-type semiconductor, whose conductivity is very sensitive to the surrounding atmosphere. Most of the explosive or toxic gases and water steam detectors are based on SnO₂ [Pop 01].

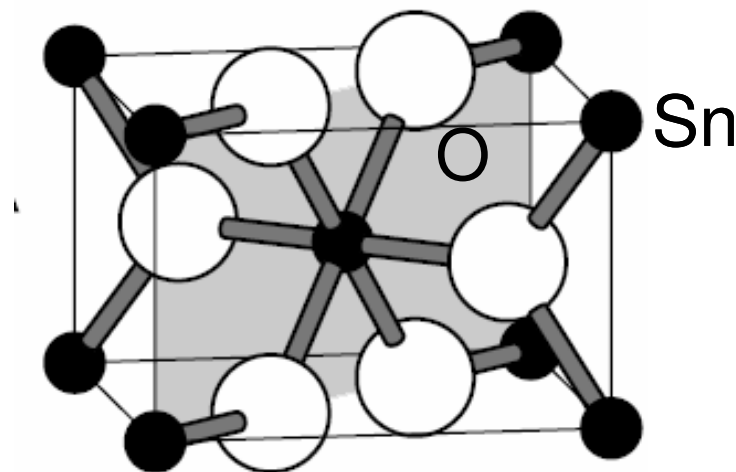


Fig. 3.3.1 Crystallite structure of SnO₂ [Cam 96], [Ham 00]

Crystalline SnO₂ (Cassiterite) has a melting temperature of 1630 °C, a density of 7020 kg.m⁻³ and possesses white or grey colour at room temperature. The SnO₂ is insoluble in water, acids and alcohols [Bla 98]. Cassiterite exhibits tetragonal crystal structure, which is shown in Fig. 3.3.1. It is a weak n-type semiconductor if deviation from the stoichiometry (oxygen deficiency) occurs. N-type conductivity could be achieved with dopants such as Sb, Cl or F [Xio 01].

3.3.1 SnO₂ thin films

SnO₂ thin films have been produced by low pressure chemical-vapour deposition (LPCVD) with tetramethyltin (TMT), oxygen, and bromotrifluoromethan (CBrF₃) as precursors. The prepared films have been treated in the temperature range from 500 to 700 °C. The films at 500 °C, have been crystallized, according to the X-ray diffraction data [Xio 01]. The electrical properties of undoped and F-doped SnO₂ films have been compared. Undoped films possess a resistivity of around 1 Ω cm and those of the doped film are around 5x10⁻⁴ Ω cm. The doping increases the carrier concentration as well as the electron mobility (μ) of the film. A mobility of ~1 cm²V⁻¹s⁻¹ and low electron concentration of 10¹⁸ cm⁻³ is reported for the undoped SnO₂ films. In contrast, the electron concentration of F-doped SnO₂ films is increased to mid-10²⁰ cm⁻³, corresponding to the F⁻ ion concentration. The electron mobility in the doped films is 40 cm²V⁻¹s⁻¹.

3.3.2 SnO₂ nano-crystals

Nano sized tin dioxide has been obtained by heating high purity metallic Sn in nitric acid for 12 h under stirring [Pop 01]. Nano-powdered SnO₂ has been separated by centrifugation, subsequently they were rinsed with distilled water and dried at 120 °C for 6 h. XRD-patterns attributed to SnO₂ were detected after drying. Grain sizes of SnO₂ in the range from 2.8 to 3.5 nm were determined by transmission-electron-microscopy. The grain

size is increased to 6nm through calcination at 500 °C. In that case, colour changes of the samples were observed, from white at 100 °C, yellow at 200 °C, to olive-green at 300 °C.

Another method used to produce nano SnO₂ is the gas-reaction method [Jia 03]. Nano-crystals of SnO₂ called nanowires, nanobelts and nanodendrites have been synthesized. The formation mechanism of these different morphologies of SnO₂ nano-crystals is dependent on the supersaturation. A low supersaturation is required for whisker growth, while a high supersaturation leads to bulk crystal growth. An intermediate supersaturation supports the growth of dendrites or platelets [Jia 03].

SnO₂ nano-powders have been also produced by slow and forced hydrolysis of aqueous SnCl₄ solutions, as well as by sol-gel routes [Ris 02]. The spectral (FTIR and Raman) properties of the SnO₂ nano-powders have been studied and compared with those of bulk SnO₂. Depending on the synthesis route the nano-powders of SnO₂ show different features in the Fourier transform infrared spectra. The Raman spectrum of nanosized SnO₂ powder, produced by forced hydrolysis showed additional bands (500, 435 and 327 cm⁻¹). In comparison that of the commercial SnO₂ have bands at 773, 630, 472 and 86 cm⁻¹ (shoulder). These additional bands are not observed for the nano-powder SnO₂ obtained by slow hydrolysis or sol-gel routes [Ris 02].

3.4 Antimony doped SnO₂ (SnO₂: Sb₂O₃ or ATO)

3.4.1 ATO thin films

Antimony doped and undoped SnO₂ films have been prepared by electron beam evaporation and spray pyrolysis methods [Sha 04]. The optical band gap of the evaporated film is in the range from 3.70 to 3.71 eV and that of spray deposited film in the range of 3.56-3.62 eV. The refractive indices measured are 1.88 and 2.03 at a wavelength of 500 nm for evaporated and spray deposited films, respectively. ATO spray deposited films have shown a sharp decrease in the resistivity. The best conductivity of the films is achieved, when the dopant is in the range of 1-2 wt%. Doping with 5 wt% leads to a higher resistance (7.5 kΩ/□) compared to undoped films (453 Ω/□) at one and the same

temperature. This effect was explained by Sb addition to SnO_2 . The incorporation of Sb atoms into the Sn^{4+} sites of the SnO_2 lattice is substitutional. In Sb doped SnO_2 films, Sb can be present in two different oxidation states, Sb^{5+} and Sb^{3+} . During the initial addition of Sb in the film, Sb^{5+} incorporated at Sn^{4+} sites acts as donor and creates excess electrons ([Moh 03], [Sha 04] compare to Fig. 3.2.1 a). Addition of Sb up to a certain level increase the carrier concentration (n) and decreases the sheet resistance of the films [Tha 02]. Film prepared at 300 °C by spraying a solution with $\text{SbCl}_3/\text{SbCl}_4 = 0.065$ led to a sheet resistance of 66.4 Ω/\square . Further addition of Sb ($\text{SbCl}_3/\text{SbCl}_4 = 0.09$), could introduce Sb^{3+} sites. They would act as acceptors-traps [Sha 04]. The Sb^{3+} species would compensate the donor levels, which are created by the Sb^{5+} sites. This leads to an increase in the sheet resistance to a value of 308 Ω/\square . The sheet resistance is decreased from 66.4 Ω/\square to 38.7 Ω/\square (by $\text{SbCl}_3/\text{SbCl}_4 = 0.065$), when the substrate temperature is increased from 300 to 350 °C. The mobility and the carrier concentration of the film are 7 $\text{cm}^2/\text{V.s}$ and $10 \times 10^{20}/\text{cm}^3$, respectively. Spray pyrolysis techniques have been used to prepare ATO thin film [Ela 04]. Sb doping levels used were 1 to 4 wt%. The dependence of the crystallinity of the films on the Sb doping level is reviewed. Films doped with 1wt% have large grains in contrast to those fabricated with higher doping levels. The sheet resistance is reduced to 2.17 Ω/\square for Sb doped films. Films doped with more than 3 wt% Sb are build by needle shaped grains. The increase of Sb doping level increases the carrier concentration, but decrease the Hall mobility.

Transparent and conducting ATO films have been deposited on glass substrates by pulse laser deposition [Kim 04]. The electrical, structural and optical properties of the films have been investigated as a function of doping level, substrate temperature and oxygen deposition pressure. For 200 nm thick films deposited at 300 °C and 45 mTorr of oxygen, an electrical resistivity of $9.8 \times 10^{-4} \Omega.\text{cm}$ is achieved. Average transmittance in the visible range of 88 % and an optical band gap of 4.21 eV are reported.

An electrical conducting ATO layer has been prepared by spinning an aqueous suspension of nano-sized ATO particles [Bom 99]. The resistance of this layer is much higher than the theoretical resistance of homogeneous ATO layers [Cho 83]. This effect has been explained in part by the small contact area between the particles. An increase of the firing

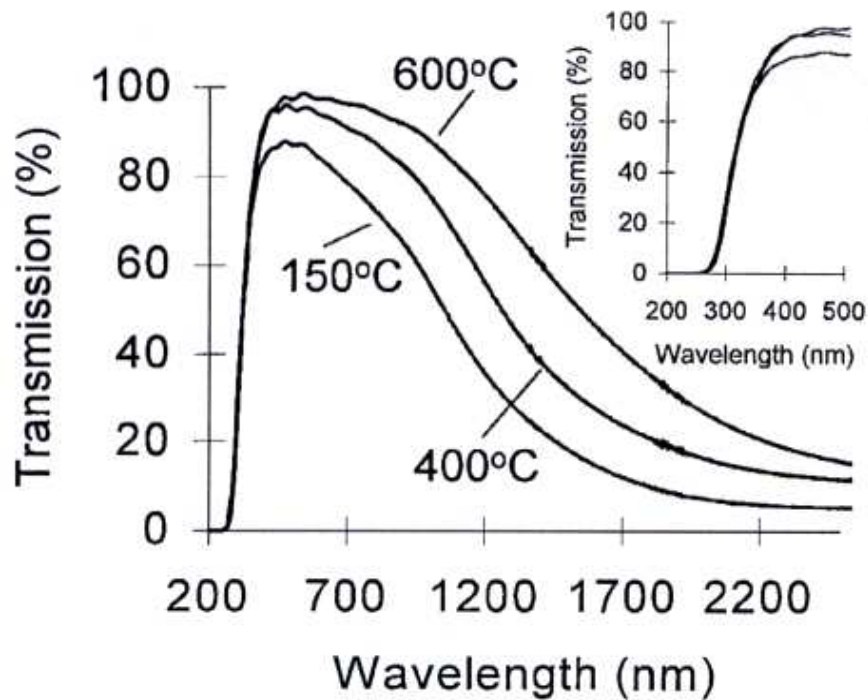


Fig.3.4.1 Optical transmission measurements of ATO particle layer on a quartz substrate [Bom 99]

temperature (150 – 400 °C) leads to a decrease in the resistance of the layer. One hypothesis is that sintering of the particles results in a larger contact surface between them, leading to a decrease in the resistance. Such a decrease could be explained by the presence of an insulating Sb-rich layer at the outside of the particle. The thickness of which could be reduced when the layer is cured. At temperatures above 700 °C, the resistivity is increased due to segregation of antimony to the surface of the particles.

The films' optical properties have been investigated as well. An increase of the annealing temperature results in a shift of the plasma edge toward higher wavelengths (see Fig. 3.4.1). This could be related to a reduction of the charge carriers concentration in the material [Hau 72].

3.4.2 ATO nano-crystals

Antimony doped tin oxide nano-particles have been synthesized by co-precipitation method [Zha 04], [Koi 02]. The starting materials used are Sb_2O_3 , dissolved in molten citric acid, and granulated Sn, dissolved in HNO_3 [Zha 04] or metal chlorides [Koi 02]. The chloride route is not preferred, because of the difficulty to rinse off the residual chloride. The presence of chlorine ions leads to the evaporation of antimony and tin compounds, which negatively affects the surface and the electrical properties. A chloride free method for the preparation of ATO-nano-particles has also been reported [Zha 04]. The crystallite size of the particles (6-20 nm) has been strongly influenced by the Sb doping level. This is in agreement with the results obtained for crystalline ATO thin film.

3.5 In- and Sn-containing glasses

Although, nano-powders are predominantly prepared by wet chemical method, the high temperature route through crystallisation and dissolution of glass is another possibility for their synthesis. Such synthesis gives a potential opportunity to control the crystal size and defects in the crystal lattice, and consequently their properties.

Nano-crystalline In_2O_3 has been obtained at crystallisation temperatures of 650 to 800 °C in the alumo-silicate system $\text{Na}_2\text{O}/\text{CaO}/\text{Al}_2\text{O}_3/\text{In}_2\text{O}_3/\text{As}_2\text{O}_3/\text{SiO}_2$ [Lös 01a]. A prerequisite for the crystallization of In_2O_3 is the presence of Al_2O_3 (typical 10 mol%). Before tempering, the glasses were transparent at wavelengths in the range from 400 to 1200 nm. This is in contrast to the samples after heat treatment. An increase of the heat treatment temperatures resulted in a shift of the UV-absorption edge toward the visible range and in an increase of the extinctions within the infrared range (Line 6 from Fig. 3.5.1). The minimum extinctions observed for glasses tempered at 750 °C and 800 °C are 0.95 and 1.78, respectively. The samples have changed their colours from colourless, after preparation to dark yellow (at 750 °C). A dark green colour of the samples has been observed at

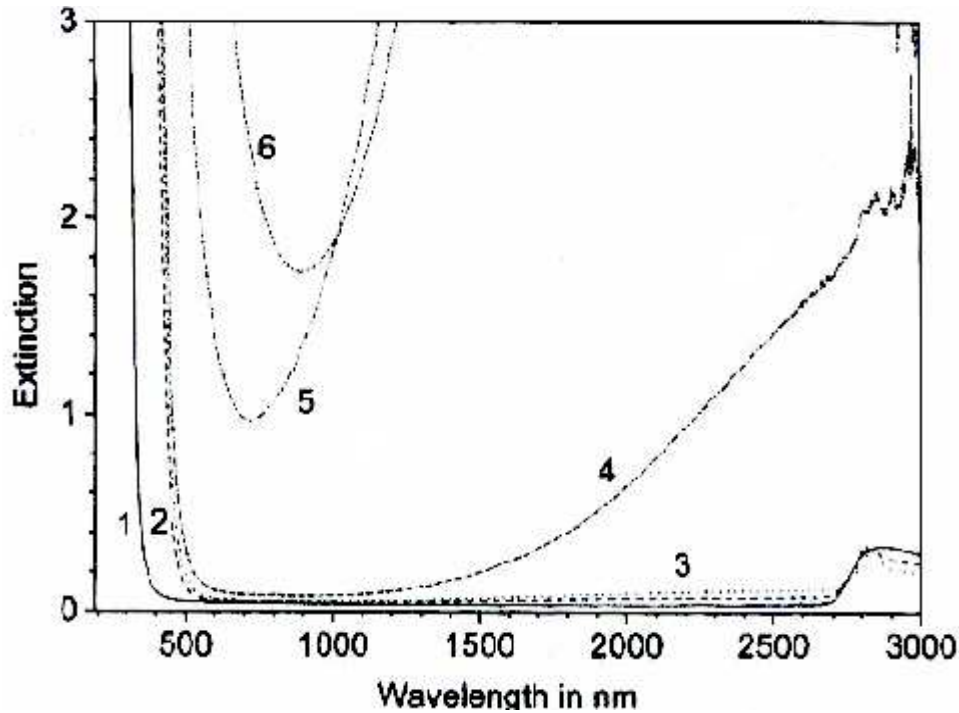
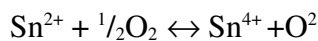


Fig. 3.5.1 Optical spectra from glass with the composition $16\text{Na}_2\text{O}\cdot 10\text{CaO}\cdot 12\text{Al}_2\text{O}_3\cdot 52\text{SiO}_2\cdot 5\text{In}_2\text{O}_3\cdot 5\text{As}_2\text{O}_3$, tempered at different temperatures, referred from [Lös 01a].

800 °C. Mean crystalline sizes in the range from 5 to 40 nm were determined, depending on the crystallisation temperature.

In conventional silicate glasses, the solubility of the SnO_2 raw material is restricted to a few percent and, furthermore, its dissolution rate is extremely low [Chi 01]. At high temperatures Sn^{2+} and Sn^{4+} form an equilibrium with the physically dissolved oxygen of the melt [Xia 97], [Ben 03], [Kum 92].

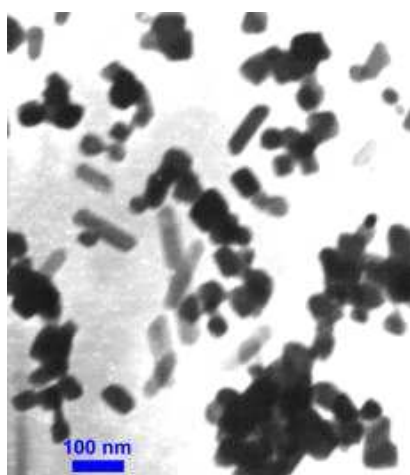


Equation 2.5.1

For the case of soda- or soda-lime-silicate glass melts in equilibrium with air at 1500 °C, the $[\text{Sn}^{2+}]/[\text{Sn}^{4+}]$ -ratio is in the range of 0.05 to 0.1 depending on the composition [Ben 03].

To our knowledges there are no literature data for synthesis of In_2O_3 , SnO_2 as well as ITO and ATO-nano-crystals trough controlled crystallisation of borate glasses. ITO- and ATO-nano-powders are predominantly used as high density targets for the fabrication of thin films.

An conformation for their usefulness and the importance of ITO-, ATO-, In_2O_3 - and SnO_2 -nano-powders is their high price. The huge increase in the price for example of In_2O_3 in the past two years can be seen in Fig. 3.5.2. The commercial In_2O_3 -nano-powder usually has crystalline size in the range from 30 to 50 nm and a purity of 99.995 % (see quoted from [Nano 03]) (Fig. 3.5.2).



Price for 5g	20 \$	145 \$
Date	09.09.02	23.06.04

Fig. 3.5.2 Commercial In_2O_3 (Nanostructured & Amorphous Materials, Inc.)
[Nano 03]

3.6 Crystallisation of melts

Crystallisation of glasses is usually designated as devitrification [Sch 90].

Thammann is probably the first who separated the crystallisation process into two independent processes: nucleation and crystal growth. The rate of nucleation J is defined by the number of crystallisation centers (N), formed per unit volume (V) and unit time (τ).

$$J = N / V \cdot \tau \quad \text{Equation 3.6.1}$$

The crystal growth velocity is defined by the formula:

$$v = l / \tau, \quad \text{Equation 3.6.2}$$

where l is the length with which the already existing crystal centers (nuclei) grow per unit time (τ) in a certain crystallographic direction. According to Tammann, both nucleation and crystallisation rates have maxima, which depend on the undercooling $\Delta T = T_m - T$, where T_m is the melting temperature [Pet 92]. Generally, these maxima do not coincide.

Figure 3.6.1 presents schematics of the nucleation rate and the crystallisation growth velocity of a glass as a function of the temperature, where T_m is melting temperature. The peak of crystal growth velocity is observed at higher temperatures (lower undercoolings) than the nucleation peak. This enables a two step crystallisation (see Fig. 3.6.1) [Gut 95]. At a first step, the glass can be tempered at temperature T_1 , in order to initialize nucleation. At T_1 , v has a small value and J is large. In a second step the formed nuclei could further grow at a higher temperature T_2 .

With increasing the superposition of the nucleation rate and crystal growth velocity, the crystal growth during cooling of the melt increases [Sch 88], [Pet 92], [Var 94].

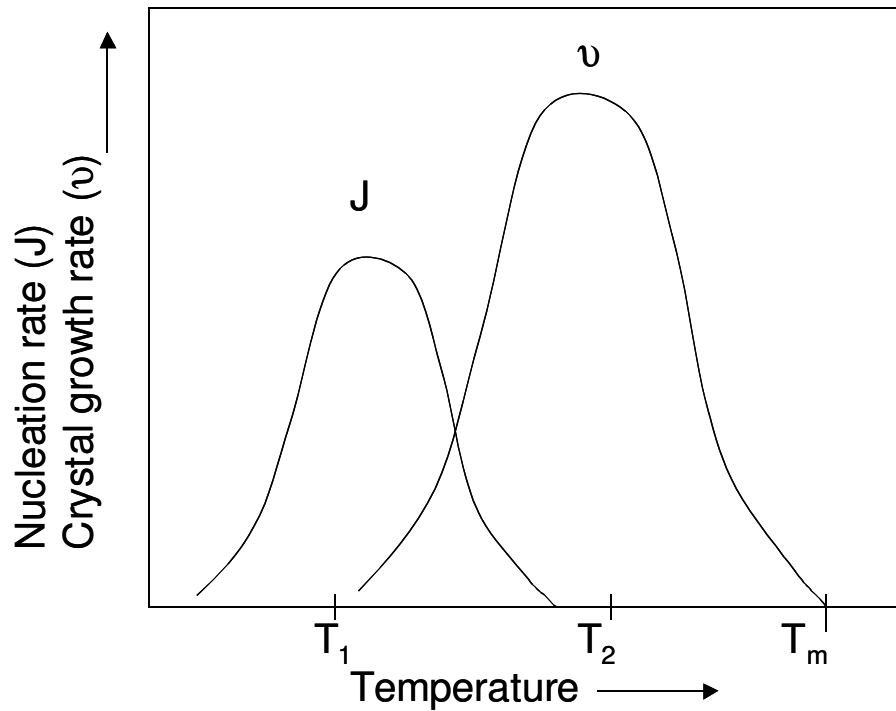


Fig. 3.6.1 Nucleation rate and crystal growth velocity as a function of the temperature [Pet 92]

3.6.1 Nano-crystallisation from glasses

Nanocrystals with proper size can be achieved by controlling the conditions during thermal treatment of the glasses. In principle, the size of the crystal is determined from the crystal growth velocity and nucleation rate. [Kas 00], [Avr 03]. In isochemical systems, small average crystallite sizes can only be obtained by high nucleation and low crystal growth rates.

3.6.2 Pendulum effect theory

A theoretical model has been developed [Avr 99], according to which needle like crystals with non-equilibrium shape grow at high supersaturation with $X/R \gg (X/R)_{eq}$, where X is the length and R the thickness of the crystal. At first, the crystals have high aspect ratios, large lengths (X) and small radii (R). Along the time at higher temperature the increase of the length of the crystal stops. Due to changes in the local concentration, the crystals get shorter. So the crystals approach their equilibrium state and the aspect ratio X/R decreases.

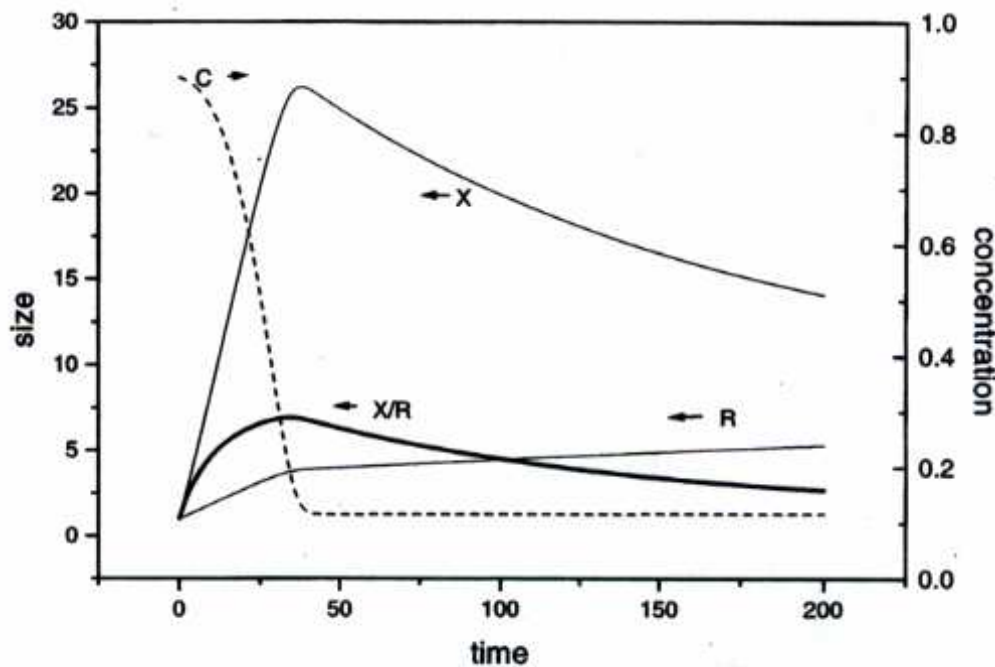


Fig. 3.6.2 Time dependence of crystal size (solid line, left axis) and matrix concentration (dashed line, right axis). The aspect ratio X/R (bold line); X : crystal length and R : radius of crystal with cylindrical shape [Avr 99]

Figure 3.6.2 shows the time dependence of crystal size and matrix concentration. At shorter times, the crystal length increases to some maximum value (solid line, left axis) and parallel the concentration of the matrix decreases (dashed line, right axis). The crystal radius increases with increasing the time. The aspect ratio X/R at first increases, reached its maximum and then gets smaller again (bold line). In summary, after reaching the maximum aspect ratio, the crystals are getting shorter and thicker with time.

4 Experimental part

4.1 Methods for analysis

4.1.1 X-ray diffraction (XRD)

X-ray diffractometry (XRD) is a useful method for the identification of crystalline substances. It is a technique at which monochromatic primary X-rays are made to fall on a studied sample substance. Because of its wave nature, like light waves, it gets diffracted to certain angles. These angles of diffraction, Θ , will give the information regarding the crystal nature of the substance.

Peaks are observed at those angles Θ , at which the Bragg's law condition:

$$n\lambda = 2d \cdot \sin \Theta \quad \text{Equation 4.1}$$

is satisfied, where 'n' is the order of reflection of X-rays, ' λ ' is the X-ray wavelength, 'd' is the interplaner spacing, which is characteristic for a crystalline plate.

X-ray diffraction can also be used for the estimation of the crystallite size through the XRD-line broadening. The mean crystalline size in a sample can be calculated using Scherrer's equation:

$$d = G \cdot \lambda / B \cdot \cos \Theta \quad \text{Equation 4.2}$$

$$B = B_0 - b_0, \quad \text{Equation 4.3}$$

where \bar{d} is the mean crystallite size, $G=0,899$ for cubic systems, λ is the wavelength (0.154 nm for $\text{Cu}_{K\alpha}$ -radiation), B real (physical) full width at half maximum (FWHM), B_o -measured width of half the maximum, b_o -the width of half maximum from macrocrystals (instrumental broadening) Θ is the Bragg angle [Mir 61].

The used technique in this work is a Siemens D 5000 diffractometer with copper anode.

A Silicon monocrystal is used in order to obtain monochromatic $\text{Cu}_{K\alpha}$ -radiation ($\lambda=0.154$ nm). The powder diffraction patterns have been measured at 2Θ values in the range from 10 to 60 °.

4.1.2 Scanning electron microscopy (SEM).

Scanning electron microscopy is widely used for inspecting the microstructure of specimens. During SEM studies, a beam of electrons is focused on a spot volume of the specimen, resulting in the transfer of energy to the spot. These bombarding electrons, also referred to as primary electrons, dislodge electrons from the specimen itself. The dislodged electrons, also known as secondary electrons, are attracted and collected by a positively biased grid or detector, and then translated into a signal.

In this work samples have been analysed with a Zeiss DSM 940 A scanning electron microscope. The surface of bulk samples have been covered with gold and studies on the crystalline character of the samples have been carried out.

4.1.3 Transmission Electron Microscope (TEM)

Transmission Electron Microscopy (TEM) is a technique used for analysis of the bulk morphology of materials. TEM provides a much higher spatial resolution than SEM, and can facilitate the analysis of features in the range of a few nanometers.

For crystalline materials, the specimen diffracts the incident electron beam, producing local diffraction intensity variations that can be translated into contrast to form an image. For amorphous materials, contrast is achieved by the variations in electron scattering as the electrons traverse the chemical and physical differences within the specimen.

In this study, size and form of crystalline powder have been determined with a 200 kV electron microscope Hitachi H-8100. For this purpose, In- and Sn-containing crystalline phases have been isolated from the glass-ceramics through dissolution of the glassy matrix and the not In- or Sn-containing crystalline phases. Subsequently dialysing the formed suspension is done (see Chapter 4.2). In this way, a suspension of the crystals in water is obtained. Some drops of it have been given to a sample holder (Cu- nets) and they have been analysed with the TEM.

4.1.4 Energy Dispersive X-ray analysis (EDX)

EDX is a technique used for identifying the elemental composition of the specimen, or an area of interest thereof. The EDX analysis system works as an integrated accessory of a scanning or a transmission electron microscope.

During EDX analysis, the specimen is bombarded with an electron beam inside the SEM or TEM. The bombarding electrons collide with the specimen atoms own electrons, knocking some of them off. A position vacated by an ejected inner shell electron is eventually occupied by a higher-energy electron from an outer shell. To be able to do so, however, the transferred outer electrons must give up some of its energy by emitting an X-ray.

The amount of energy released by the transferring electrons depends on which shell it is transferring from, as well as which shell it is transferring to. Furthermore, the atom of every element releases X-rays with unique amounts of energy during the transferr process. Thus, measuring the energy of the X-rays being released by a specimen during electron beam bombardment, enables to identify the atoms from which the X-rays were emitted.

The output of an EDX analysis is an EDX spectrum. The EDX spectrum is just a plot of how frequently an X-ray is received for each energy level. An EDX spectrum normally displays peaks corresponding to the energy levels for which the most X-rays had been

received. Most of these peaks are unique to an atom, and therefore correspond to a single element. The more intense a peak in a spectrum, the more concentrated the element is in the specimen.

4.1.5 Differential Thermal Analyse (DTA)

This technique measures the temperature difference between a sample and a reference material as a function of temperature as they are heated or cooled or kept at a constant temperature (isothermal). In actual practice, sample and reference material are simultaneously heated or cooled at a constant rate. Reaction or transition temperatures are then measured. It provides vital information of the materials regarding their endothermic and exothermic behaviour at high temperatures.

The DTA measurements have been carried out with Shimadzu DTA-50. Samples have been in powder form and a Pt-crucible was used. The measurements were performed with a heating rate of 10 K/ min up to 1400 °C.

4.1.6 UV-VIS-NIR-spectrometry

UV-VIS-NIR-spectrometer Shimadzu UV 3101 PC was used to study glass samples as well as nano-powders dispersed in different matrices (solution, polystyrene or paraffin oil).

4.1.7 Fourier-Transform-Infrared Spectrometry (FTIR)

Fourier Transform Infrared Spectroscopy is an analysis technique that provides information on the chemical bonding or molecular structure of materials, whether organic or inorganic. It is used to identify unknown materials present in a specimen.

The technique works on the fact that bonds and groups of bonds vibrate at characteristic frequencies. A molecule that is exposed to infrared radiation absorbs infrared energy at frequencies which are characteristic to that molecule. During FTIR analysis, a spot on the

specimen is subjected to a modulated IR beam. The specimen's transmittance or reflectance of the infrared rays at different frequencies is translated into an IR absorption plot consisting of reverse peaks. The resulting FTIR spectral pattern is then analysed and matched with known signatures of identified materials in the FTIR library.

4.2 Procedure for preparation of In_2O_3 -, $\text{In}_2\text{O}_3\text{:SnO}_2$ -, SnO_2 - and $\text{SnO}_2\text{:Sb}_2\text{O}_3$ - nano-powders from glasses

The used method for the preparation of In_2O_3 -, $\text{In}_2\text{O}_3\text{:SnO}_2$ -, SnO_2 - and $\text{SnO}_2\text{:Sb}_2\text{O}_3$ - nano-powders consists of some steps as followed:

- Preparation of borate glasses with relatively high In_2O_3 and/or SnO_2 concentrations
- Crystallisation of the desired crystalline phase from the glasses
- Dissolution of the glass matrix and non In- or Sn-containing crystalline phases, except the desired nano-crystalline phase.
- Separation of the nano-crystalline phase through dialysis or centrifugation

Glasses were prepared from reagent grade B(OH)_3 , Na_2CO_3 , Al(OH)_3 , In_2O_3 , SnO_2 and Sb_2O_3 . The 20 g batches were melted in a platinum crucible at 1250 to 1500 °C in a resistance heated furnace and soaked for 15 min to 1 h. The melts were quenched on a copper block. The obtained glasses were subsequently heat treated at temperatures in the range from 500 to 820 °C for 20 min to 16 h. The samples were tempered in air or in Ar/ H_2 gas (5 % H_2 + 95 % Ar). The crystallized samples were studied by x-ray diffraction (Siemens D 5000, $\text{Cu}_{K\alpha}$). In order to dissolve the glass matrix and the non In- and/or Sn-containing crystalline phases, 1 g of the powdered samples were dissolved in distilled water (50 ml) for 6 days at 40 °C, in acetic acid (0.6 N CH_3COOH) or in 5 % HF + 20 % HNO_3 mixture for 1 day. The crystalline residue was separated by centrifugation with tetra chlor methan (CCl_4) or by dialysis.

Due to the nano crystallinity, the separation of the crystals from the solution (i.e. the salt) could not be completely achieved by simple filtration. Therefore, the solutions containing dissolved salts and nano crystals were given inside a cellulose membrane of a type usually applied for dialysis of macromolecular solutions with a molecular weight cut off of 12 kDa. It is supposed, that the pores of the membranes are smaller than the nano crystals. The filled tubes were closed from both ends and given to a vessel with distilled water (Fig. 4.2.1). The membrane is semi permeable and allows the salt to diffuse into the distilled water. The pH value of the water was measured. When the pH value changed from neutral pH to a value from 2 or 3, then the water in the vessel have been changed with a new one. This procedure has been done until the pH had a constant value equal to pH 7. Consequently the nanocrystal-water suspension have been taken from the membranes and dried at 40 °C. The as obtained powder was characterized by XRD, FTIR and TEM using an acceleration voltage of 200 kV.

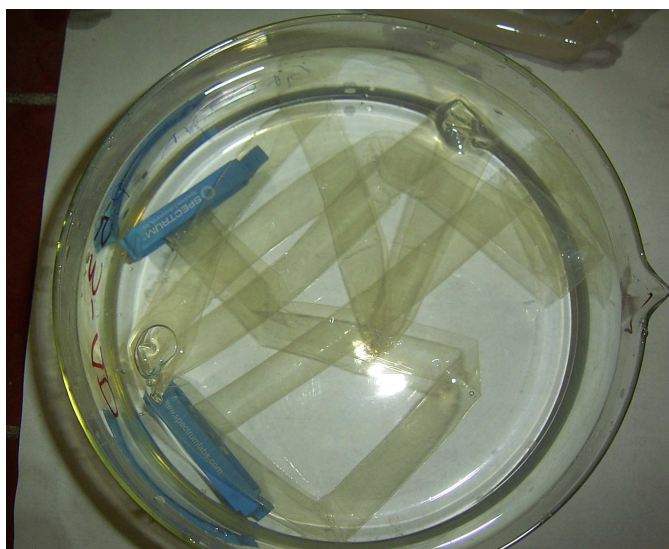


Fig.4.2.1 Cellulose membranes filled with suspension (dissolved powder from crystallized sample in acid)

5 Results

5.1 Synthesis and optical properties of In_2O_3 -nano-powder

5.1.1 Choice of the glass system

The ideal glass for the purpose of the work should contain relative high concentration of In_2O_3 from which during thermal treatment In_2O_3 - nano-particles crystallize. The glass should be chemically not stable in comparison to the desired nano-crystalline phase, in order to facilitate the separation of nano-crystalline powder.

The silicate glass used in [Lös 01a] possesses high chemical durability. Therefore it is not suitable for the preparation of pure In_2O_3 nano-powder, because of the lack of a solvent in which the glass matrix is soluble, but the nano-crystals insoluble. A promising glass matrix, for this purpose could be a glassy matrix with low chemical resistivity. The matrix should be easily soluble in water or acids in which the desired crystalline phase is insoluble. First of all, borate glasses are promising candidates.

The glass system B_2O_3 Na_2O Al_2O_3 In_2O_3 was chosen due to the relatively large glass formation range (GFRs) of the three component systems as shown on Fig. 5.1.1 and Fig. 5.1.2.

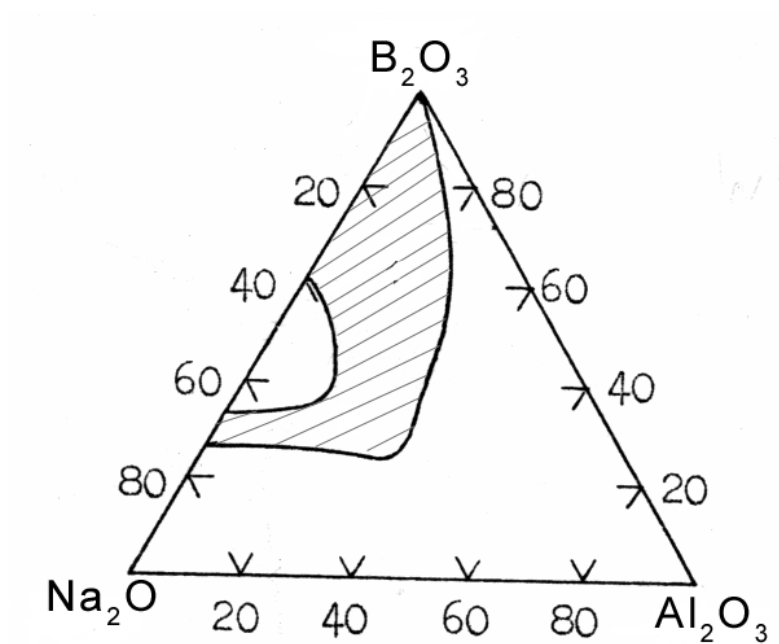


Fig. 5.1.1 Glass formation range of the system $\text{Na}_2\text{O} \cdot \text{Al}_2\text{O}_3 \cdot \text{B}_2\text{O}_3$ in Mol% [Maz 91]

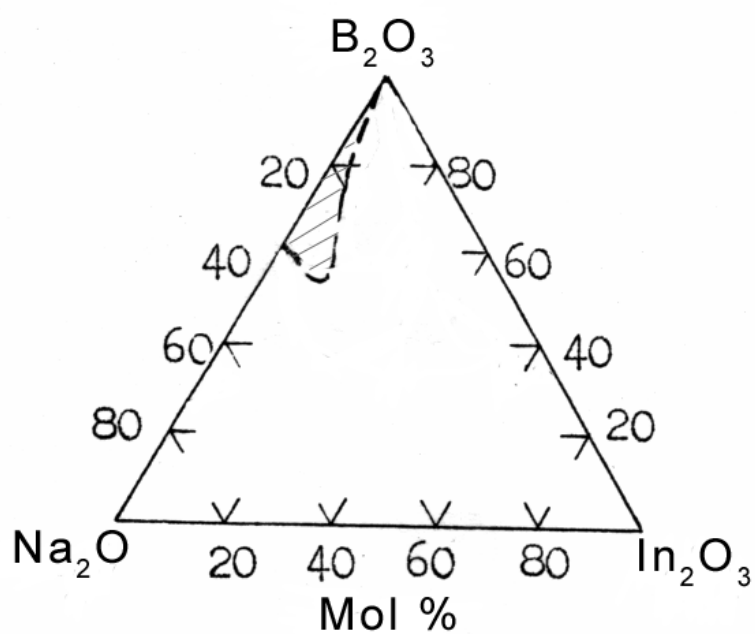


Fig. 5.1.2 Glass formation range of the system $\text{Na}_2\text{O} \cdot \text{In}_2\text{O}_3 \cdot \text{B}_2\text{O}_3$ in Mol% [Maz 91]

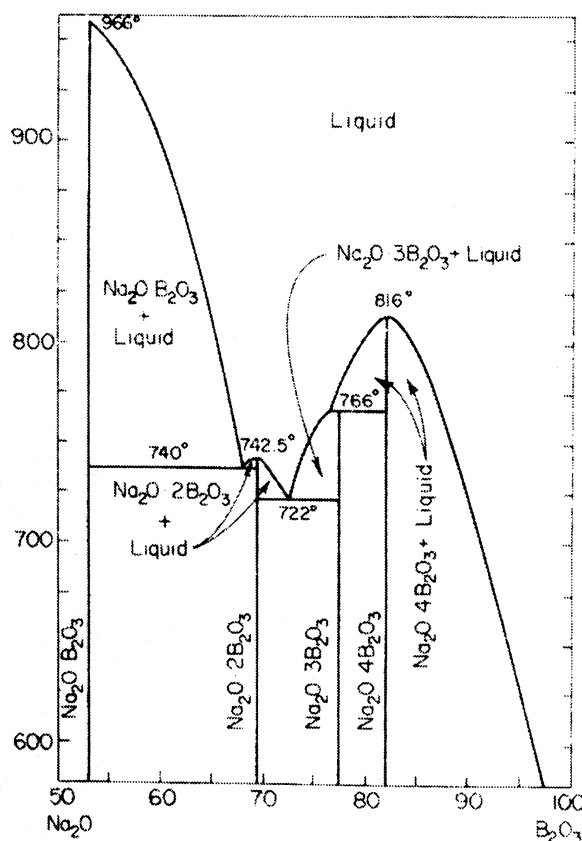


Fig. 5.1.3 Phase diagram of binary system Na₂O- B₂O₃ [Lev 64]

Information about the possible formation of crystalline phases in systems could be obtained from the phase diagrams. The ternary phase diagram Na₂O·Al₂O₃·B₂O₃ is not known. The binary systems Na₂O-B₂O₃ and In₂O₃-B₂O₃ have the following binary phase diagram shown on Figs. 5.1.3 and 5.1.4.

Only one binary compound, InBO₂, exists in the In₂O₃-B₂O₃ system. The thermal stability of the compound was measured by DTA [Saj 93], and no phase transition, melting or decomposition is observed in the temperature range up to 1773 K. It was reported by Levin

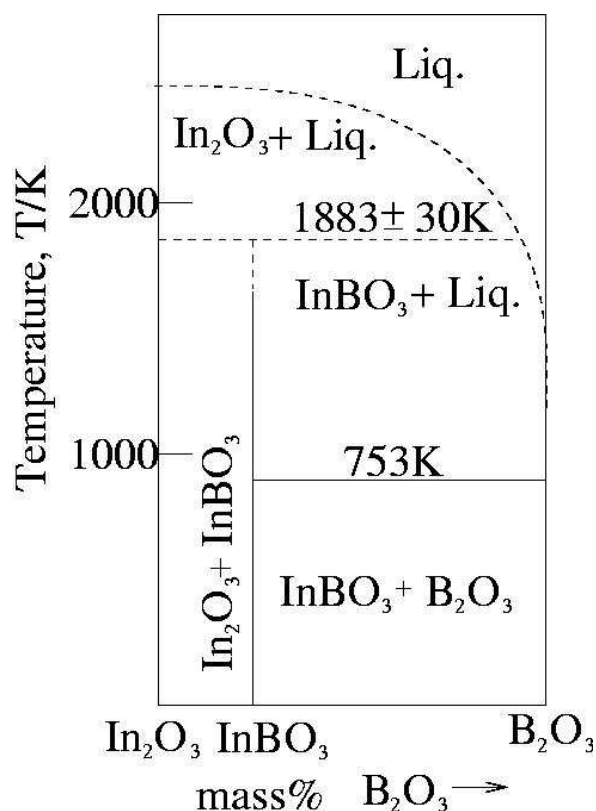


Fig.5.1.4 Phase diagram of binary system
In₂O₃- B₂O₃ [Saj 93]

et al. [Lev 61] that the InBO₃ compound melts at 1883±30 K. Studies of the structural relations among double oxides of trivalent elements [Kei 54] found that after a few minutes at 1973 K the InBO₃ compound lost B₂O₃ and yielded In₂O₃.

5.2 Melting and thermal treatment of glasses

Several compositions in the system B₂O₃·Na₂O·Al₂O₃·In₂O₃ have been investigated and summarised in Tab.5.2.1. During melting, all the compositions were completely dissolved and homogeneous melts have been formed. Glass compositions with 5 and 7 mol% In₂O₃ have been melted in order to achieve relatively large In₂O₃ concentrations. In the system studied, compositions with more than 7 mol% In₂O₃ could not be transferred into homogeneous melts at temperatures ≤ 1500 °C.

An important factor which influences the crystallisation of In_2O_3 is the molar ratio $[\text{Na}_2\text{O}]/[\text{B}_2\text{O}_3]$. Therefore glass compositions with molar ratios from 1.375 to 0.613 have been studied. At high Na_2O concentrations ($\text{Na}_2\text{O}/\text{B}_2\text{O}_3 > 1.2$), NaInO_3 crystallises after heat treatment of glasses, as will be discussed later. At low Na_2O concentrations, no crystallisation was observed. A value of at about 1.1 for the $[\text{Na}_2\text{O}]/[\text{B}_2\text{O}_3]$ ratio enabled controlled In_2O_3 crystallisation. Another factor which could affect the In_2O_3 crystallisation is the Al_2O_3 concentration as reported for silicate glasses [Lös 01a]. In relation to this, compositions with Al_2O_3 concentration from 0 to 15 mol% have been prepared and analysed. The glasses with 12 and 15 mol% Al_2O_3 (samples K and L) allow largest amount of In_2O_3 to be dissolved in the melts, however they require high melting temperatures. Therefore, glass compositions with Al_2O_3 concentrations ≤ 10 mol% were preferred.

During quenching of the melt, under the conditions supplied, fully transparent and X-ray amorphous glasses were obtained from the sample compositions D, E, G, H, K and M. The samples B, C and L were opaque and contained large quantities of crystals, while in the samples A, F and I trace amounts of crystalline phase were seen.

In Fig. 5.2.1 the DTA profile of sample H is shown. A glass transition temperature $T_g = 385$ °C and a softening temperature $T_s = 420$ °C are determined. Two crystallisation peaks T_{c1} at 530 °C and T_{c2} at 607 °C and a melting temperature of 740 °C are recorded as well.

The as quenched glasses and the samples after heat treatment have been characterized with X-ray diffractometry.

The XRD-patterns of quenched glass samples B, H, I and K are shown in Fig. 5.2.2 The patterns of samples H and K do not show any sharp peak caused by crystalline phases, while samples I shows small peaks attributed to In_2O_3 (JCPDS-file No.: 6-0416). In the XRD -pattern of the opaque sample B, intense lines indicated the crystallisation of NaBO_2 (JCPDS-file No.: 32-1046) and In_2O_3 .

Tabl. 5.2.1 Chemical compositions of the In_2O_3 containing samples (in mol%). The glasses were: T- transparent, C-with small quantity of crystalline phase and O- opaque

Sample	Na_2O	B_2O_3	Al_2O_3	In_2O_3	SnO_2	Sample	$[\text{Na}_2\text{O}]/[\text{B}_2\text{O}_3]$	In-containing crystalline phase	non In-containing phase
A	55.0	40.0	-	5,0	-	C	1,375	NaInO_2^*	NaBO_2
B	49.9	45.1	-	5,0	-	O	1,106	In_2O_3^*	NaBO_2
C	45.1	49.9	-	5,0	-	O	0,904	In_2O_3^*	NaBO_2
D	36.1	58.9	-	5,0	-	T	0,613	--	NaBO_2
E	47.5	42.7	4,8	5,0	-	T	1,112	In_2O_3	$\text{Na}_2\text{B}_2\text{O}_4$
F	45.0	40.0	8,0	7,0	-	C	1,125	In_2O_3^*	NaBO_2
G	35.0	50.0	10,0	5,0	-	T	0,700	---	---
H	45.0	40.0	10,0	5,0	-	T	1,125	In_2O_3	NaBO_2
I	44.0	39.0	10,0	7,0	-	C	1,128	In_2O_3^*	NaBO_2
K	42.9	38.1	12,0	7,0	-	T	1,125	In_2O_3	NaBO_2
L	41.3	36.7	15,0	7,0	-	O	1,125	In_2O_3^*	--
M	44,55	39,6	9,9	4,95	1,0	T	1,125	In_2O_3	NaBO_2 , $\text{Na}_2\text{Al}_2\text{B}_2\text{O}_7$

*-spontaneous crystallisation during quenching

XRD-patterns of heat treated glasses with the compositions A, E, G, I and K can be seen in Fig. 5.2.3. In sample A, distinct lines attributed to NaInO_2 (JCPDS-file No.:24-1037) are observed. In the XRD-patterns of sample G, lines caused by any indium containing crystalline phase were not detected. Samples E, I and K show lines attributed to crystalline In_2O_3 . Besides, in sample I notable quantities of NaBO_2 (JCPDS-file No.: 12-0492) are detected. In sample K, minor concentration of NaBO_2 occur. The crystallisation of In_2O_3 is also observed in samples B, F and H, while in sample D the crystal phases formed are $\text{Na}_2\text{B}_2\text{O}_4$ and $\text{Na}_2\text{B}_4\text{O}_7$. In sample A besides NaInO_2 , sodium borate is formed.

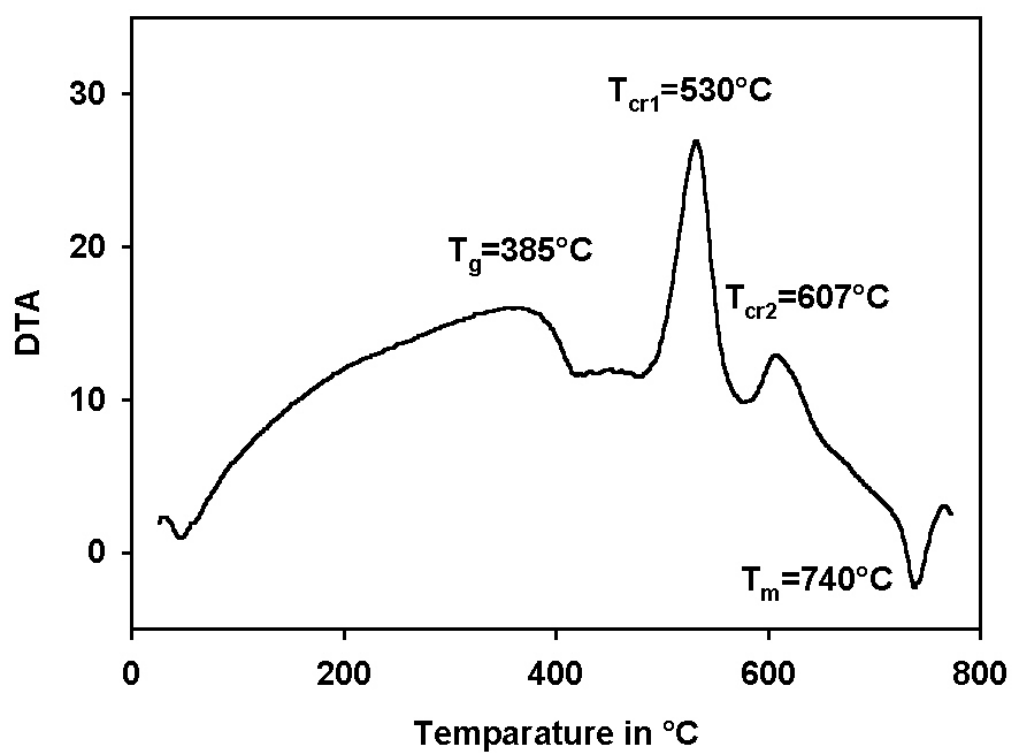


Fig. 5.2.1 DTA-profile of sample H

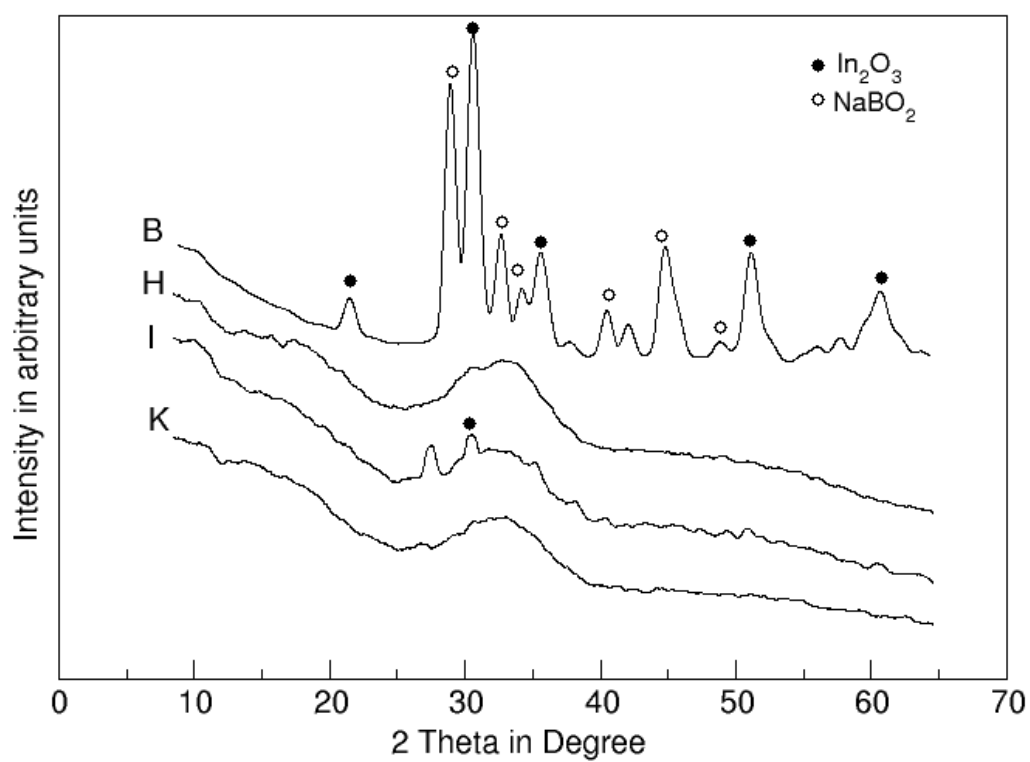


Fig. 5.2.2 XRD-patterns of quenched samples B, H, I and K

The phases formed during tempering depend not only on the composition, but also on the crystallisation conditions applied as shown in Fig. 5.2.4, for sample H. Without tempering or after thermal treatment at 500 °C for 20 min, distinct lines are not observed. After tempering at 500 °C for 80 min, first lines due to NaBO_2 are seen. Thermal treatment at 530 °C for 80 min resulted in the crystallization of small quantities of In_2O_3 as well as in the occurrence of NaBO_2 . At temperatures of 560, 600 and 700 °C, In_2O_3 is the main crystalline phase formed. The intensities of the peaks attributed to In_2O_3 increase and the lines get narrower with increasing temperatures. Besides In_2O_3 and NaBO_2 , an additional phase, possibly $\text{Na}_2\text{Al}_2\text{B}_2\text{O}_7$ occurs, as indicated by the peak at 23 °.

Sample H (5 mol% In_2O_3) was heat treated at 630 °C for 20, 40, 60 and 100 min, in order to study the change in the crystallite size of In_2O_3 (see Fig. 5.2.5). Tempering for 20 min results in the mean crystallite size of 16 nm, calculated using Scherrer's equation (see Equation 4.2.). Thermal treatment for 40 and 60 min leads to mean crystallite sizes of 19 and 21 nm, respectively. After tempering for 100 min, a further increase in the crystallite size is not observed within the limits of experimental error.

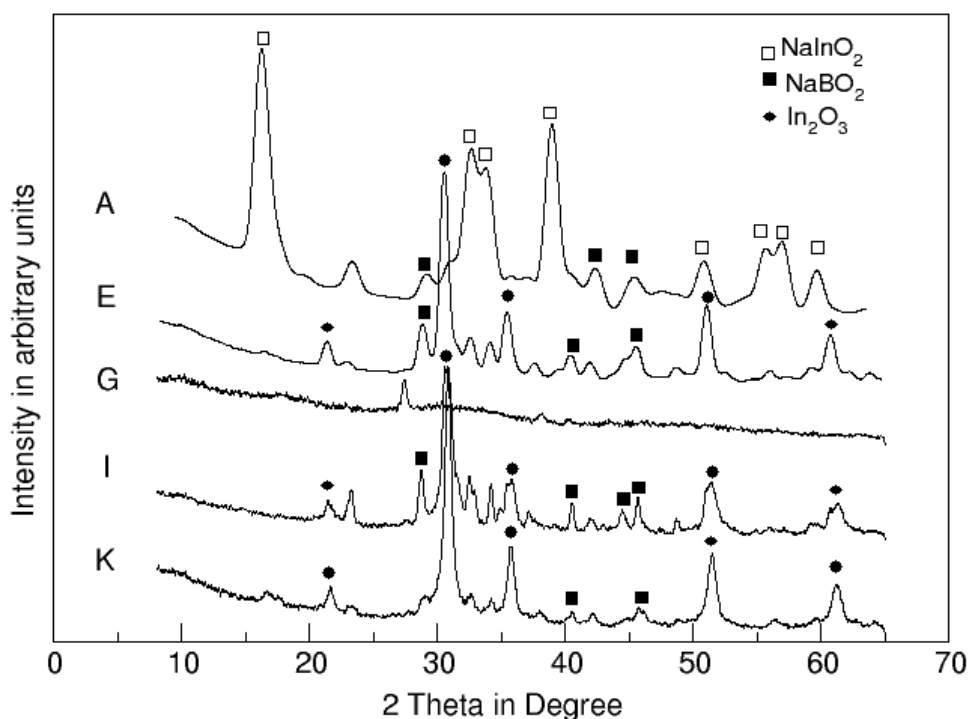


Fig. 5.2.3 XRD-patterns of tempered samples A (700 °C, 3 h), E (700 °C, 1 h), G (580 °C, 20 min), I (580 °C, 20 min) and K (590 °C, 30 min)

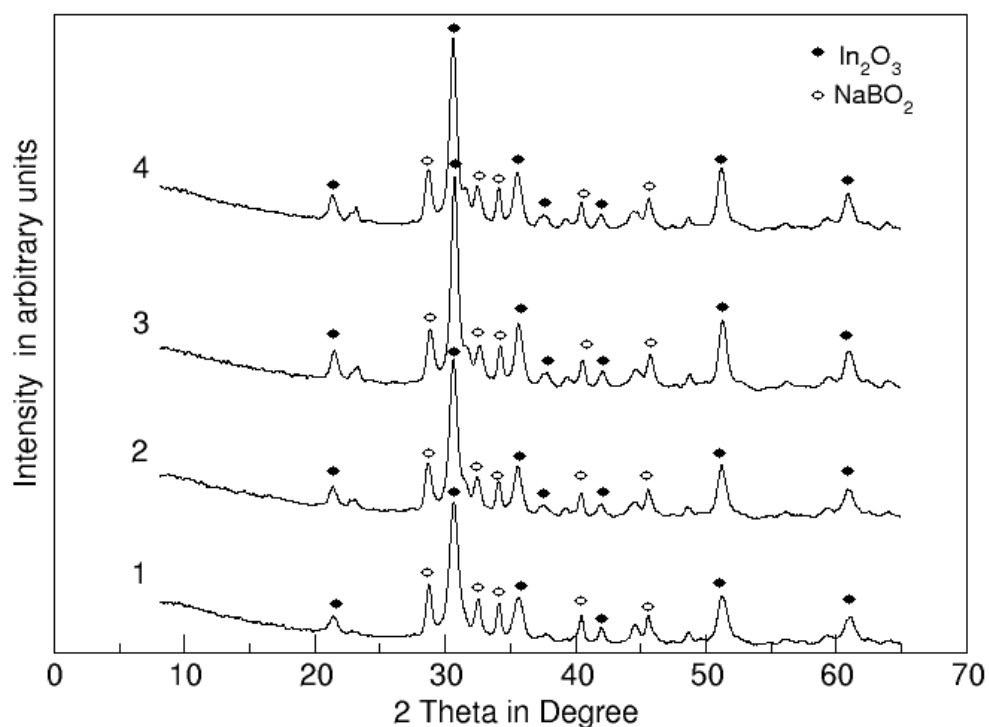


Fig. 5.2.4 XRD-patterns of sample H after thermal treatment at 630 °C for: 1: 20 min, 2: 40 min, 3: 60 min and 4: 100 min

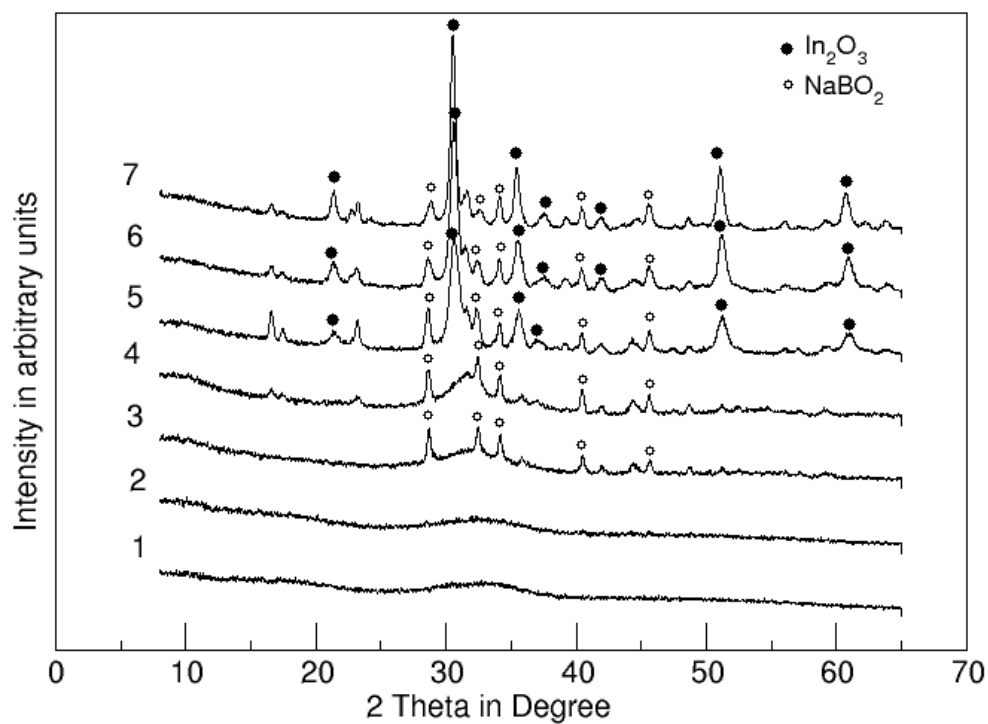


Fig. 5.2.5 XRD-patterns of sample H. 1: without thermal treatment, 2: 500 °C, 20min; 3: 500 °C, 80 min; 4: 530 °C, 80 min; 5: 600 °C, 80 min; 6: 600 °C, 60 min and 7: 700 °C, 60 min

Sample K (7 mol% In_2O_3) was heat treated at 590, 620 and 700 °C for 30, 20 and 60 min, respectively, in order to compare the crystallite sizes with those of sample H (5 mol% In_2O_3) (see Fig. 5.2.6). It can be seen that the non tempered sample K is amorphous (Fig. 4.3.10, curve 1). Tempering at 590 °C for 30 min resulted in broadened XRD-lines attributed to In_2O_3 and NaBO_2 (curve 2). Increasing the temperature (620 and 700 °C) leads to narrowing of the XRD-lines. This indicates that the In_2O_3 particle size increases with increasing temperature. The XRD-lines of In_2O_3 in the XRD-patterns of sample K are narrower than those of sample H. This supposes smaller In_2O_3 crystallite sizes for sample H. Parallel, the line intensities attributed to NaBO_2 are smaller than those observed in sample H (see Fig. 5.2.5). Therefore, the formed NaBO_2 quantity is supposed to be smaller than in sample H.

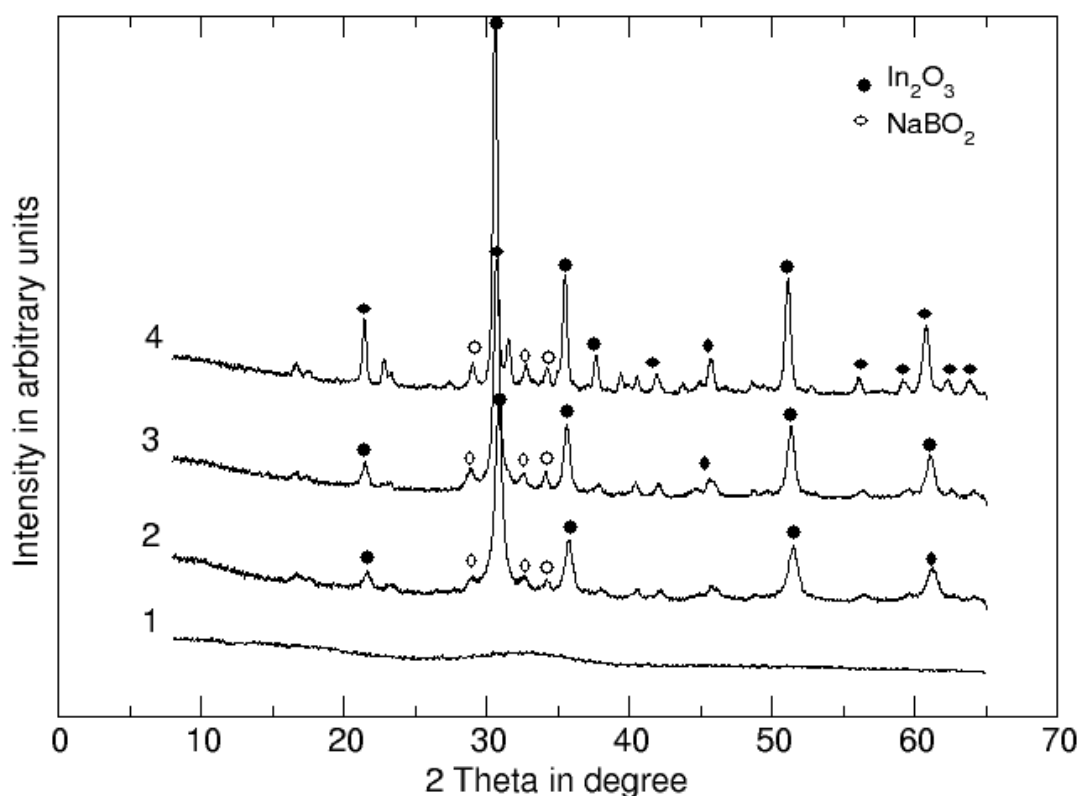


Fig. 5.2.6 XRD-patterns of sample K: 1: without thermal treatments; 2: 590 °C, 30 min; 3: 620 °C, 20 min; and 4: 700 °C, 60 min

To compare the In_2O_3 crystallite sizes for samples H (10 mol% Al_2O_3) and K (12 mol% Al_2O_3), after thermal treatment for 60 min at temperature from 560 to 700 °C, the mean

crystallite sizes have been calculated from the XRD-line broadening by Scherrer's equation. The results are plotted in Fig. 5.2.7. It can be seen that the mean crystallite sizes of both samples increase with increasing temperature. The crystallite sizes of sample H are notably smaller than those of sample K, probably due to the higher concentration of Al_2O_3 .

In summary, the sample H was chosen as optimum for the aim of the recent research work. The concentration of 5 mol% In_2O_3 is relatively high and a complete dissolution of In_2O_3 in the melt is observed. A molar ratio $[\text{Na}_2\text{O}]/[\text{B}_2\text{O}_3] = 1.125$ and an Al_2O_3 concentration of 10 mol% enabled the crystallisation of In_2O_3 with crystallite sizes in the nano-range, as already shown. Therefore, the further investigations are focused on this glass composition and relative to it as sample M.

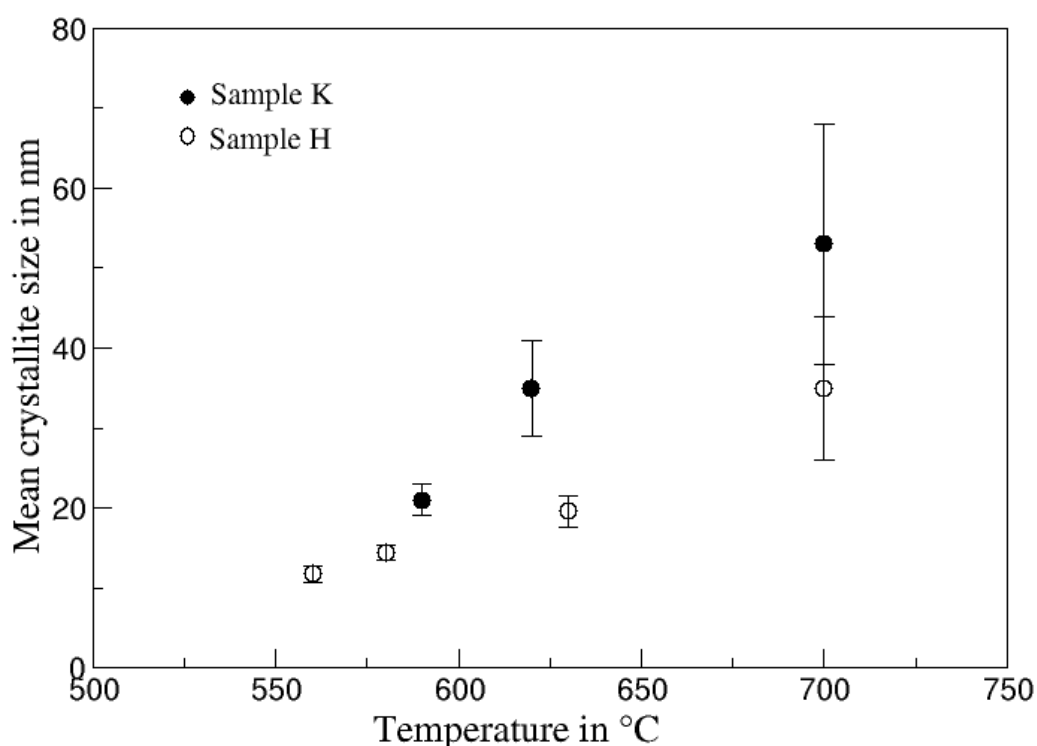


Fig. 5.2.7 Mean crystallite size of In_2O_3 in the samples H and K as a function of the temperature after tempering for 60 min.

5.3 Dissolution of the glass matrix and of non In- containing phases

The glass matrix and the non In-containing crystalline phases should be dissolved in, in order to obtain pure In_2O_3 nano-powder. For this purpose, 1 g of a powdered sample is given to 50 ml distilled water for 6 days. The obtained suspension (nano-crystals and water) is dried and the obtained powder is analysed with X-ray diffractometry.

In Fig. 5.3.1 an XRD-pattern of the powder, obtained after dissolution of sample H (tempered at 700 °C for 60 min.) in water and drying the suspension are shown. Only lines attributed to nano-crystalline In_2O_3 are observed. Using Scherrer's equation, a crystallite size of 47 nm is calculated.

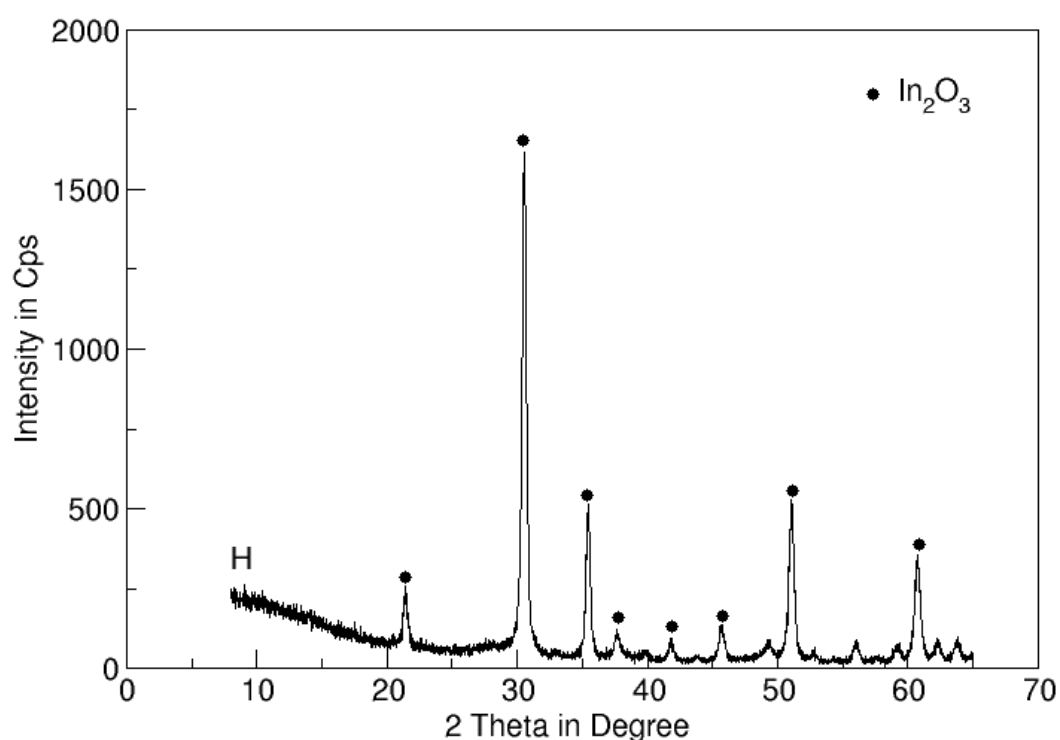


Fig. 5.3.1 XRD-pattern of the residue obtained after dissolution of the glass-ceramic of sample H (previously tempered at 700 °C for 60 min in air) in water.

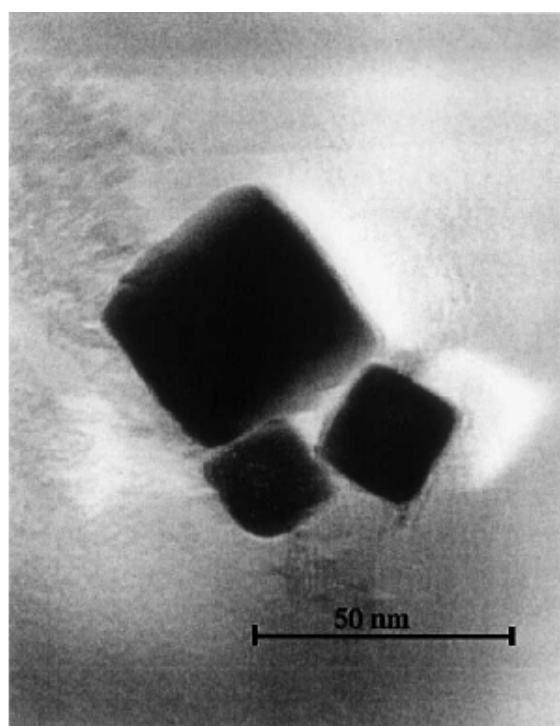


Fig. 5.3.2 TEM-micrograph of the residue obtained by dissolution the glassy phase of sample H (tempered at 700 °C for 60 min) in water.

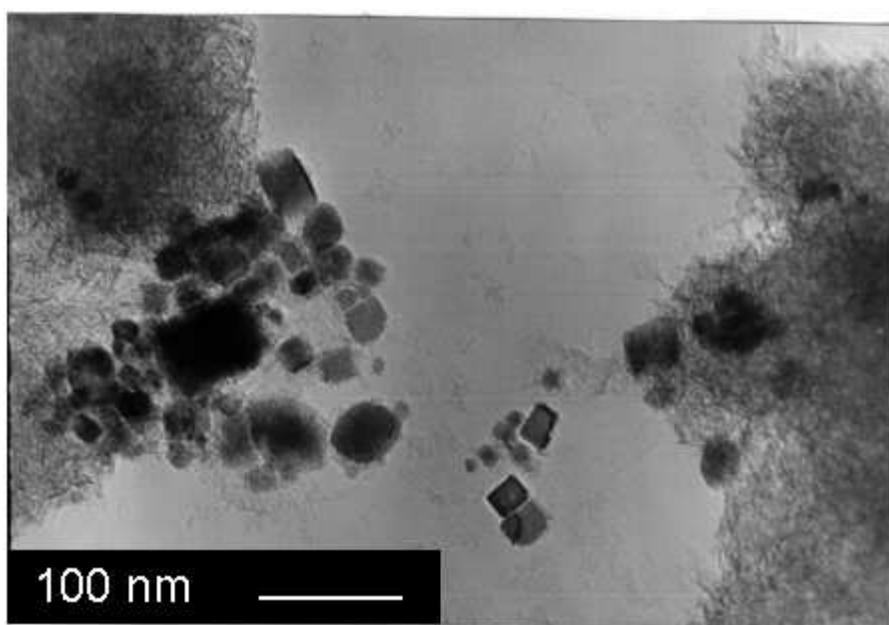


Fig. 5.3.3 TEM-micrograph of In_2O_3 nano-particles with some residual glass obtained by dissolution of the glassy phase of sample H (tempered at 700 °C) in water and separated by centrifugation.

Crystals with sizes from 30 to 50 nm are observed from the TEM micrograph of the In_2O_3 nano-particles, obtained through centrifugation from suspension (dissolution the matrix of sample H (700 °C, 60 min) in water) (see Fig. 5.3.2). Some residual glass is found in the In_2O_3 powder as seen from the TEM-micrograph in Fig. 5.3.3. The existence of a residual glass is due to incomplete dissolution of the matrix in water.

The glass-ceramics have been further dissolved in acetic acid, in order to achieve complete dissolution of the glassy phase and to obtain pure nano In_2O_3 powder. The samples have been given to 0.6N acetic acid for 1day. The formed suspension have been dried at 80 °C and the obtained powder was analysed with XRD.

5.4 Separation of In_2O_3 nano-particles

The XRD-patterns of sample H without thermal treatment, after heat treatment at 580 °C for 1 h and after dissolution in diluted acetic acid are represented in Fig. 5.4.1. The glass before heat treatment is X-ray amorphous (Curve 1) in contrast to the XRD-pattern of the sample heat treated at 580 °C for 1 h (Curve 2). The crystalline phases determined after tempering are In_2O_3 , NaBO_2 and $\text{Na}_2\text{Al}_2\text{B}_2\text{O}_7$. Curve 3 shows the XRD-patterns of the sample after dissolution in acid and after subsequent drying. The only crystalline phases detected after drying are In_2O_3 and CH_3COONa .

The In_2O_3 phase has to be separated from the acid solution, before drying. For this purpose the method of centrifugation and dialysis have been applied. The CCl_4 used by the centrifugation is toxic, therefore the dialysis method is preferred. This method is well known as appropriate for organic macromolecules separation. Dialysis is the diffusion of a solute across a selectively permeable membrane along a concentration gradient, from an area of higher solute concentration to an area of lower solute concentration. In comparison to the centrifugation, this method has the advantage to separate all In_2O_3 nano-particles from the formed salts after dissolution of the matrix.

The samples have been dialysed as described before (see paragraph 4.2) and the obtained suspension (In_2O_3 nano-crystals in water) from the dialysis tubing have been dried at 80°C. The obtained nano-powders were investigated by means of XRD, FTIR and TEM.

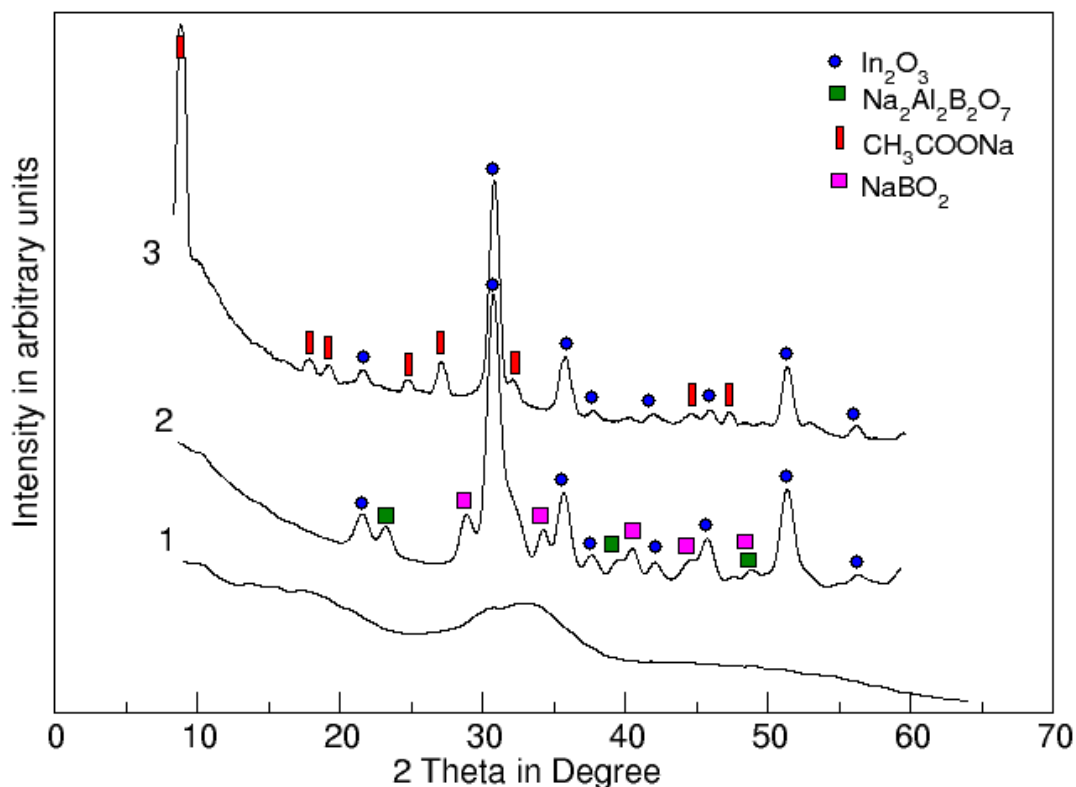


Fig. 5.4.1 XRD-patterns of sample H: 1: without thermal treatment, 2: 580 °C for 1 h, 3: after dissolution in acid

XRD-patterns of dissolved and dried sample H (580 °C, 1 h) and after dialysis are compared in Fig. 5.4.2. The lines attributable to CH_3COONa are not observed after dialysis (curve 2 compare with curve 1), only the In_2O_3 crystalline phase is detected.

The XRD method could not be used for the determination of the eventually undissolved glass matrix and/or non dialysed amorphous salts in the obtained In_2O_3 powder. Therefore, FTIR spectrometry has been carried out. Fig. 5.4.3 shows the FTIR- spectra from glasses before heat treatment, after heat treatment at 580 °C for 1 h, after dissolution of the sample and the sample after dialysis. Characteristic vibrations of borate bonds could be seen in the range from 1500 to 600 cm^{-1} [Nyg 97], [Bai 02] and other lines due to In_2O_3 in range from 500 to 200 cm^{-1} . After heat treatment the sample show sharper peaks attributed to the formation crystalline phases $\text{Na}_2\text{B}_4\text{O}_7 \cdot 5\text{H}_2\text{O}$ (1480 and 1250 cm^{-1}), $\text{Na}_2\text{Al}_2\text{B}_2\text{O}_7$ (~750 cm^{-1}) and In_2O_3 (Curve 2). Curve 3 represents the spectra of the glass-ceramics dissolved in acid, where sharp peaks at ~1620 and at ~1320 cm^{-1} are observed. They could be assigned to

CH_3COONa [Nyg 97]. As expected the sharp peaks corresponding to $\text{Na}_2\text{Al}_2\text{B}_2\text{ONa}_2$ and $\text{Na}_2\text{B}_4\text{O}_7 \cdot 5\text{H}_2\text{O}$ are not observed in that case. The characteristic vibrations of the O-H bond are observed (3400 and 1650 cm^{-1}) in all samples. The spectrum of In_2O_3 nano-powder after dialysis shows only peaks attributed to In_2O_3 ($> 500\text{ cm}^{-1}$). No borate groups are detected in the dried In_2O_3 powder after dialysis. This proves that the dialysis is a successful method for separation of nano-particles in our case.

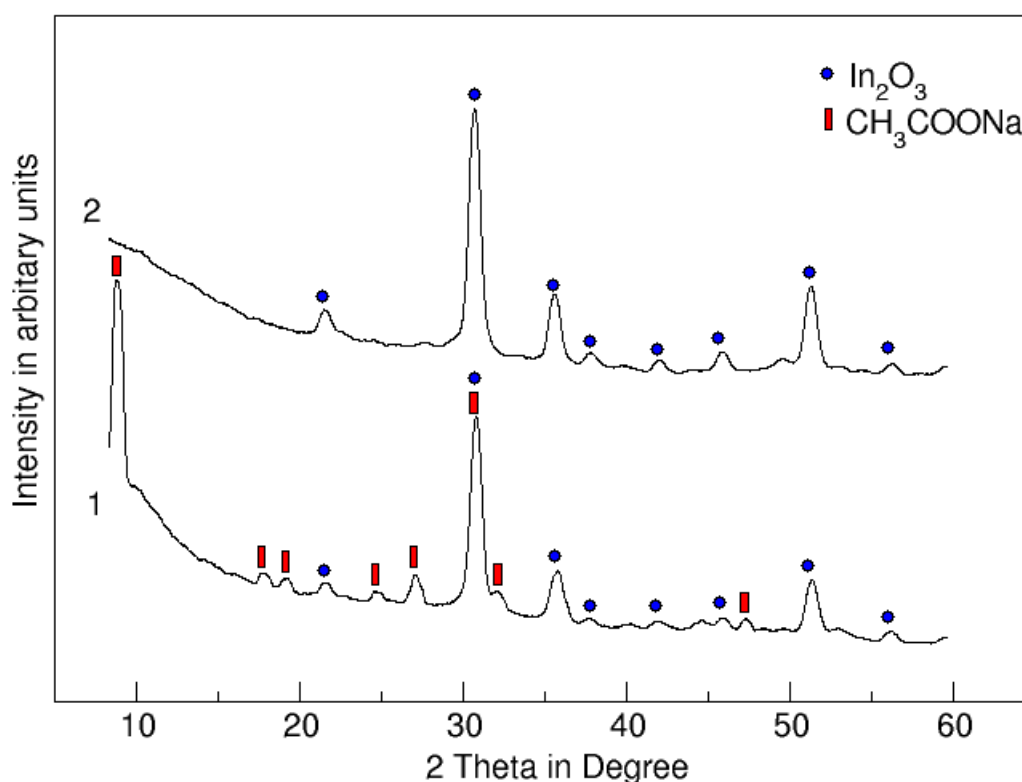


Fig. 5.4.2 XRD-patterns of sample H; 1: $580\text{ }^\circ\text{C}$, 1h, 2: after Dialysis

TEM-micrographs of the In_2O_3 nano-crystals have been taken from sample H heat treated at $580\text{ }^\circ\text{C}$ for 1h after dialysis. The average crystallite size for the sample treated at $580\text{ }^\circ\text{C}$ for 1 h in air, is $16 \pm 3\text{ nm}$, calculated by Scherrer's equation. This is in agreement with the TEM-micrographs, where crystals with an average size ~ 15 to 30 nm are observed (Fig. 5.4.4). TEM-micrographs of single In_2O_3 crystals and their size distribution are shown in Fig. 5.4.4 a and Fig. 5.4.4 b, respectively. No glass matrix is observed in the TEM- images.

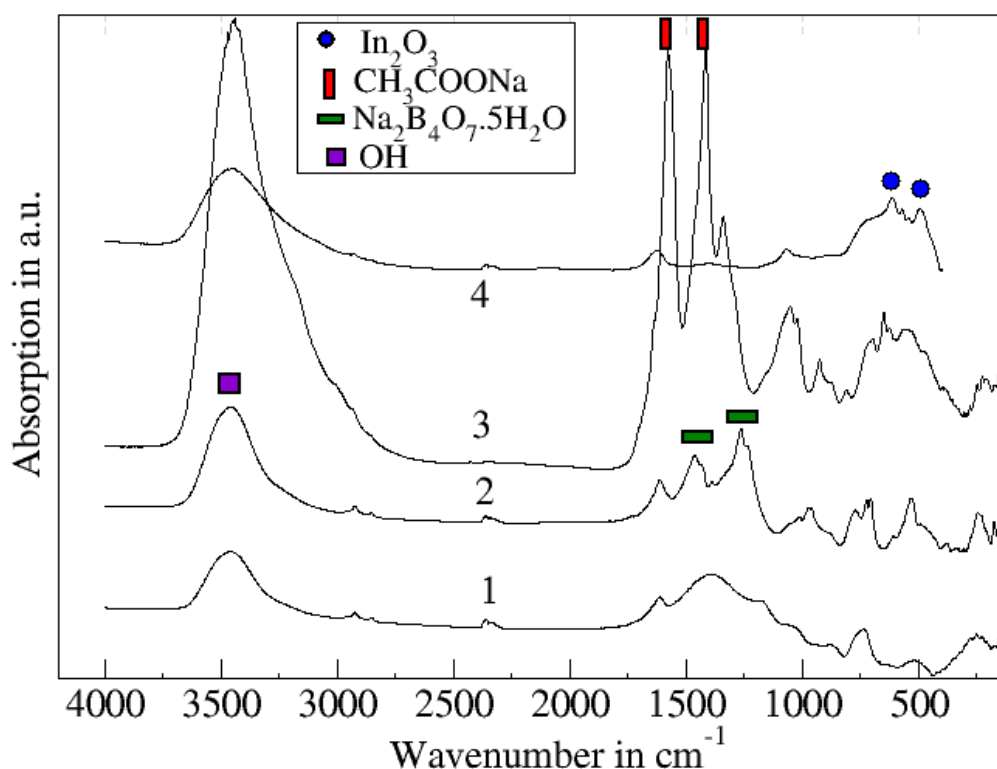


Fig.5.4.3 FTIR-Spectra from sample H; 1: without heat treatment, 2: 580 °C, 1 h, air 3: after dissolution the sample in acid, 4: after dialysis

Crystals with size of ~ 25 nm and ~ 45 nm are observed from TEM images of sample H heat treated at 630 °C and 700 °C for 1 h in air, respectively (Figs. 5.4.6 and 5.4.7). Sizes of 21 nm and 47 nm are estimated from the XRD-line broadening, which are in good agreement with the previously obtained results.

The mean crystallite size from TEM-micrographs is specified with the help of image analysing software “Optimas 6.2”. The diagonal from the particles is measured as main crystallite size in the case of cubic-shaped crystals (Fig. 5.4.5). The data have been used to create characteristic particle sizes histograms from the TEM- images of sample H heat treated in the temperature range from 580 to 700 °C as shown in Figs. 5.4.8, 5.4.9 and 5.4.10, respectively.

In summary, In_2O_3 nano-powder with adjustable mean crystal size could be produced through controlled crystallisation of In-containing borate glasses, dissolution in acetic acid and separation by dialysis.

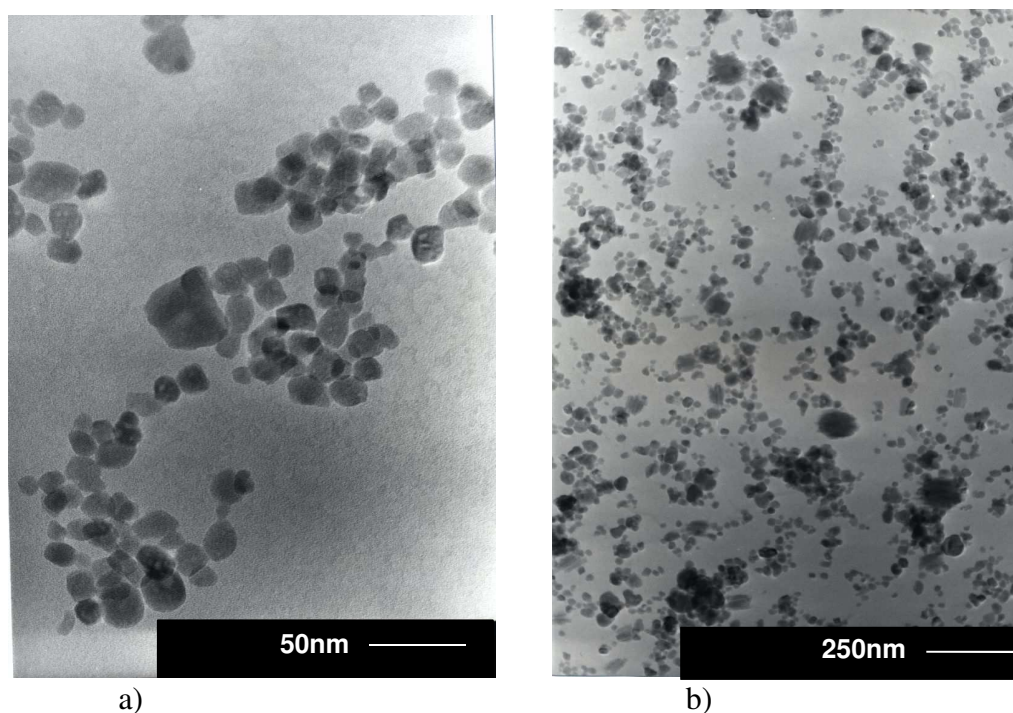


Fig. 5.4.4 TEM -micrograms from In₂O₃ nano-crystals from sample H (580 °C, 1 h, in air) after Dialysis; a) single crystals, b) distribution of the nano-crystals.

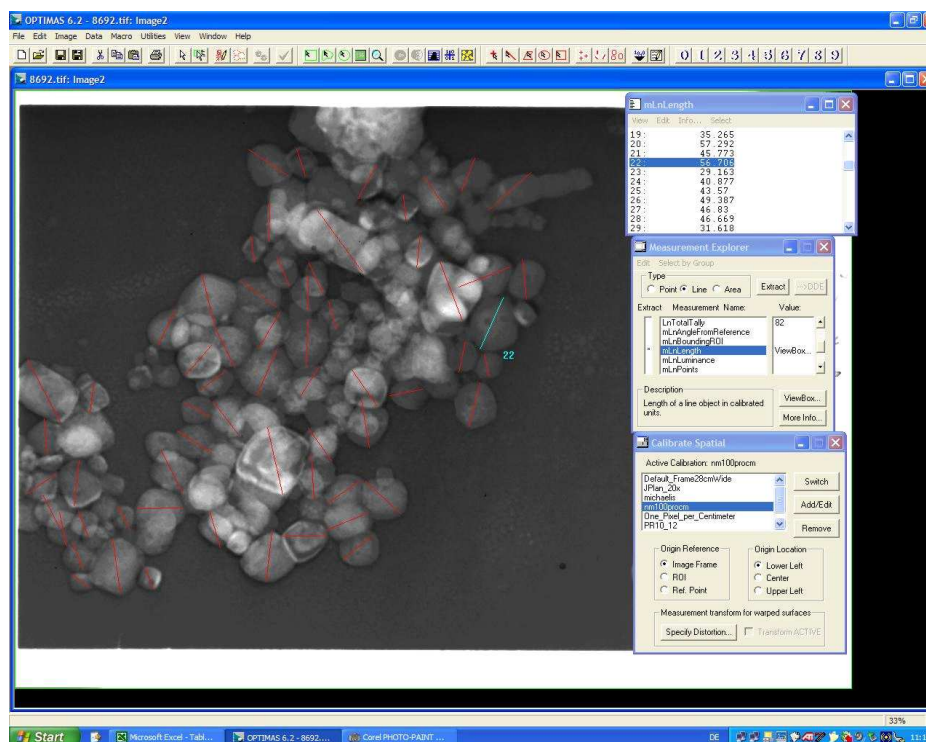


Fig. 5.4.5 Measurement of the crystalline size from In₂O₃ nanoparticles from TEM-image, Sample H (580 °C, 1 h, in air) with “Optimas 6.2” software

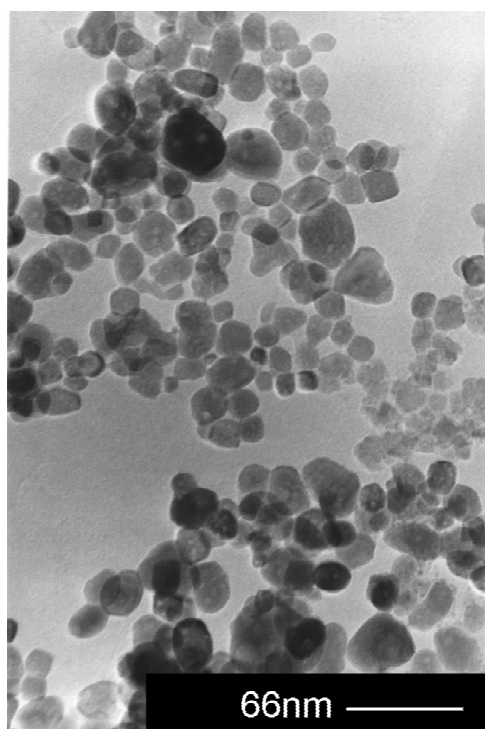


Fig. 5.4.6 TEM-image of sample H, thermal treated at 630 °C for 1 h in air

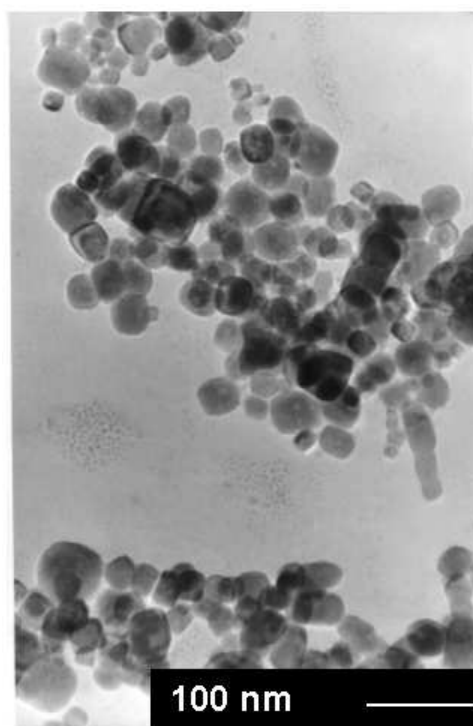


Fig. 5.4.7 TEM-image of sample H, thermal treated at 700 °C for 1 h in air

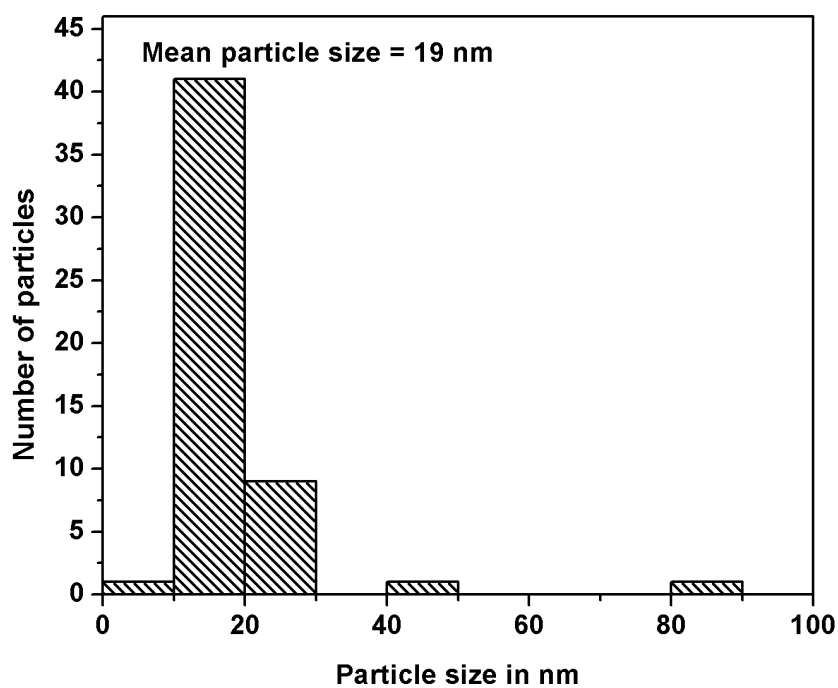


Fig. 5.4.8 Characteristic particle size histogram from TEM image of sample H (580 °C, 1 h)

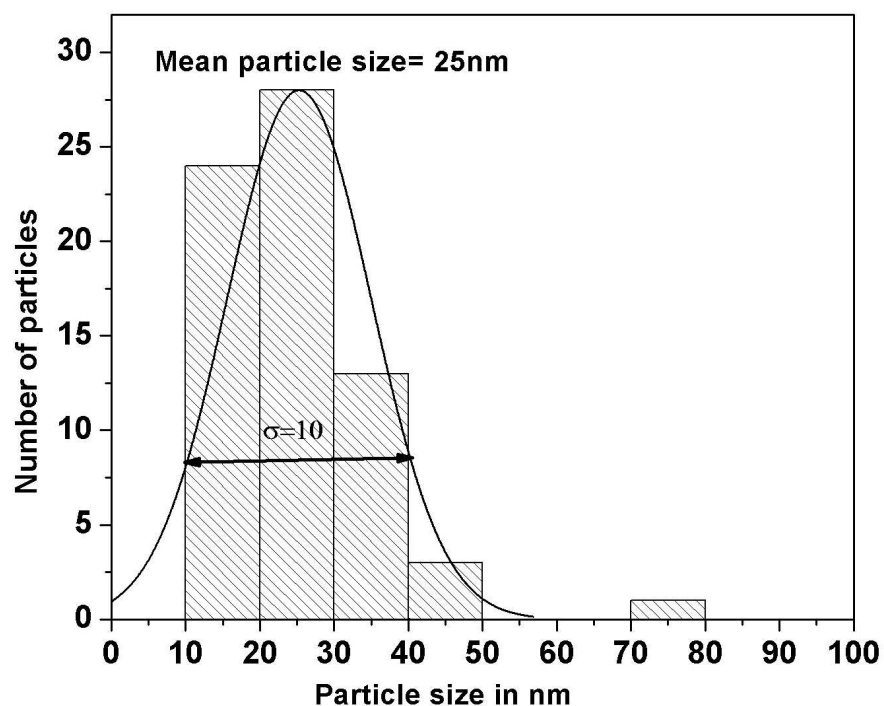


Fig. 5.4.9 Characteristic particle size histogram from TEM image of sample H (630 °C, 1 h)

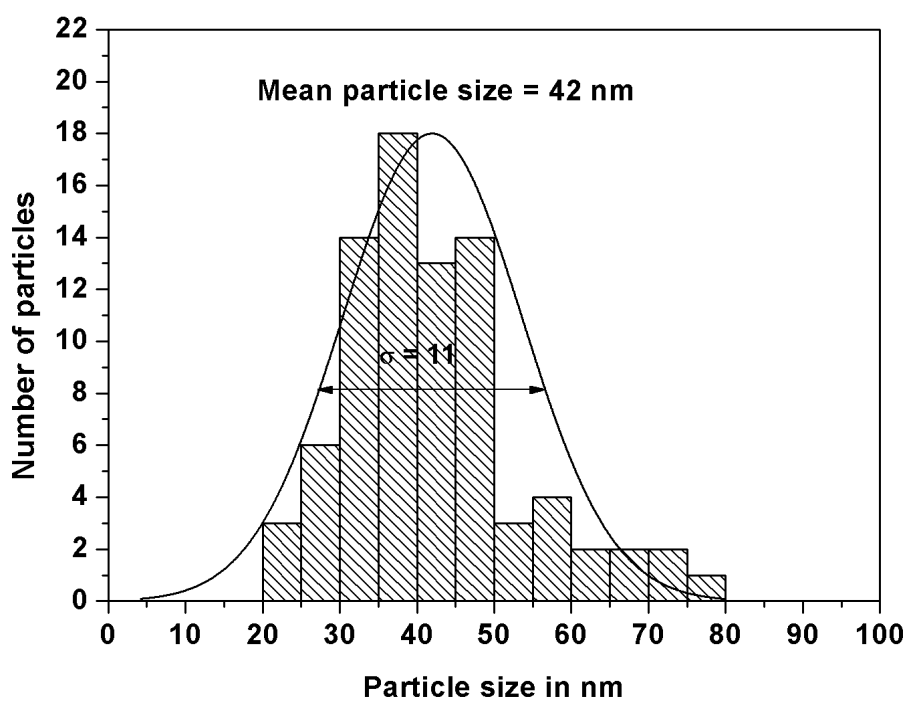


Fig. 5.4.10 Characteristic particle size histogram from TEM image of sample H (700 °C, 1 h)

5.5 Optical properties of the In_2O_3 nano-particles

One of the goals of the present work is to obtain nano-particles, which are transparent in the visible and non-transparent in the near infrared spectral region. Hence, the UV-VIS-NIR spectra of the prepared nano-powder, suspended in different matrices are studied.

5.5.1 Heat treatment in air

The In_2O_3 nano-powder obtained from sample H (580 °C, 1 h, air), have been immersed in polystyrene melt, polystyrene-chloroform solution and in paraffin oil, in order to study their optical spectra. In a first attempt, the In_2O_3 -powder have been mixed with powdered polystyrene. The prepared mixture have been heated until the polystyrene melts ($T_m = 180$ °C). The polystyrene melt, possesses high viscosity, which hinders the homogenisation of the nano-powder and results in a muddy material.

As a second step the nano-powder has been immersed in polystyrene, dissolved in chloroform. Paraffin oil has been also used as immersion liquid for the nano-powder. Figure 5.5.1 shows the optical spectra from samples with In_2O_3 nano-powder and polystyrene (curves 1 and 3) as well as a sample of In_2O_3 nano-powder in paraffin oil. The spectra 1 was recorded with air as reference and spectra 2 and 3 against reference of the respective sample (polystyrene or paraffin) to evaluate the spectra only of the nano-powder.

The studied In_2O_3 nano-particles do not have the desired non-transparency in the NIR range. This behaviour could be explained with the fact that the synthesised In_2O_3 is stoichiometric [Xir 98].

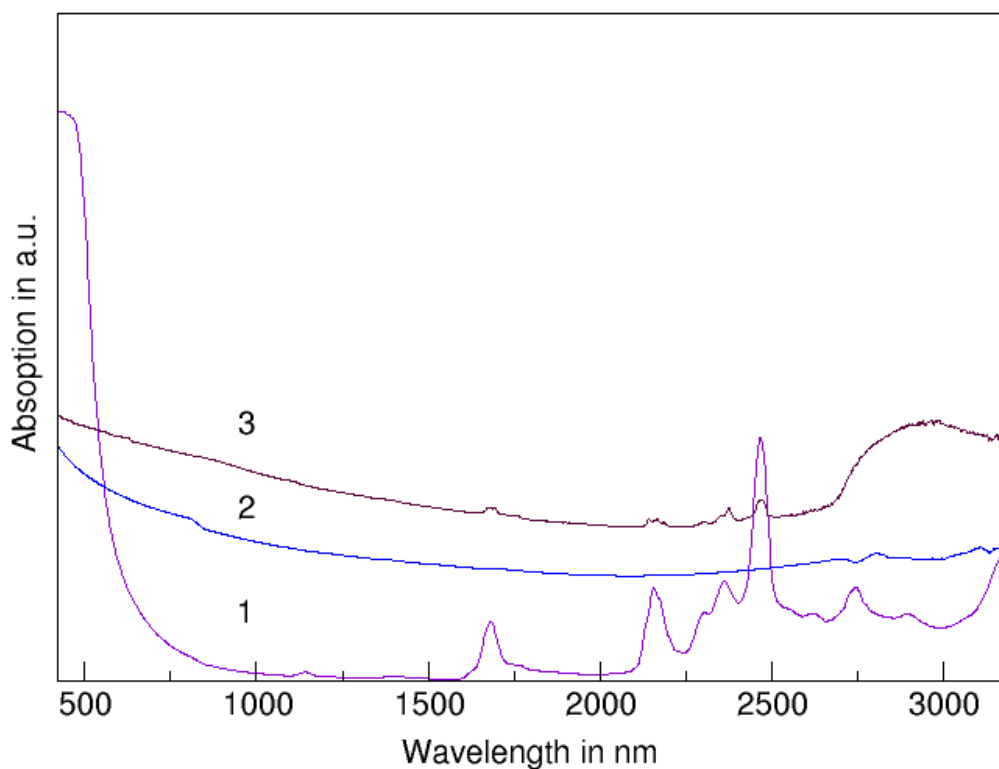


Fig. 5.5.1 Optical spectra from In₂O₃ nano-powder of sample H (580 °C, 1 h, air) in different matrices: 1: in molten polystyrene against air, 2: in paraffin oil against reference paraffin oil, 3: in polystyrene dissolved in chloroform against reference chloroform

5.5.2 Influence of the heat treatment atmosphere

According to the literature, one method to achieve non-transparency in NIR is to induce oxygen vacancies to the In₂O₃ nano-crystals is through reduction [Ede 03], [Abe 03], [Bur]. To reduce the samples H, the crystallisation have been carried out in forming gas (95 % Ar-5 %H₂). The heat treatment conditions for sample H and the formed crystalline phases are presented in Table 5.5.2

All samples crystallise during heat treatment. The samples H, heat treated in reductive atmosphere exhibit light green (540 °C, 2 h) to dark green (700 °C, 1 h) colour. In comparison, the samples H heat treated in air, possess yellow colour.

The reduction of the In_2O_3 nano-crystals with forming gas is not sufficient to obtain the desired optical properties from the spectrum from powder sample H (700 °C, 1 h, forming gas) in acid solution as seen in Fig. 5.6.4, Curve 3.

Table 5.5.2 Heat treatment conditions of sample H

T [°C]	τ [h]	Atmosphere of heat treatment	Colour of the glass-ceramic	In-containing cryst. phase
540	2	air forming gas	yellow light green	In_2O_3
540	6	air forming gas	yellow green	In_2O_3
580	1	air forming gas	yellow green	In_2O_3
700	1	air forming gas	yellow dark green	In_2O_3

5.6 Synthesis, characterisation and optical properties of $\text{In}_2\text{O}_3\text{:SnO}_2$ nano-powder

The optical properties of In_2O_3 nano-powder could be also influenced through proper additives, the most common of which is SnO_2 . Therefore, a glass composition M similar to the composition H, but with the addition of 1 mol% SnO_2 (Table 5.2.1) was studied in order to achieve oxygen deficiency in the In_2O_3 crystals and non transparency in the NIR range. The glass M was transparent and X-ray amorphous before tempering and forms coloured glass-ceramics after different thermal treatments, as shown in Table 5.6.1.

Photos from sample M heat treated at 560 °C for 6 h in air and in forming gas are shown in Fig. 5.6.1. The change in the colour of sample M depends on the heat treatment atmosphere. The heat treated sample in air exhibited yellow colouration and that heat

Table 5.6.1 Heat treatment conditions and crystalline phases of sample M

T (°C)	τ (h)	Atmosphere of heat treatment	Colour of the glass-ceramic	In-containing cryst. phases
540	2	air	dark yellow	In ₂ O ₃
		forming gas	yellow-green	In ₂ O ₃
	6	air	dark yellow	In ₂ O ₃
		forming gas	dark blue	In ₂ O ₃
580	1	forming gas	dark blue	In ₂ O ₃
700	1	air	dark yellow	In ₂ O ₃
		forming gas	dark blue	In ₂ O ₃

treated in forming gas possess dark blue colour. In both cases crystalline phases attributed to In₂O₃, NaBO₂ and Na₂Al₂B₂O₇ are observed by XRD-analysis.

In order to separate the crystals from the glass matrix and the additional non In-containing crystalline phases, the samples were soaked in 0.6N acetic acid. Figure 5.6.2 shows suspensions from powders of sample M (560 °C, 6 h, in air or in forming gas) dispersed in 0,6N CH₃COOH. The samples have been kept in the acid for 1 d and consequently dialysis has been done. In₂O₃-nano-powder have been obtained after drying the dialysed nano-crystal dispersion at 80 °C. The powder was investigated by XRD, TEM and EDX.

The XRD -patterns of the ITO-powder, obtained from sample M (700 °C, 1 h, air) and those of In₂O₃ nano-powder from sample H (700 °C, 1 h, air) are shown in Fig. 5.6.3. Notable differences between the XRD-patterns of the both powders are not observed, as expected. Only a weak shift to smaller 2 Theta is observed of the ITO powder (Curve 1) in comparison to the maximum intensity [222] peak of In₂O₃ nano-powder (Curve 2) [Nad 88], as shown in Fig. 5.6.4.

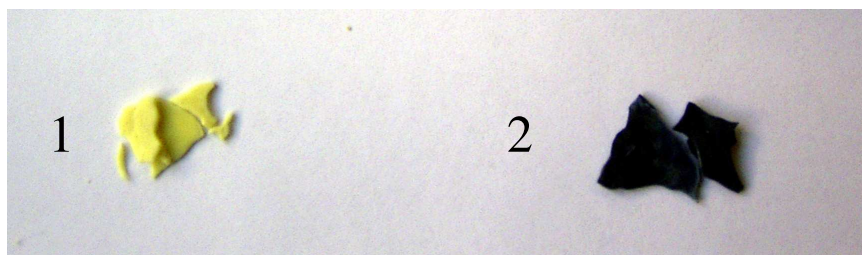


Fig. 5.6.1 Sample M heat treated at 560 °C for 6 h:
1: in air, 2: in forming gas



Fig. 5.6.2 Powders from sample M
(560 °C for 6 h) dispersed in 0,6N
CH₃COOH: 1: in air, 2: in forming gas

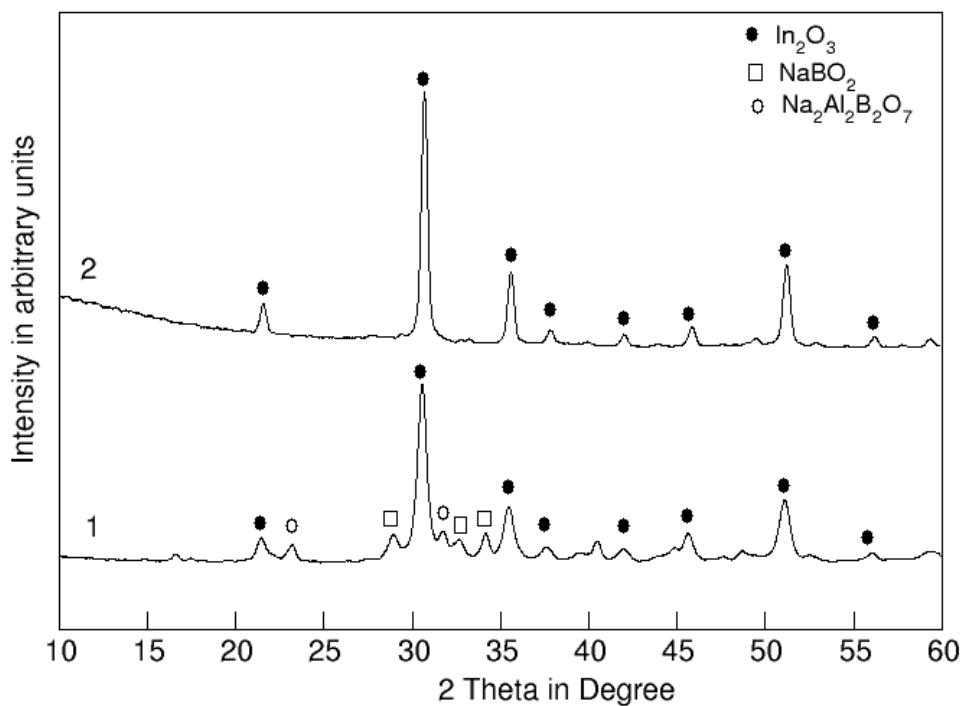


Fig. 5.6.3 XRD patterns of samples heat treated at 700 °C for 1 h in air 1: $\text{In}_2\text{O}_3\text{:SnO}_2$ from sample M and 2: In_2O_3 nano-powder from H

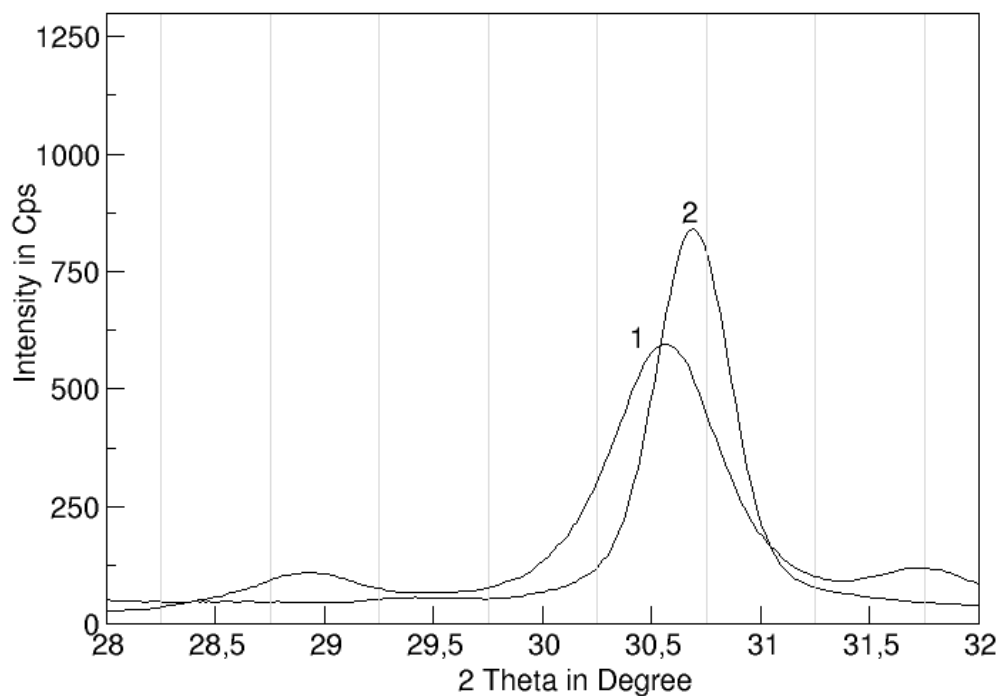


Fig. 5.6.4 XRD peak [222] of undoped and SnO_2 doped Indium oxide from samples heat treated at 700 °C for 1 h in air 1: $\text{In}_2\text{O}_3\text{:SnO}_2$ from sample M and 2: In_2O_3 nano-powder from H

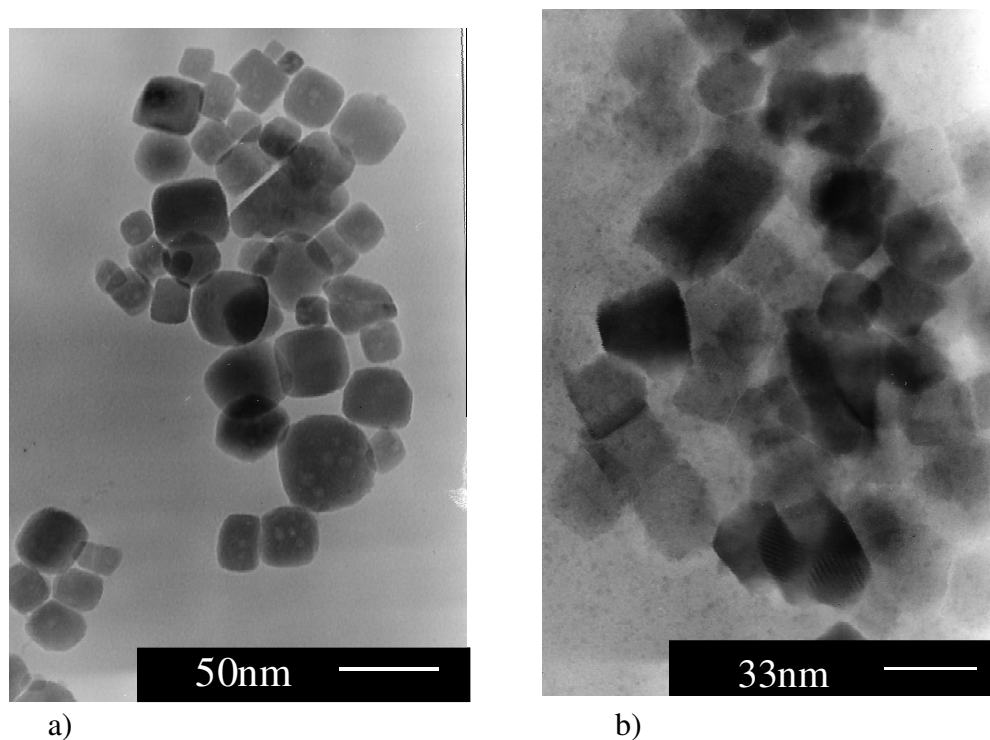


Fig 5.6.5 TEM-images of crystals from samples heat treated at 700°C, 1h in forming gas: a) sample H and b) sample M.

The In_2O_3 - and $\text{In}_2\text{O}_3\text{:SnO}_2$ -powders obtained from samples H and M, treated at 700 °C for 1 h in air are shown in the TEM-micrographs in Fig. 5.6.5 and those heat treated in forming gas in Fig. 5.6.6. A mean crystallite size of ~ 40 nm is observed for the In_2O_3 nano-crystals (Fig. 5.6.5 a) and those of $\text{In}_2\text{O}_3\text{:SnO}_2$ possess sizes of ~25 nm (Fig. 5.6.5 b). The smaller particle sizes in the case of SnO_2 doping could be based on Sn inhibition of the In_2O_3 crystallisation. Heat treatment of both samples H and M in forming gas leads to the formation of crystals with a mean size of 25 nm (Fig. 5.6.6 a and 5.6.6 b).

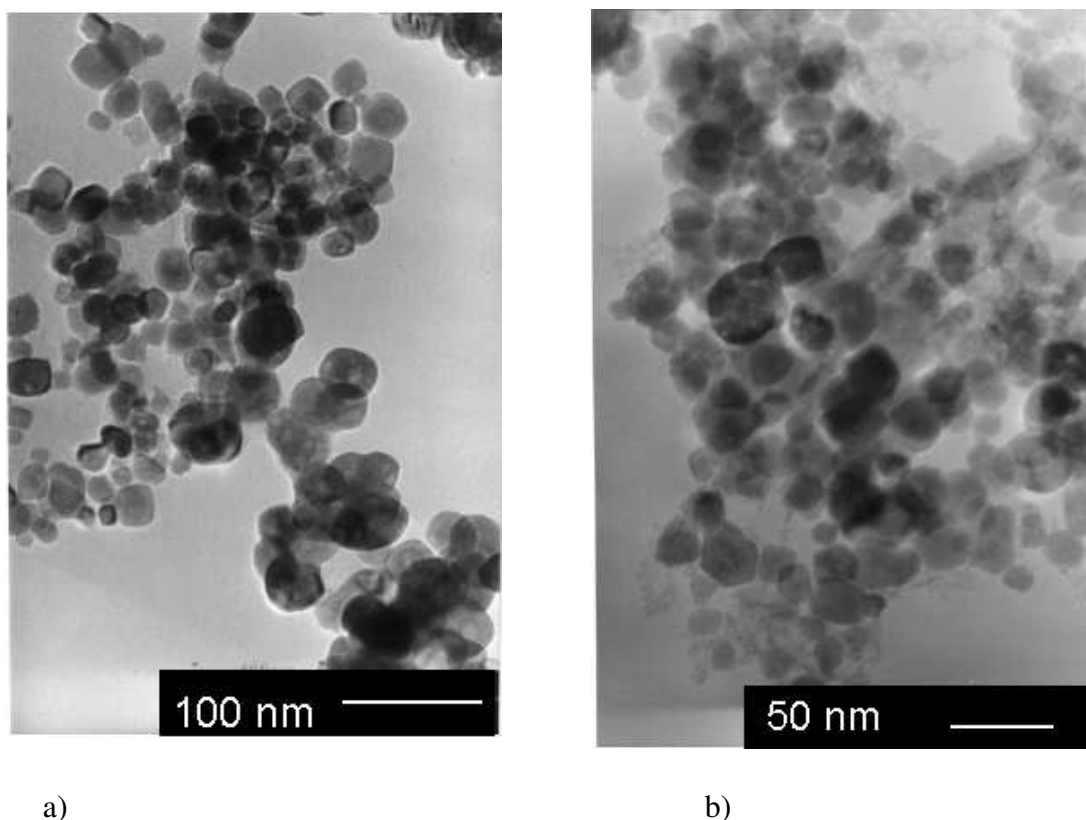


Fig. 5.6.6 TEM-images of crystals from samples heat treated at 700 °C, 1 h in air
a) In_2O_3 nano-crystals from sample H. and b) $\text{In}_2\text{O}_3:\text{SnO}_2$ nano-crystals from sample M

In order to determine if there is an incorporation of tin in the In_2O_3 crystals, energy dispersed X-ray analysis have been carried out.

In Fig. 5.6.7 an EDX analysis from one nano crystal, obtained from sample M (700 °C, 1 h) is shown. Signals attributed to In and Sn are detected as well as Cu from the sample holder (Cu-nets). This result proves the incorporation of Sn in the In_2O_3 crystal lattice as already reported [Qua 98], [Free 00].

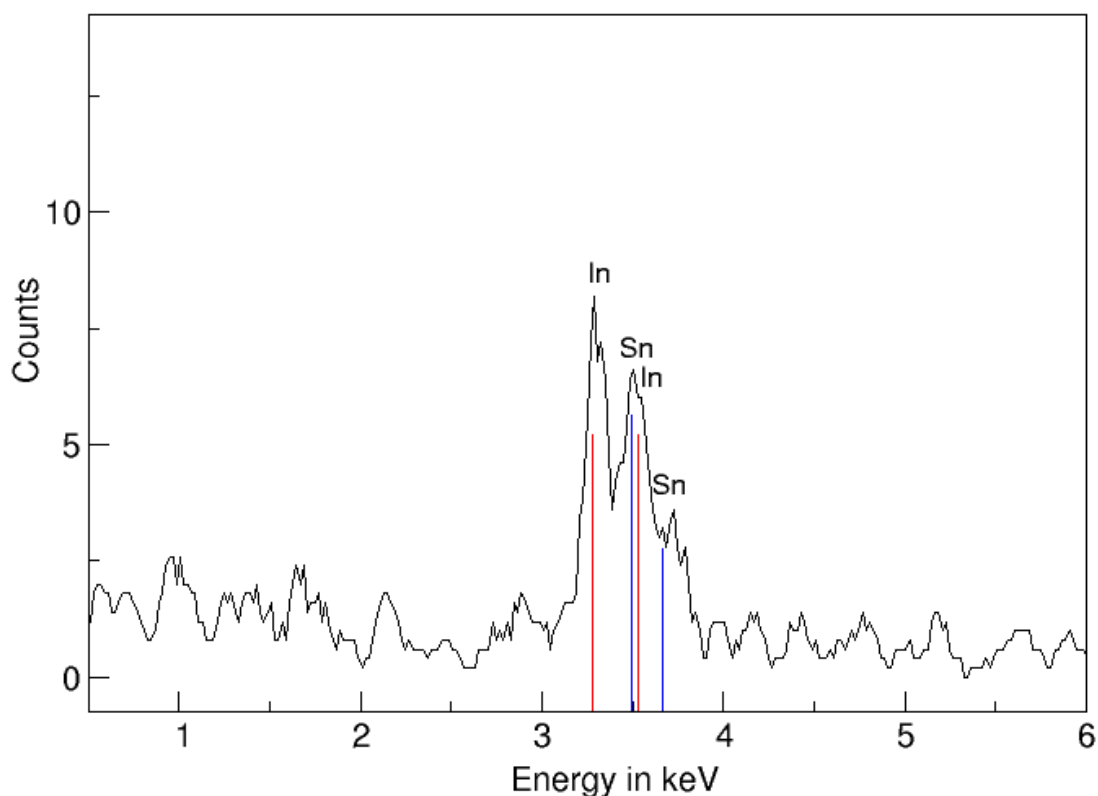


Fig. 5.6.7 EDX analysis of nano-crystal from sample M (700 °C, 1 h, forming gas)

One of the aim of the work is to achieve non-transparency in the NIR range through nano-powders. According to this, UV-VIS-NIR measurements of In_2O_3 - and ITO nano-powders have been carried out. For this purpose, suspensions of the powders from sample H and M heat treated at 700 °C for 1 h in air or in forming gas and acetic acid solution have been studied. The spectra have been recorded against acetic acid solution as reference (Fig. 5.6.8). Samples M ($\text{In}_2\text{O}_3\text{:SnO}_2$) and H (In_2O_3) heat treated in air show no absorption at wavelengths between 800 and 1500 nm (Line 2 and 4), as well as by heat treatment in forming gas (see sample H (Line 3)). By contrast, sample M heated in forming gas shows an increase in the absorption (Line 1) and the desired NIR cut-off.

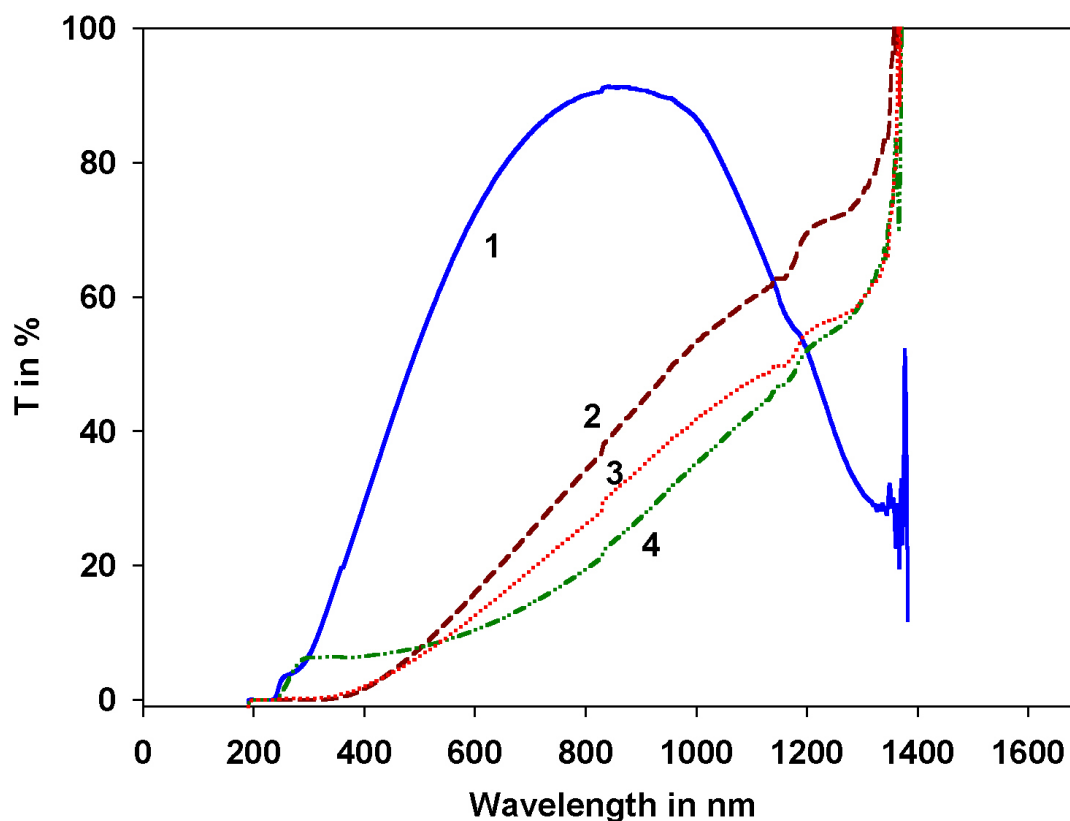


Fig. 5.6.8 Transmission spectra from sample: heat treated at 700 °C, 1 h, acetic acid solution: 1: powder from sample M (in forming gas); 2: powder from sample M (air); 3: powder from sample H (in forming gas); 4: powder from sample H (air)

For comparison in Fig. 5.6.9 the transmissions spectra of ITO nano-powder from the dialysed sample M (540 °C, 6h) in water and that of a commercial ITO nano-powder dispersed in polystyrene matrix are presented. A transmission of 72 % and 58 % at 300 to 1000 nm is recorded for powder sample M and the industry sample, respectively. The behaviour of the two curves is identical. Both samples exhibit an NIR-cut-off (see the right shoulder of the curve).

In summary, the desired non-transparency in NIR range could be achieved through combination of Sn-doping and heat treatment in reducing atmosphere of In_2O_3 -containing glasses.

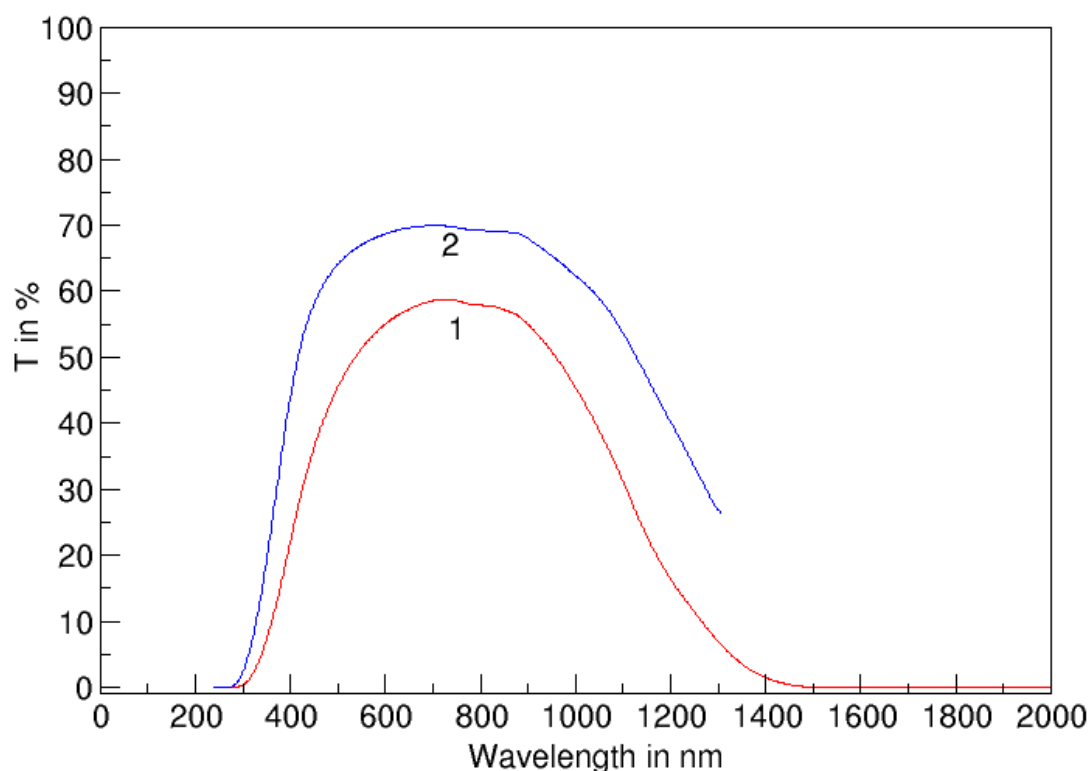


Fig. 5.6.9 UV-VIS Spectra: 1: industrial sample with In_2O_3 - nano-crystals in polystyrene, 2: $\text{In}_2\text{O}_3\text{:SnO}_2$ - nano-crystals in water (dialysed sample M, 540 °C, 6 h in forming gas)

5.7 Synthesis of SnO_2 nano-powder

5.7.1 Choice of the glass system

Glass compositions in the system $\text{B}_2\text{O}_3 \cdot \text{Na}_2\text{O} \cdot \text{Al}_2\text{O}_3 \cdot \text{SnO}_2$ were studied in order to obtain SnO_2 nano-powder. The system is chosen in similarity to that from which In_2O_3 and $\text{In}_2\text{O}_3\text{:SnO}_2$ nano powders were successfully obtained.

The starting glass composition R34 is similar to sample H, where 5 mol% In_2O_3 are substituted against 5 mol% SnO_2 . The prepared glass compositions are summarized in Tab. 4.5.1. To study the influence of $[\text{Na}_2\text{O}]/[\text{B}_2\text{O}_3]$ molar ration upon the crystallisation of SnO_2 , series of glass compositions have been investigated. To achieve large amounts of crystalline SnO_2 after thermal treatment, the glass compositions should contain a maximum tin concentration.

Therefore, sample compositions with SnO_2 concentration from 4.5 to 12 mol% have been melted. Compositions with more than 10 mol% SnO_2 could not be transferred in homogeneous melts at temperatures $\leq 1300^\circ\text{C}$.

The influence of the SnO_2 crystallisation from the Al_2O_3 concentration has been investigated. In the case of In_2O_3 nano-crystallisation, Al_2O_3 have played a key role (see Chapter 5.2). Therefore sample composition with Al_2O_3 concentration from 0 to 10.47 have been studied (Table 5.7.1).

Table 5.7.1 Glass compositions by synthesis in mol%, * spontaneous crystallisation

Sample	$[\text{B}_2\text{O}_3]$	$[\text{Na}_2\text{O}]$	$[\text{Al}_2\text{O}_3]$	$[\text{SnO}_2]$	$[\text{Sb}_2\text{O}_3]$	$[\text{Na}_2\text{O}]/[\text{B}_2\text{O}_3]$	Sn-containing crystalline phase
R44	31.4	54.1	9,5	5	--	1,723	Na_2SnO_3
R30	40.2	55.3	-	4,5	--	1,38	Na_2SnO_3 *
R33	39.1	44	9,8	7,1	--	1,125	$\text{Na}_2\text{Sn}_2\text{O}_5$
R34	40	45	10	5	--	1,125	$\text{Na}_2\text{Sn}_2\text{O}_5$
R29	40.2	45.2	10,1	4,5	--	1,125	$\text{Na}_2\text{Sn}_2\text{O}_5$
R35	37.9	42.6	9,5	10	--	1,125	$\text{Na}_2\text{Sn}_2\text{O}_5$
R36	37	41.7	9,3	12	--	1,125	SnO_2
R37	42.2	47.5	5	5,3	--	1,125	SnO_2
R39	40.2	40.2	9,5	10,1	--	1,0	SnO_2
R40	42	38.4	9,5	10,1	--	0,914	SnO_2
R42	50.6	44.9	-	4,5	--	0,887	SnO_2
R51	46	40	7	7	--	0,869	SnO_2
R47	53	31	9	7	--	0,585	SnO_2
R45	54.1	31.4	9,5	5	--	0,580	SnO_2
R52	65.3	23,7	5	5	1	0,363	SnO_2
R55	65	24,6	5	5	0,4	0,378	SnO_2
R49	66.5	19	9,5	5	--	0,286	SnO_2 *

5.7.2 Melting procedure

5.7.2.1 SnO₂ raw material

SnO₂ raw material has a low dissolution rate in the borate melts. In our compositions, SnO₂ in high concentration, more than 4.5 mol %, was not completely dissolved and was found as a residue at the bottom of the crucible, and in the glass. SEM-images of residual SnO₂ crystals with a size of around 30 μm are observed in glass sample R40 (Fig. 5.7.1). Residual SnO₂ crystals are also found after heat treatment of the sample. (Fig. 5.7.2)

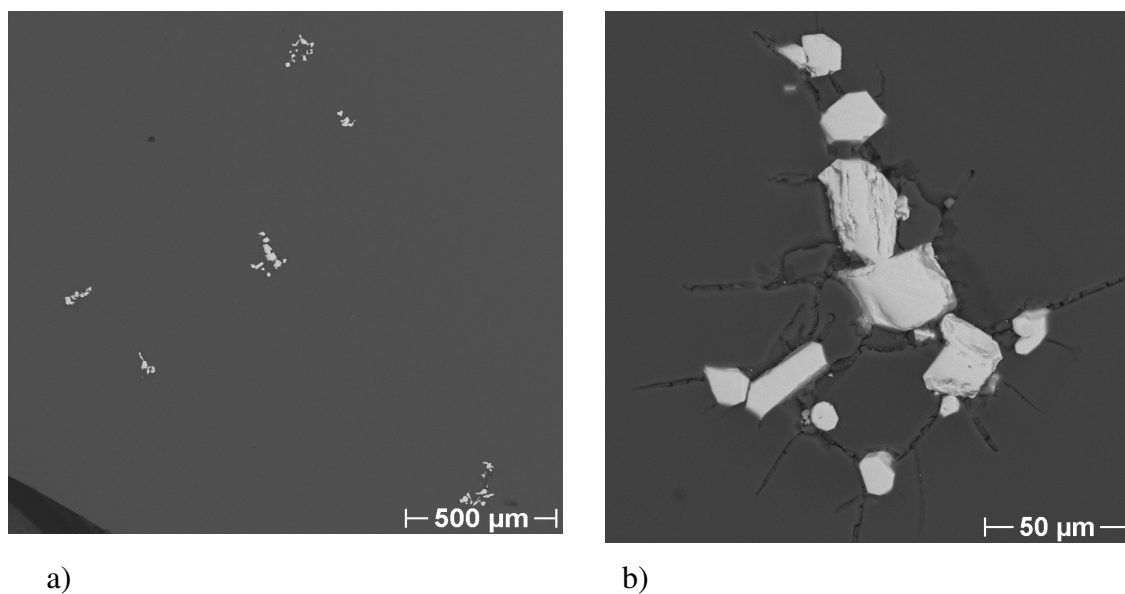


Fig. 5.7.1 SEM-images from the residual SnO₂ crystals in glass sample R40: a) distribution of the crystals in the sample, b) SnO₂ crystals

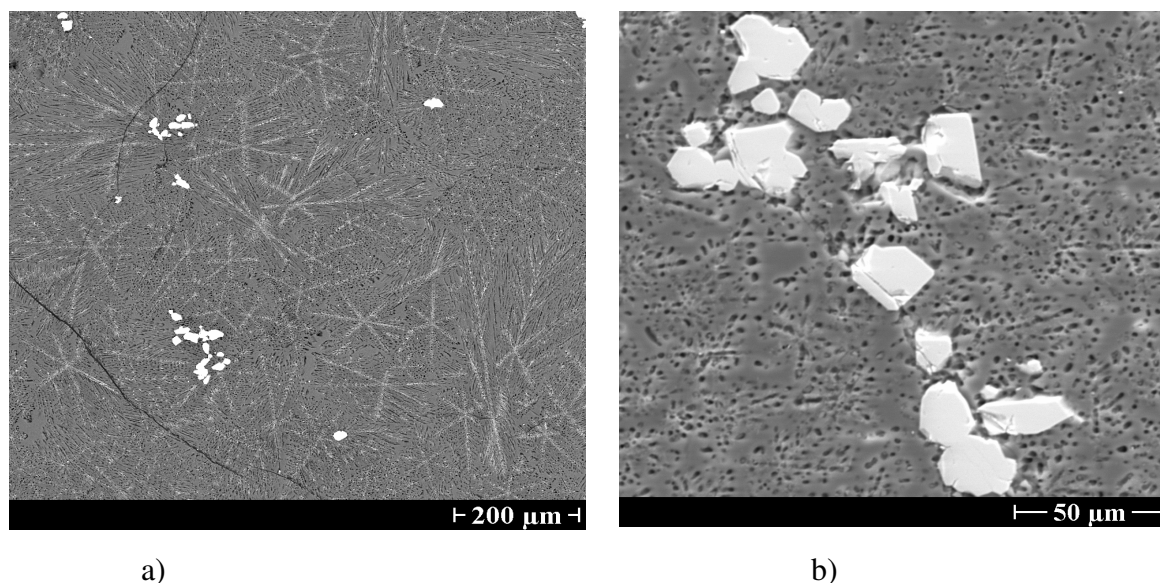


Fig. 5.7.2 SEM-images from the residue of SnO_2 crystals in sample R40, after heat treatment: a) distribution of the crystals in the sample, b) SnO_2 crystals

One possible reason for slow dissolution of the SnO_2 raw material in the borate melts, is as follows: The borate glasses have a low temperature of melting in comparison to SnO_2 (1630 °C). Reaching the liquidus temperature of the raw materials, except of SnO_2 , the viscosity of the melt drops rapidly. In this case, due to the high density of SnO_2 crystals (7020 kg.m^{-3}), they sediment on the bottom of the crucible. Hence, the surface contact between the melt and the SnO_2 raw material is not enough for its fast dissolution.

5.7.2.2 Complete dissolution of SnO_2 in the melt

To achieve a complete dissolution of the SnO_2 raw material in the melt, fine dispersed powder have been prepared by a wet chemical method. In this case, the SnO_2 crystals (raw material) are much smaller than the commercial ones. The surface of the crystals will be surrounded by the melt and thus could affect the SnO_2 -dissolution kinetics.

The fine dispersed SnO_2 raw material have been prepared by a wet chemical method from the precursor $\text{SnCl}_2 \cdot 2\text{H}_2\text{O}$, H_2O_2 , NH_3OH and dist. H_2O . They have been mixed and the product from the reaction was dried at 40 °C. The product was analysed with XRD. The

crystalline phase detected is attributed to NH_4Cl (Fig. 5.7.3, Curve 1).

Consequently the dried powder have been heat treated at $500\text{ }^\circ\text{C}$ for 1 h, in order to obtain fine dispersed crystalline SnO_2 . The X-ray diffractogram determines patterns attributed only to SnO_2 (Curve 2). The characteristic SnO_2 peaks are much broader than those of the commercial SnO_2 raw material (Curve 3). The morphology of the SnO_2 raw material obtained through wet chemical synthesis, can be seen on the TEM-micrographs in Fig. 5.7.4. Needle-like crystals, possessing lengths from 20 to 600 nm are observed.

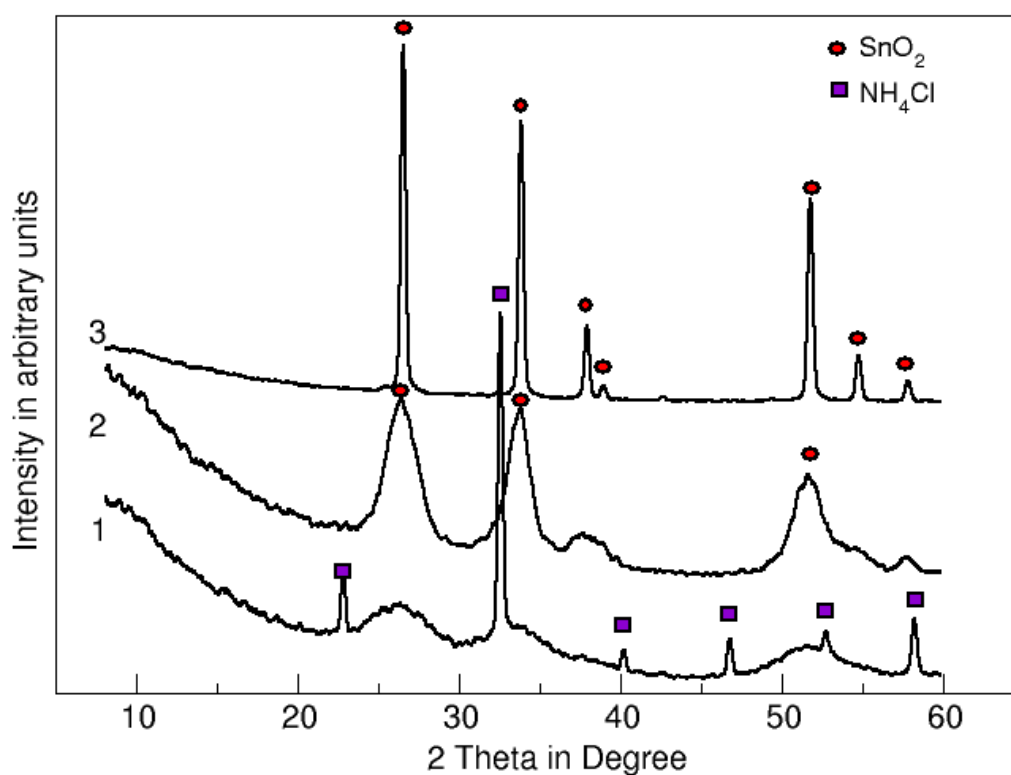


Fig. 5.7.3 XRD patterns from products of the wet chemical synthesis: 1 after drying at $40\text{ }^\circ\text{C}$, 2: after thermal treatment at $500\text{ }^\circ\text{C}$ for 1 h, 3: SnO_2 commercial raw material

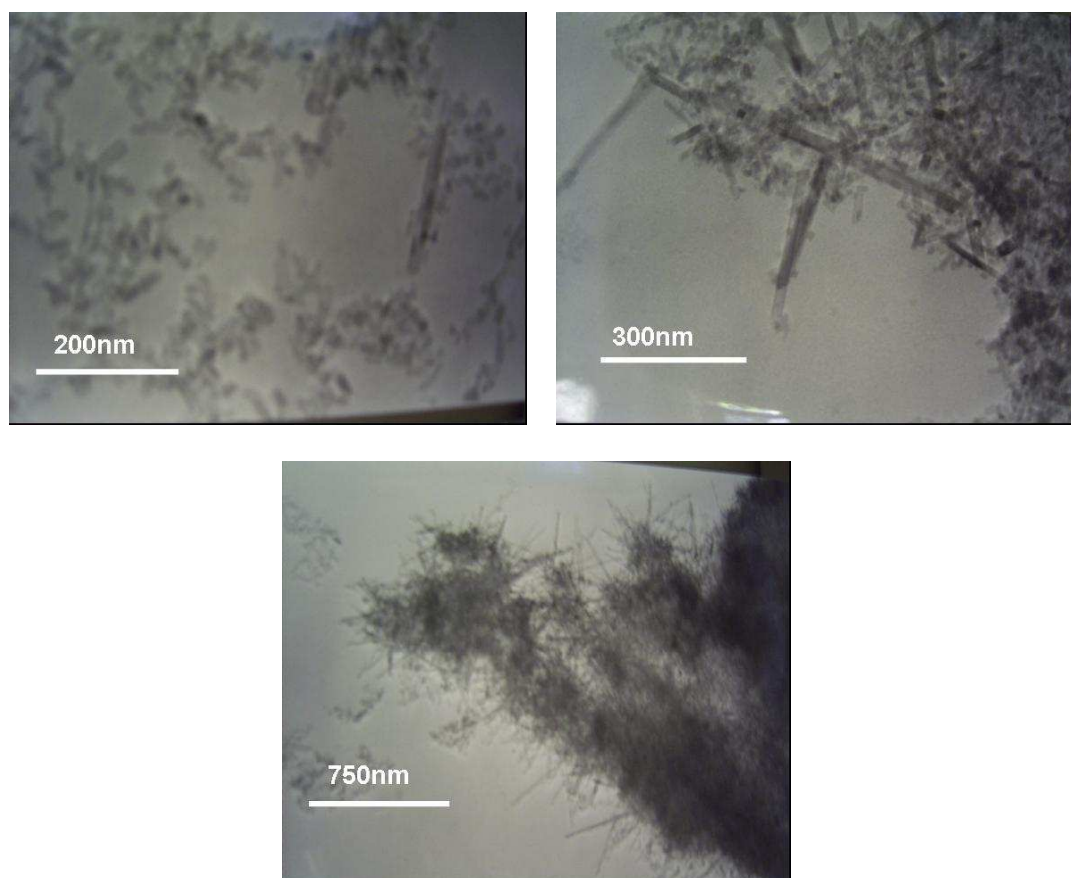


Fig. 5.7.4 TEM – micrographs of SnO₂-crystals prepared by wet chemical synthesis

Another factor, which affects the dissolution as a kinetic process is the time for contact of the raw material crystals with the melt. Also by keeping higher viscosity of the melt, using lower temperatures, it could be avoid the SnO₂ crystals to sediment. According to this, two steps melting process have been carried out. The samples were hold at temperatures in the range from 800 to 900 °C for 8 to 20 h (depending on the composition) and consequently melted at 1300 °C for 30 min.

Homogeneous glasses have been obtained (see Table 5.7.1), where the whole amount of SnO₂ was dissolved. The complete dissolution of SnO₂ in the melt is achieved by using the combination of fine dispersed SnO₂ raw material and a two step melting procedure.

5.7.3 Glass samples thermal treatment

The quenched glass samples have been heat treated in air at temperatures in the range from 500 to 820 °C for 0.5 to 16 h.

In Fig. 5.7.5 the XRD-patterns of sample R34 after quenching (Curve 1) and after tempering at 700 °C for 2 h (Curve 2) are presented. After quenching the sample is X-ray amorphous and after tempering, lines attributed to $\text{Na}_2\text{Sn}_2\text{O}_5$, NaBO_2 and $\text{Na}_2\text{Al}_2\text{B}_2\text{O}_7$ (Curve 2) are detected.

To avoid the $\text{Na}_2\text{Sn}_2\text{O}_5$ crystallisation, the glass compositions with decreasing Na_2O - and increasing B_2O_3 - concentration, i.e. with smaller molar ratio $[\text{Na}_2\text{O}]/[\text{B}_2\text{O}_3]$ have been prepared. Figure 5.7.6 shows XRD-patterns of samples R30 (curve 1), R35 (curve 2) and R39 (curve 3). XRD-lines attributable to SnO_2 , NaBO_2 and $\text{Na}_2\text{Al}_2\text{B}_2\text{O}_7$ are observed. By contrast, the patterns of sample R30 do not exhibit lines due to SnO_2 . The lines shown belong to NaBO_2 and Na_2SnO_3 . Low intensity lines of $\text{NaBO}_2 \cdot 2\text{H}_2\text{O}$ are additionally seen. In the pattern of sample R35, lines due to NaBO_2 , $\text{Na}_2\text{Al}_2\text{B}_2\text{O}_7$ and $\text{Na}_2\text{Sn}_2\text{O}_5$ are observed. By analogy, the patterns of samples R33 and R29 show lines attributable to $\text{Na}_2\text{Sn}_2\text{O}_5$, while in that of sample R44, lines caused by Na_2SnO_3 are observed.

Figure 5.7.7 shows XRD-patterns of sample R40 after thermal treatment at 650 °C for 60 min (see curve 2) and 670 °C for 80 min (see curve 3). Both patterns show lines attributed to crystalline SnO_2 (cassiterite) and furthermore lines due to NaBO_2 and $\text{Na}_2\text{Al}_2\text{B}_2\text{O}_7$. The patterns of sample R40 has approximately the same shape as that of sample R39. Lines attributed to SnO_2 are also seen in the patterns of sample R39, R42, R47, R45 and R52. In all these samples the molar ratio $[\text{B}_2\text{O}_3]/[\text{Na}_2\text{O}]$ has a value ≤ 1.125 . This means that the ratio $[\text{B}_2\text{O}_3]/[\text{Na}_2\text{O}] \leq 1$ favours the SnO_2 crystallisation from the studied borate glasses.

The Al_2O_3 has a main role in the controlled In_2O_3 crystallisation, as already reported. To study the dependence of the SnO_2 crystallisation from the Al_2O_3 concentration, the aluminium oxide free samples R42 and R30 have been prepared and compared with sample R40 containing 10 mol% Al_2O_3 . Figure 5.7.8 presents XRD-patterns of sample R42, after quenching and after thermal treatment. After casting, the sample is amorphous

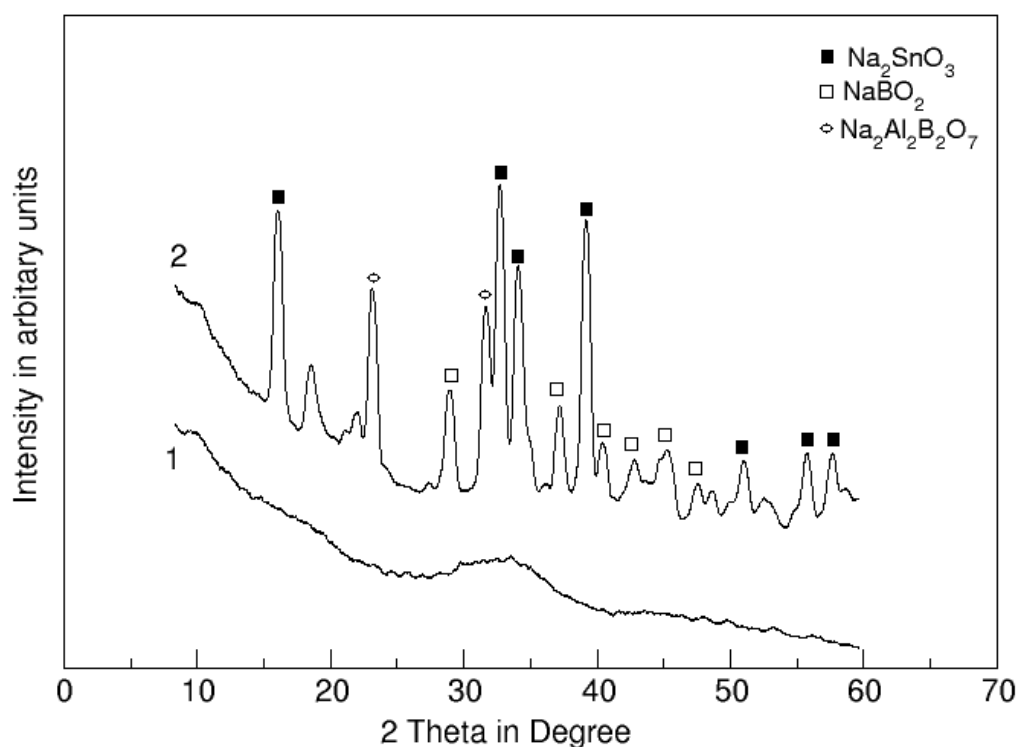


Fig. 5.7.5 XRD-patterns of sample R34: 1: without thermal treatment, 2: after thermal treatment at 700 °C for 2 h

(curve 1). This is in contrast to Fig. 5.7.6 (sample R30), where spontaneous crystallisation of Na_2SnO_3 occurs. Thermal treatment at 580 °C for 4 h (see curve 2) results in distinct notably broadened lines, all attributed to NaBO_2 . Lines caused by SnO_2 are observed after tempering at 650 °C for 4 h (see curve 3).

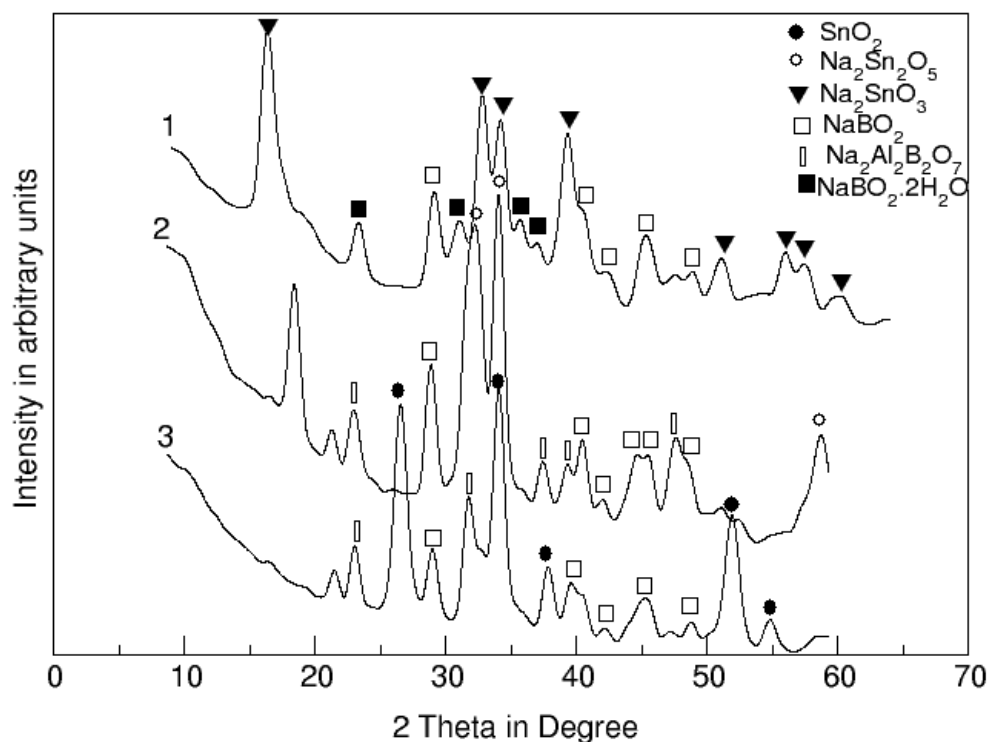


Fig 5.7.6 XRD-patterns of samples: 1: sample R30,
2: sample R35 (650 °C, 60 min), 3: sample R39 (650 °C, 60 min)

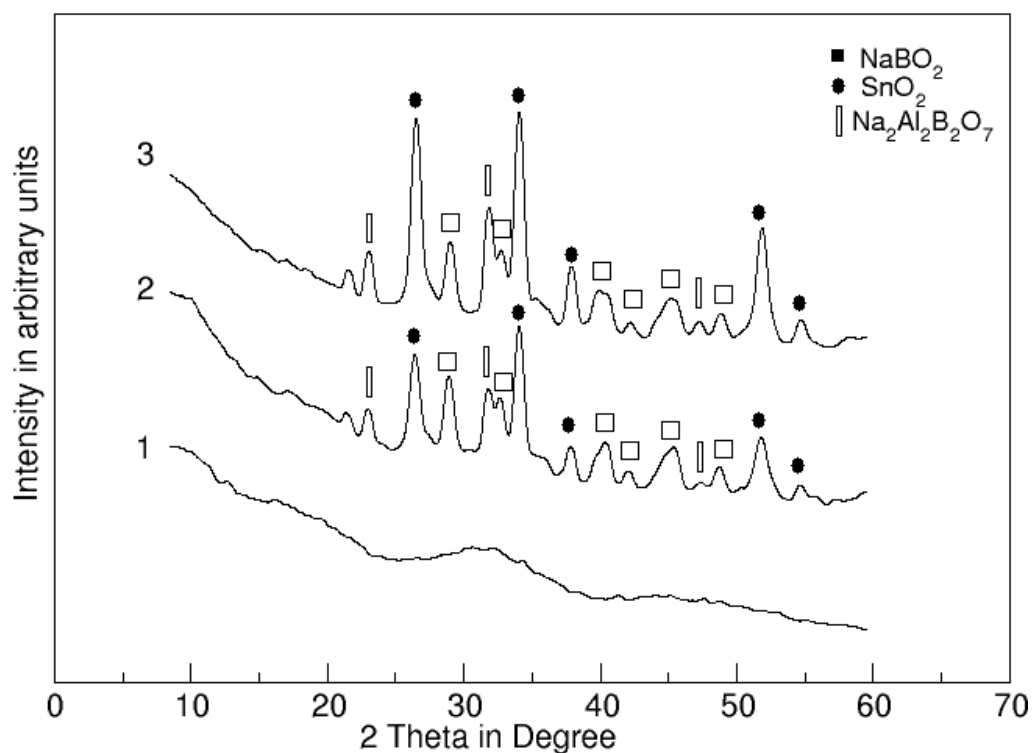


Fig. 5.7.7 XRD-patterns of sample R40; 1: without thermal treatment,
2: after thermal treatment at 650 °C for 60 min and 3: at 670 °C for 80 min.

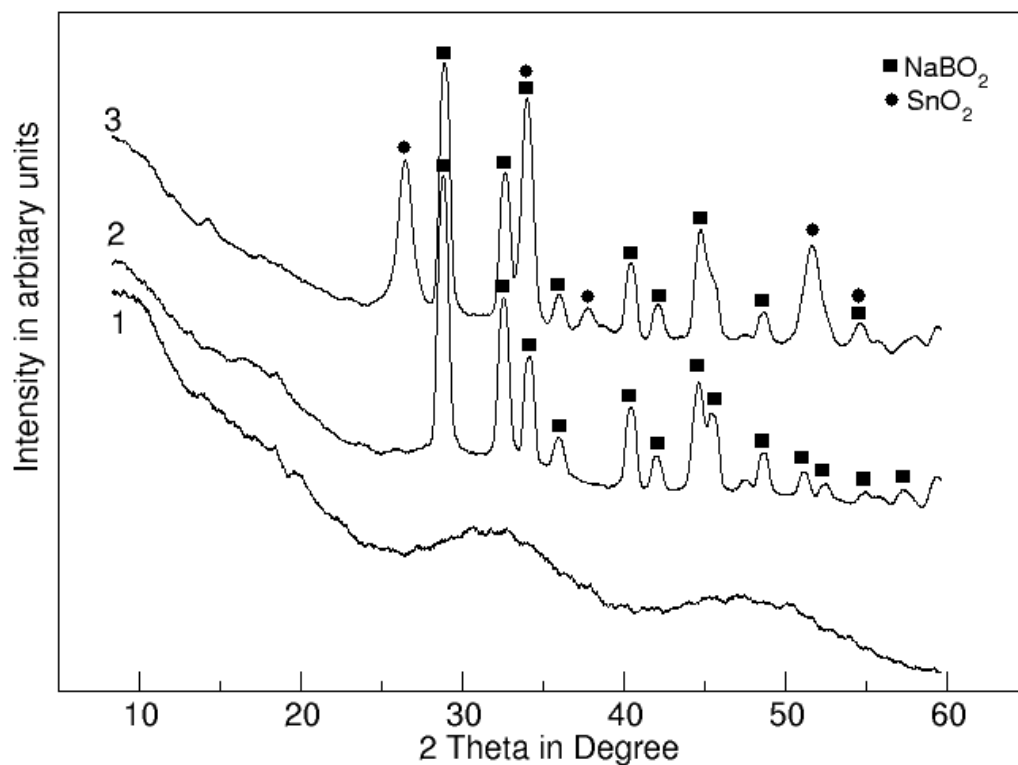


Fig. 5.7.8 XRD-patterns of sample R42; 1: without thermal treatment, 2: 580 °C, 4 h and 3: 650 °C, 4 h

XRD-patterns of sample R40 and R42 thermally treated at 650 °C for 1 h are shown in Fig. 5.7.9. The samples contain 9.47 and 0 mol% Al₂O₃, respectively. In both samples, lines attributed to SnO₂ and NaBO₂ are observed. Peaks attributed to NaBO₂·2H₂O (supposedly formed by corrosion of the powdered glass) and Na₂Al₂B₂O₇ are determined in sample R40. Obviously, the Al₂O₃ concentration has not a notable influence on the SnO₂ crystallisation.

Samples R40 and R39 possess similar glass compositions, with molar ratio [Na₂O]/[B₂O₃] of 0.914 and 1, respectively. The mean SnO₂ crystallite sizes in these samples, heat treated at the same thermal conditions are calculated from Scherrer's equation, from the [110] peak. The estimated values are plotted as a function of the crystallisation temperature in Fig. 5.7.10. Crystallite sizes of 18 and 32 nm are determined for SnO₂ in samples R39 and

R40 (tempered at 650 °C), respectively. An increase of the heat treatment temperature leads to an increase of the crystal size. Crystallite sizes of 25 and 60 nm are observed in samples R39 and R40 nm (670 °C), respectively. Tempering at 690 °C results in crystallite sizes of 30 and 70 nm, respectively. At 710 °C, a crystallite size of 58 nm is reached for sample R39. The crystallite sizes of sample R40 are larger than those of sample R39, for one and the same thermal history of the samples. Nevertheless, in glasses with a molar ratio $[\text{Na}_2\text{O}]/[\text{B}_2\text{O}_3] = 1.125$, crystallisation of SnO_2 can occur as well as that of Na_2SnO_3 .

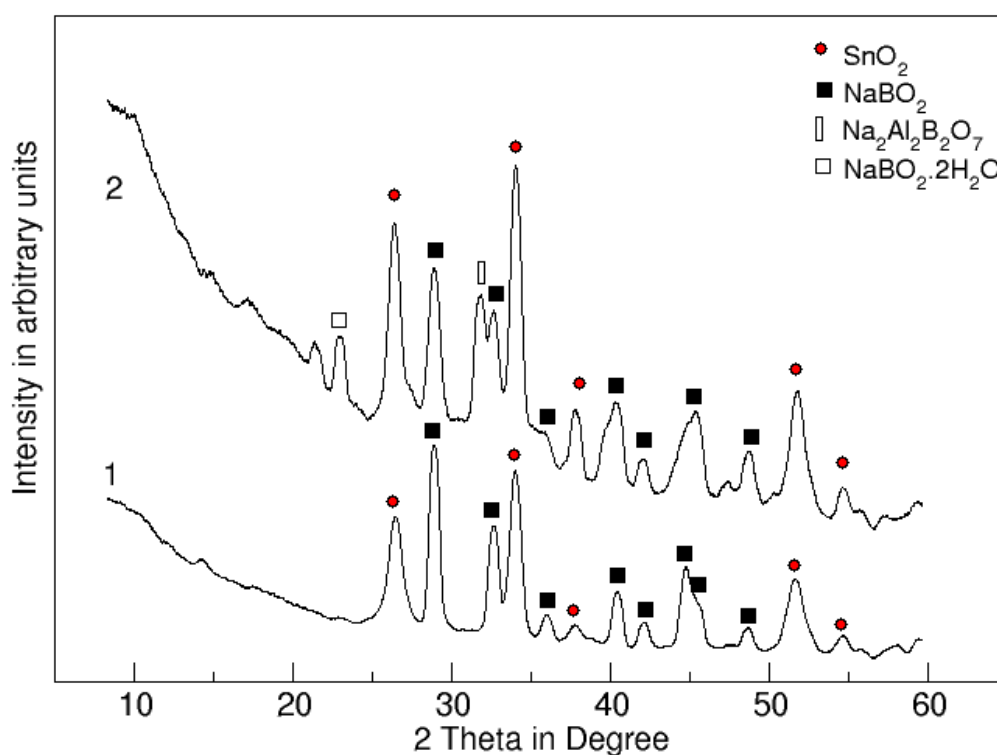


Fig. 5.7.9 XRD-patterns of samples thermal treated at 650 °C for 1 h:
1: R40 and 2: R42

It seems that this is a limiting value, therefore to avoid eventual Na_2SnO_3 -crystallisation, the sample R40 (10 mol% SnO_2 and molar ratio = 0.914) was preferred for further investigations. Another sample suitable for further studies is sample R37 with 5 mol%. This sample was modified by adding Sb_2O_3 : R52 (5 mol% SnO_2 , 1 mol% Sb_2O_3) and R55 (5 mol% SnO_2 , 0.4 mol% Sb_2O_3).

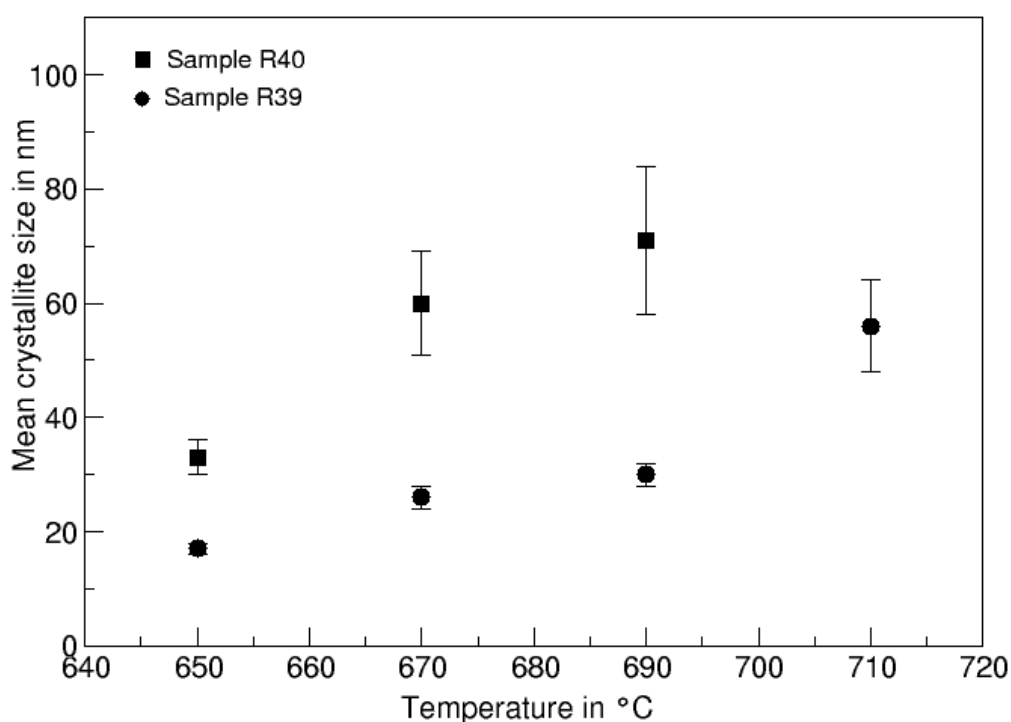


Fig. 5.7.10 SnO₂ crystallite size calculated from XRD-line broadening of samples after thermal treatment at temperatures in the range from 650 to 710 °C for 1 h

5.7.4 Dissolution of the matrix

In order to obtain SnO₂ nano-powder, the matrix and the not Sn-containing crystalline phases have been dissolved in 0.6N acetic acid or in a mixture of 5 % HF and 20 % HNO₃ acid.

XRD-patterns of sample R40 without thermal treatment, after thermal treatment at 670 °C for 80 min and after dissolution and subsequent drying are shown in Fig. 5.7.11. The sample after quenching (Curve 1) is X-ray amorphous, while lines attributed to SnO₂, NaBO₂ and Na₂Al₂B₂O₇ are observed after tempering (Curve 2). SnO₂ and CH₃COONa crystallisation is detected after sample dissolution in diluted acetic acid (Curve 3). The crystalline phases of NaBO₂ and Na₂Al₂B₂O₇ are not any more observed, due to their dissolution in the acid.

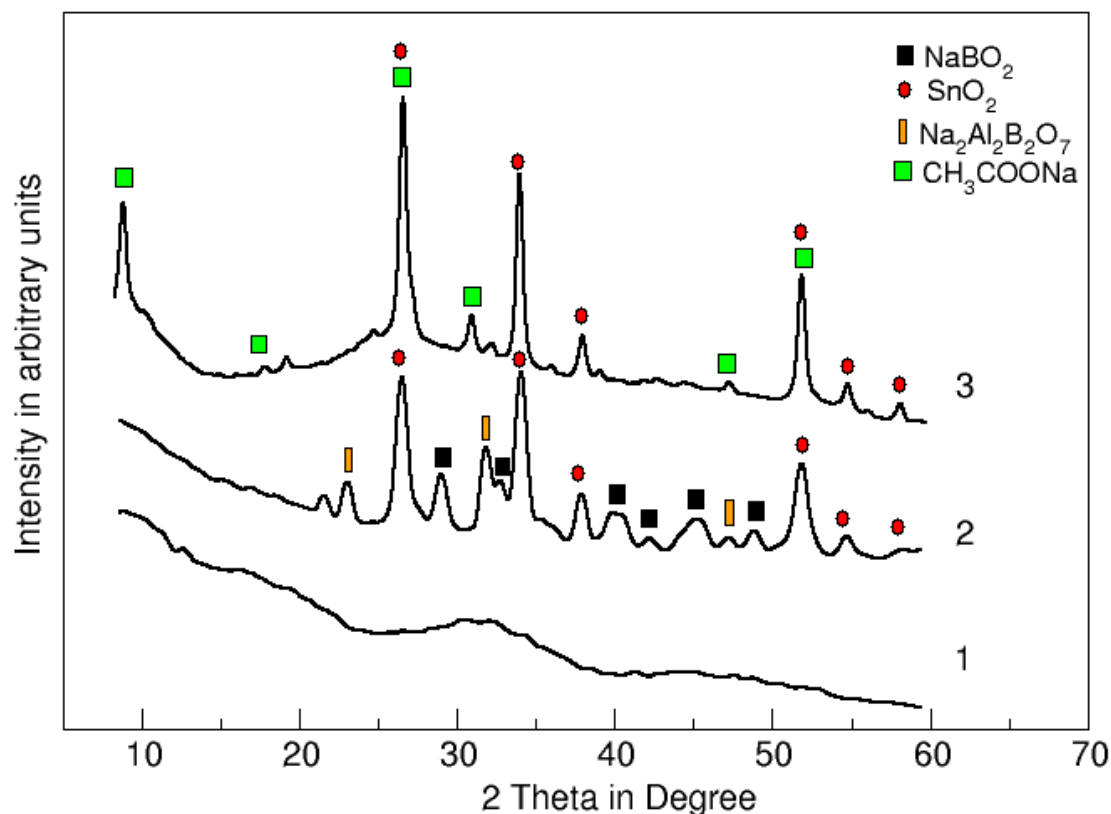


Fig. 5.7.11 XRD-patterns of sample R40: 1: without thermal treatment; 2: after thermal treatment at 670 °C for 80 min; 3: after dissolution in acetic acid

5.7.5 Separation of the SnO_2 nano-crystals

Successful separation of In_2O_3 and $\text{In}_2\text{O}_3\text{:Sb}_2\text{O}_3$ nano-powders from the formed salts have been achieved by dialysis. This method was also used to separate SnO_2 and $\text{SnO}_2\text{:Sb}_2\text{O}_3$ powders.

In Figure 5.7.12 XRD-patterns of sample R40 (670 °C for 80 min) after dissolution and after dialysis are shown. The lines attributable to sodium acetate (see Curve 1) do not occur after dialysing the sample. Only lines caused by SnO_2 crystalline phase are detected.

In summary, dialysis is a successful method for the separation of nano-crystals from salt solutions. It allows the transport of the dissolved salts (dissolved glass matrix, not In or Sn-containing phases and the formed sodium acetate) through the cellulose membrane and the separation of the nano-crystals.

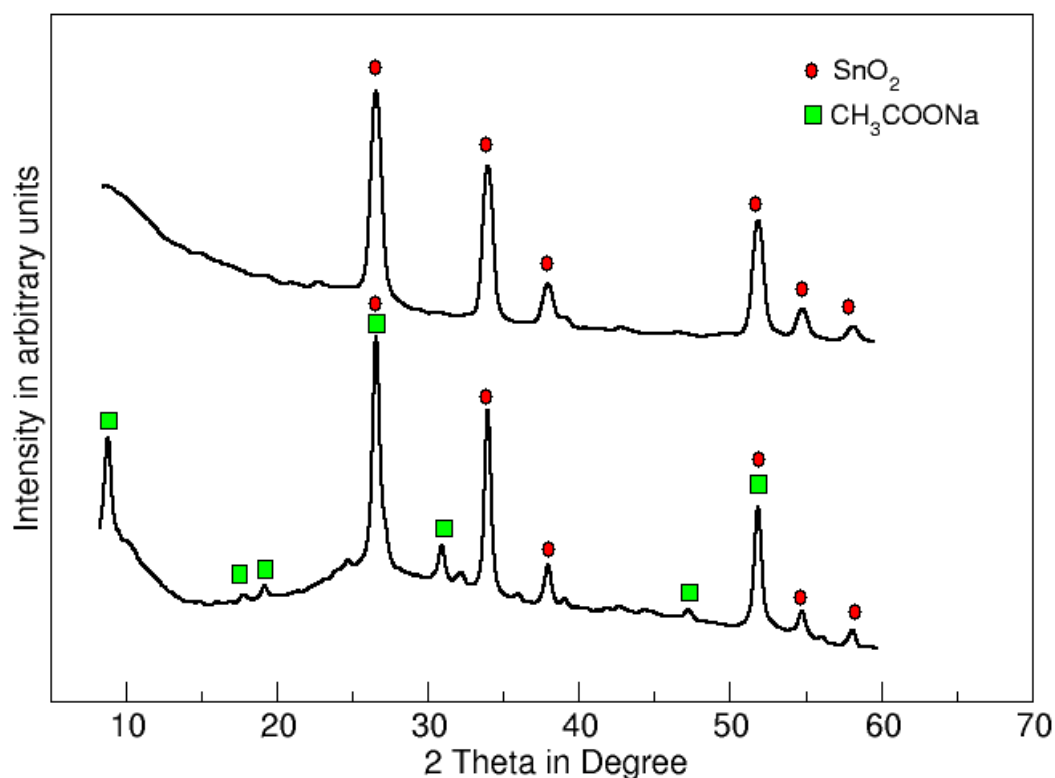


Fig. 5.7.12 XRD-patterns of sample.R40 tempered at 670 °C for 80 min:
1. after dissolution in acetic acid, 2: after dialysis

5.7.6 Characterisation of SnO₂ nano-crystals

SnO₂ nano-powders, obtained after dissolution of the glass-ceramic matrix and the subsequent separation of the crystals, have been characterised by TEM. SnO₂ powders from samples with 5 mol% SnO₂ (sample R37) and with 10 mol% (samples R39 and R40) are studied.

Figure 5.7.13 shows TEM micrographs of tempered sample R37, with 5 mol% SnO₂. Needle-like SnO₂ crystals are seen after tempering the sample at 600 °C for 4 h (Fig. 5.7.13 a). The crystals have a thickness in the range from 4 to 7 nm and lengths in the range from 25 to 100 nm. After tempering sample R37 at 700 °C for 18 h (Fig. 5.7.13 b), the SnO₂ crystals have the same needle-like morphology. They possess thicknesses of around 250 nm and lengths in the range from 1.2 to 2 μm.

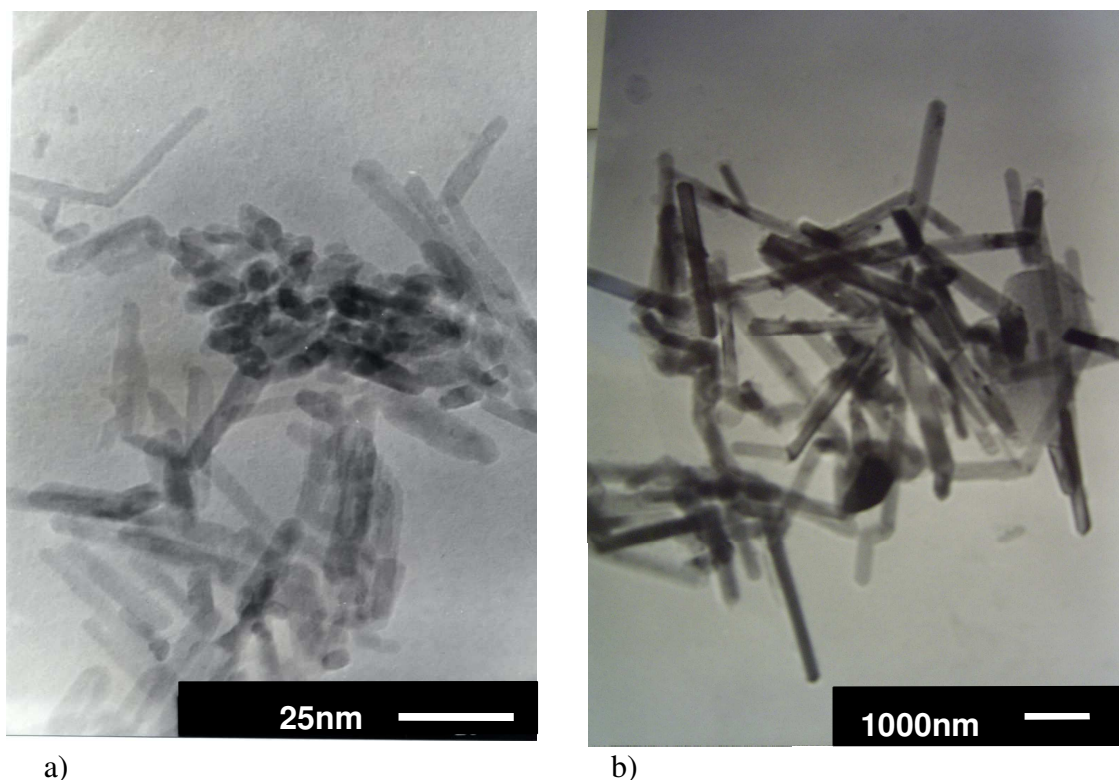


Fig. 5.7.13 TEM- micrographs of SnO₂ crystals from sample R37, tempered at a) 600 °C for 4 h and b) 700 °C for 18 h

A mean crystal thickness of 17 nm and a mean length of 160 nm are determined, after tempering sample R39 (10 mol% SnO₂) at 650 °C for 1 h (Fig. 5.7.14 a). Further increasing the temperature to 700 °C for 1 h (Fig. 5.7.14 b) results in a crystal thickness of 40 nm and a length of 1200 nm. An increase of the heat treatment temperatures increases the crystalline sizes i.e. their thicknesses and lengths.

In the TEM-micrograph of sample R40, tempered at 650 °C for 1 h, crystals with thicknesses of around 30 nm and lengths of ~1.8 µm are seen (see Fig. 5.7.15 a). After heat treatment of this sample at 820 °C for 1.5 h, the observed crystals possess lengths in the range from 400 to 800 nm (see Fig. 5.7.15 b). In this case, increasing the temperature leads to decreasing crystals lengths. This behaviour could be explained with the “Pendulum effect theory” [Avr 99] (see paragraph 3.6.2).

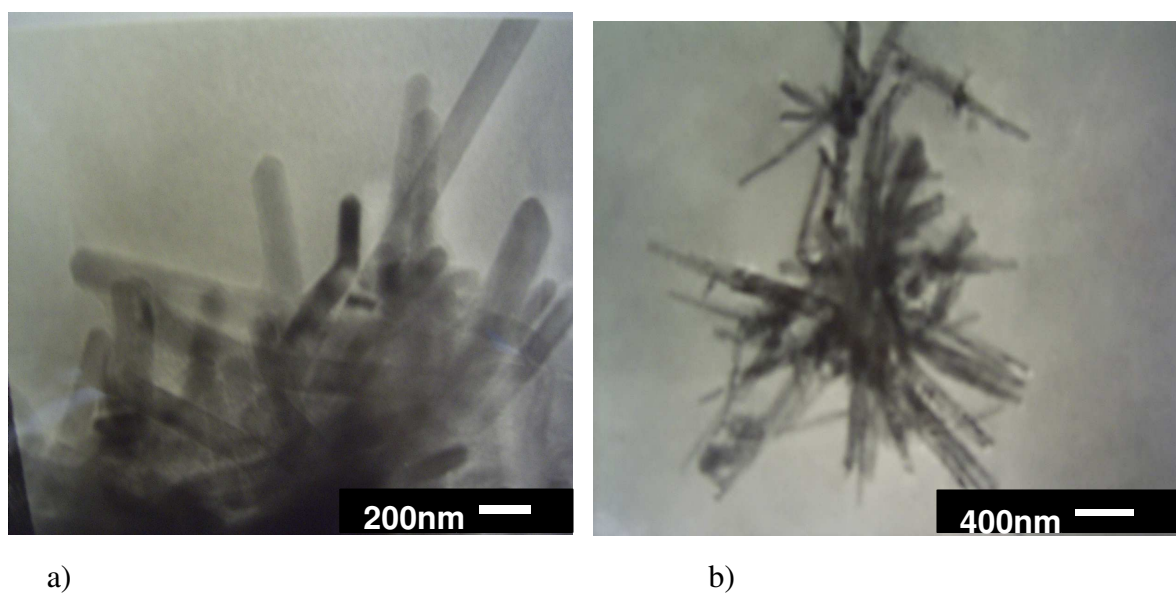


Fig. 5.7.14 TEM- micrographs of SnO₂ crystals from sample R39, tempered at a) 650 °C for 1 h and b) 700 °C for 1 h

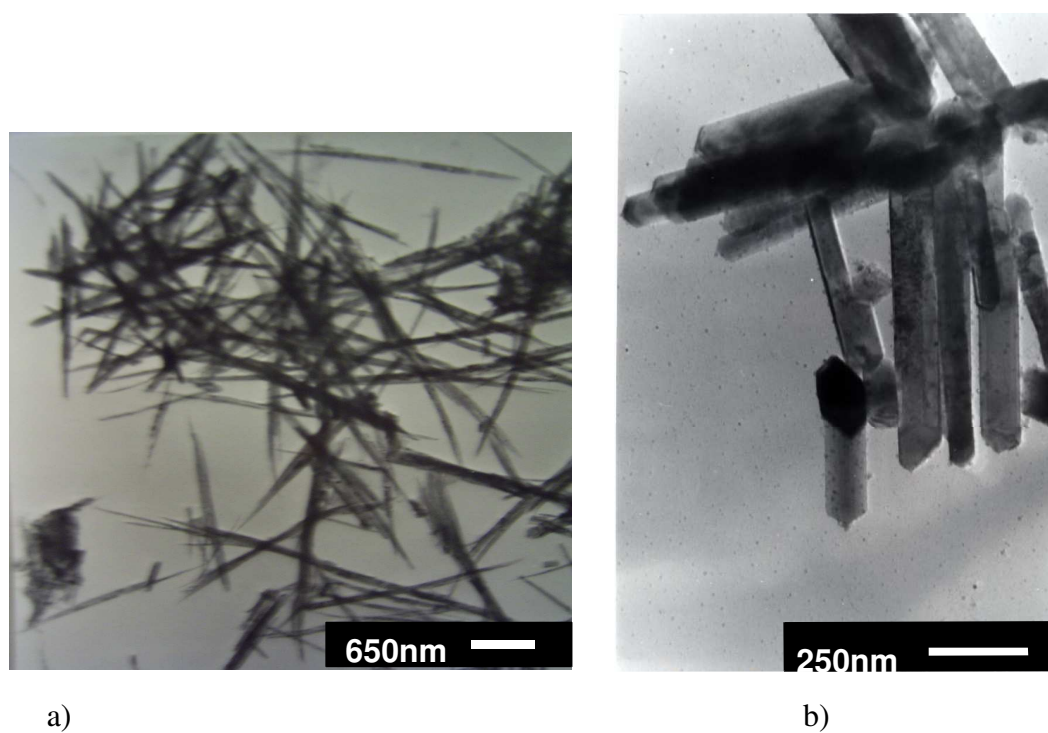


Fig. 5.7.15 TEM- micrographs of sample R40, tempered at: a) 650°C for 1 h and b) 820 °C for 1.5 h

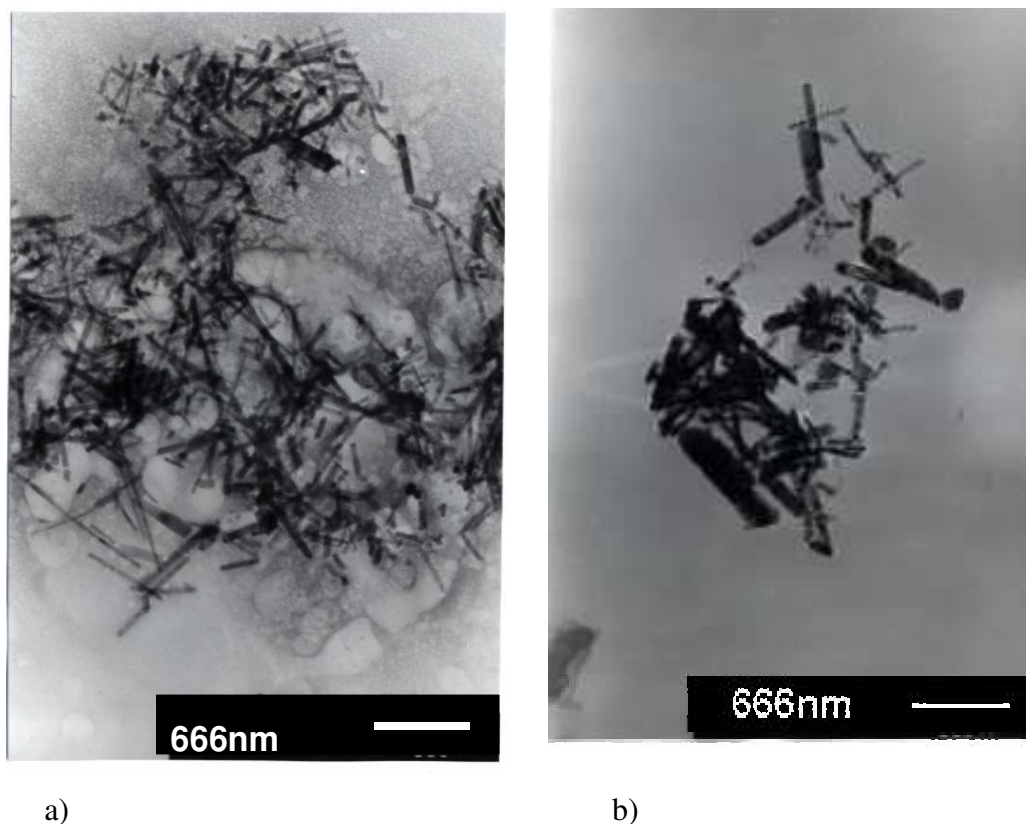


Fig. 5.7.16 TEM- micrographs of sample R37, tempered at 820 °C for:
a) 0.5 h and b) 8 h

In order to achieve smaller crystals and to prove the “Pendulum effect theory”, crystals from sample R37 have been tempered at 820 °C for 0.5 and 2 h. While the SnO₂ crystals in the sample tempered for 0.5 h are thin and long (Fig. 5.7.16 a), those tempered for 2 h are notably thicker and shorter (Fig. 5.7.16 b).

Figure 5.7.17 shows XRD-patterns of sample R37 thermal treated at 820 °C for 0.5 h (curve 1), 2 h (curve 2), 8 h (curve 3) and 16 h (curve 4). The XRD-line broadening of SnO₂ peak [110] increases with increasing the temperature (Fig. 5.7.18). Having in mind that the broader the XRD-lines, the smaller are the crystals. In the case of SnO₂ needle-like crystals, the peak [110] responds to the thickness of the crystals [Lei 03]. These means that the SnO₂ crystals become thicker and shorter with increasing time of thermal treatment, which is in agreement with the “Pendulum effect theory”.

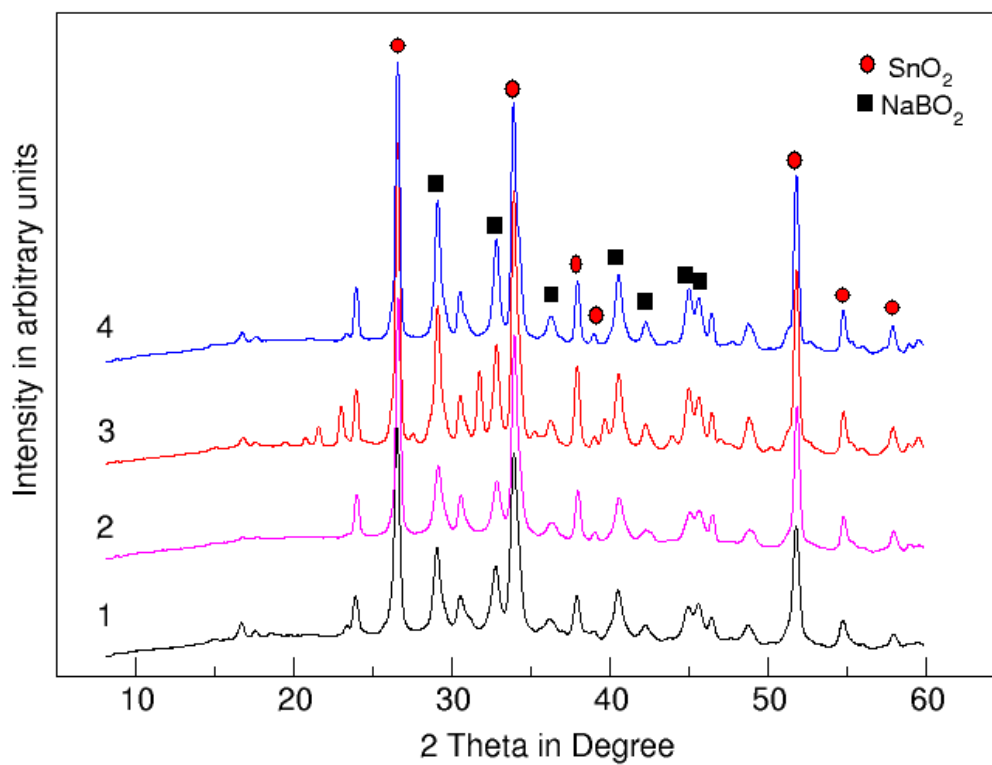


Fig. 5.7.17 XRD-patterns of sample R37 thermally treated at 820 °C for: 1: 0.5 h, 2: 2 h, 3: 8 h and 4: 16 h

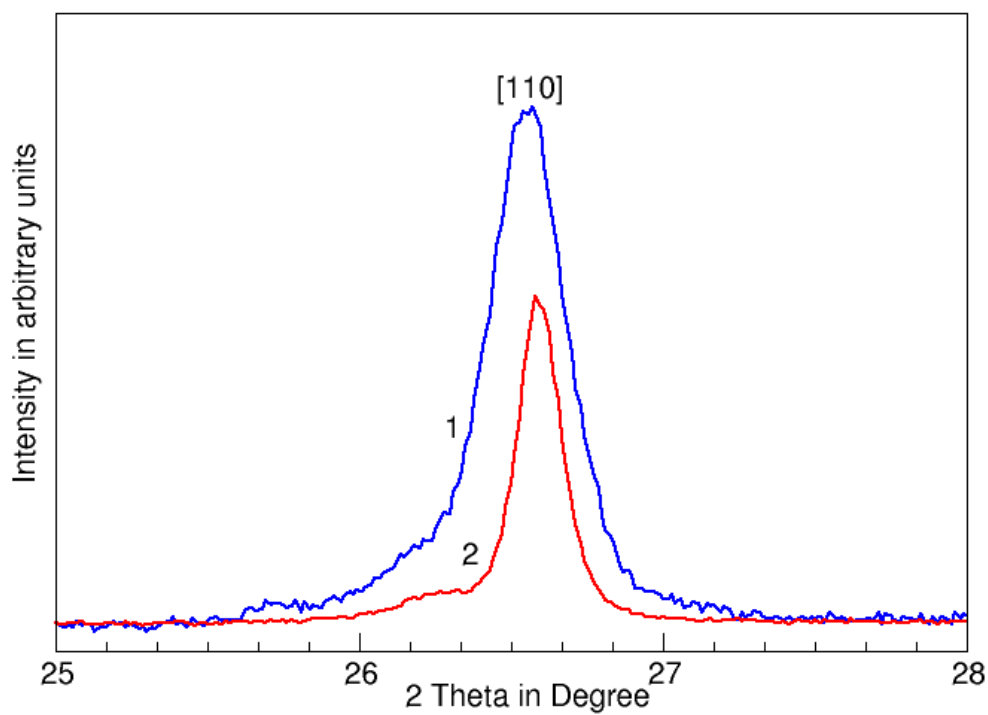


Fig. 5.7.18 XRD-patterns of the SnO_2 peak [110], obtained from sample R37 thermally treated at 820 °C for: 1: 0.5 h and 2: 16 h.

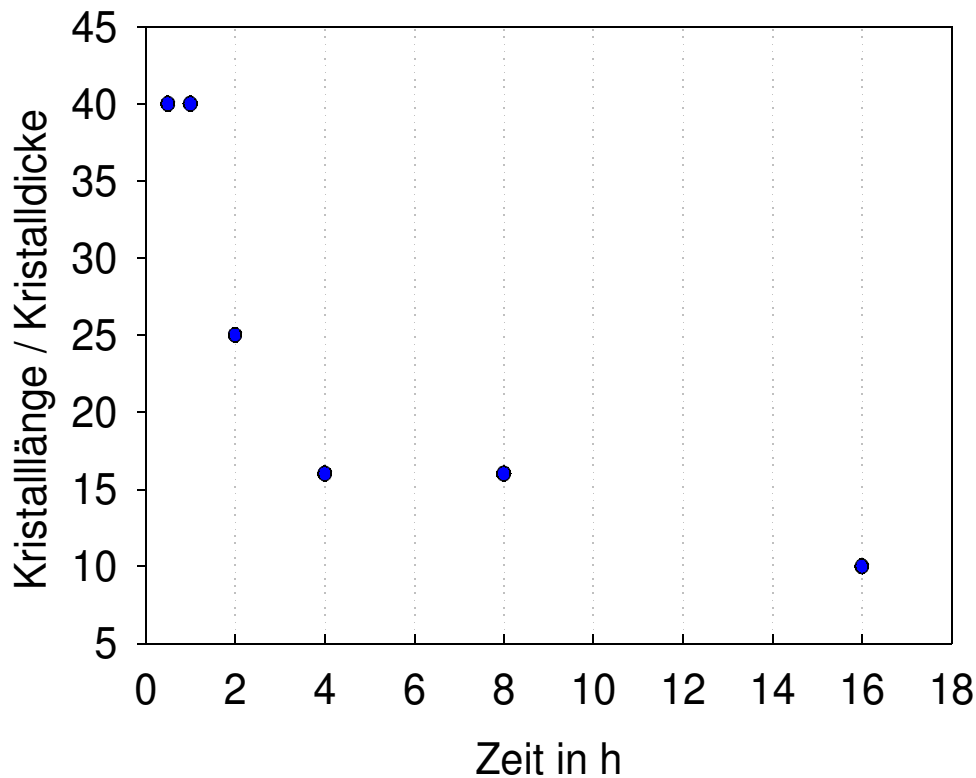


Fig. 5.7.19 Aspect ration versus time of crystals from sample R37 thermal treated at 820 °C

The aspect ratio length/ thickness of the crystal as a function of the time is shown in Fig. 5.7.19. The data are taken from the TEM-micrographs of sample R37 tempered at 820 °C for times in the range from 0.5 to 16 h. An increase of the time results in a decrease of the aspect ratio.

Due to large supersaturations (high SnO_2 concentration and high temperatures) non-equilibrium needle-like crystals grow. The growth of the crystals leads to decreasing SnO_2 concentration in the matrix. As a result, SnO_2 -concentration in the melt approaches a constant value [Avr 99].

This behaviour of decreasing the aspect ratio Length/ Thickness of the crystals from sample R37 proves the “Pendulum Effect theory”. According to which, the needle-like crystal is thermodynamically not favoured and transfer into a shorter and thicker crystal in order to minimize the surface energy. The shape of the crystal approaches an equilibrium state. Within this process, in a first approximation the volume of the crystal remains almost constant.

5.8 Synthesis and optical properties of SnO_2 : Sb_2O_3 nano-powder

Glass composition R52 with 5 mol% SnO_2 and doping of 1 mol % Sb_2O_3 have been studied in order to achieve ATO nano-powders [Ela 04]. The glass composition is chosen similar to composition R37, but with smaller $[\text{Na}_2\text{O}]/[\text{B}_2\text{O}_3]$ ratio, in order to avoid sodium stannate crystallisation (see Tab. 5.7.1).

After quenching, the glass R52 is transparent and X-ray amorphous. Subsequently the glasses have been heat treated and studied using XRD and TEM. The thermal conditions and the formed crystalline phases are summarized in Tab. 5.8.1.

Lines attributed to sodium borate are observed after tempering the sample at 620 °C for 10 h. No Sn-containing phase is detected after thermal treatment. Hence, to achieve SnO_2 : Sb_2O_3 crystallisation, a two step crystallisation procedure is carried out (see paragraph 3.6). To initialize nucleation, the sample is tempered at 500 °C for 24 h. Forming gas is used as atmosphere during heat treatment in order to reduce the formed SnO_2 : Sb_2O_3 crystallites and to achieve NIR-non transparency (similar to the obtained ITO nano-powder). As a second step, the sample is treated at a temperature of 620 °C for 10 h in air, in order to obtain suitable crystallisation conditions and enable crystal growth.

Table 5.8.1: Heat treatment conditions and crystalline phases formed from sample R52

Heat treatment T in °C t in h		Atmosphere	Sn-containing crystalline phase	other crystalline phases
500	24	Forming gas	SnO_2	NaBO_2
620	10	Air		
620	10	Air	---	NaBO_2
650	18	Air	SnO_2	NaBO_2
700	6	Forming gas	SnO_2	NaBO_2

SnO_2 lines are observed as a result of the two step crystallisation procedure. Additional lines attributed to NaBO_2 are also detected. By comparison, no SnO_2 lines are reported from glass M, heat treated directly at 620 °C for 10 h (Fig. 5.8.1). In Fig. 5.8.2, the differences in the XRD-patterns of the sample M, heat treated with two step crystallisation and directly at 620 °C are compared in a narrow 2 Theta- interval.

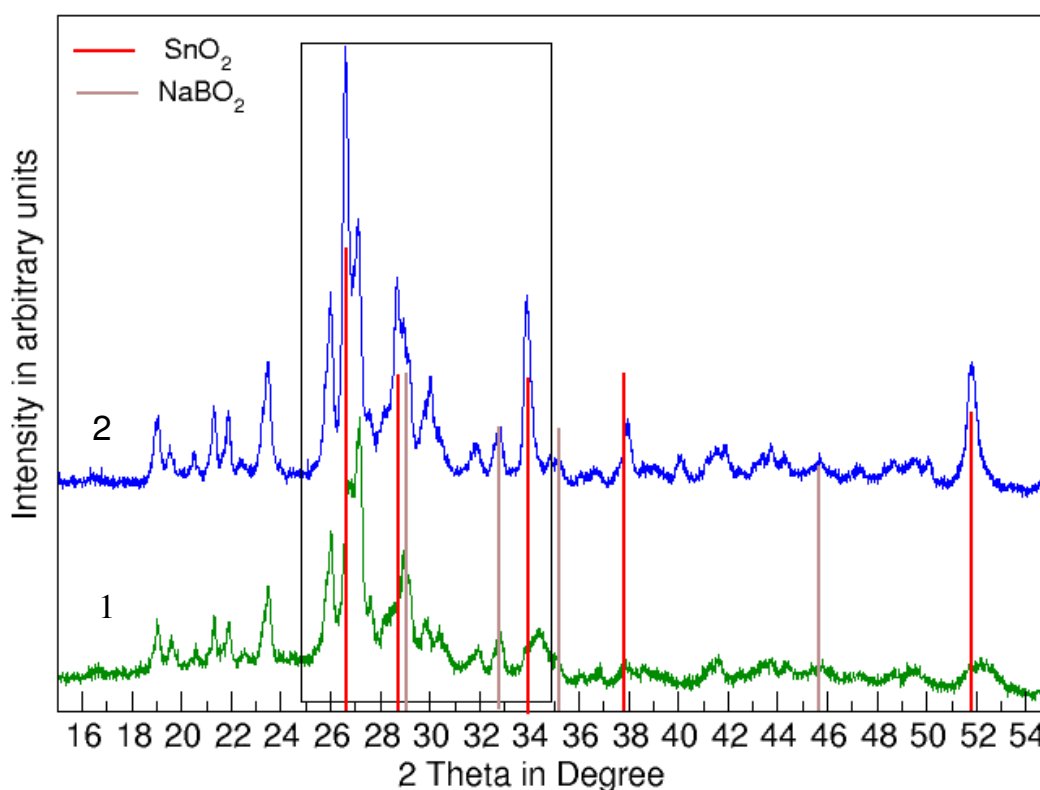


Fig. 5.8.1 XRD-patterns of sample M heat treated at : 1. 620 °C for 10 h and 2. 500 °C for 24 h and subsequently at 620 °C for 10 h

Powders from doped SnO_2 crystals are obtained again by dissolution of the glass-ceramic matrix and subsequent dialysing the formed salts. As expected, the obtained crystals have needle-like shape as seen in sample R52 heat treated first at 500 °C for 20 h and then at 600 °C for 10 h. They possess lengths from around 300 to 600 nm and thicknesses of around 50 nm (see Fig. 5.8.3).

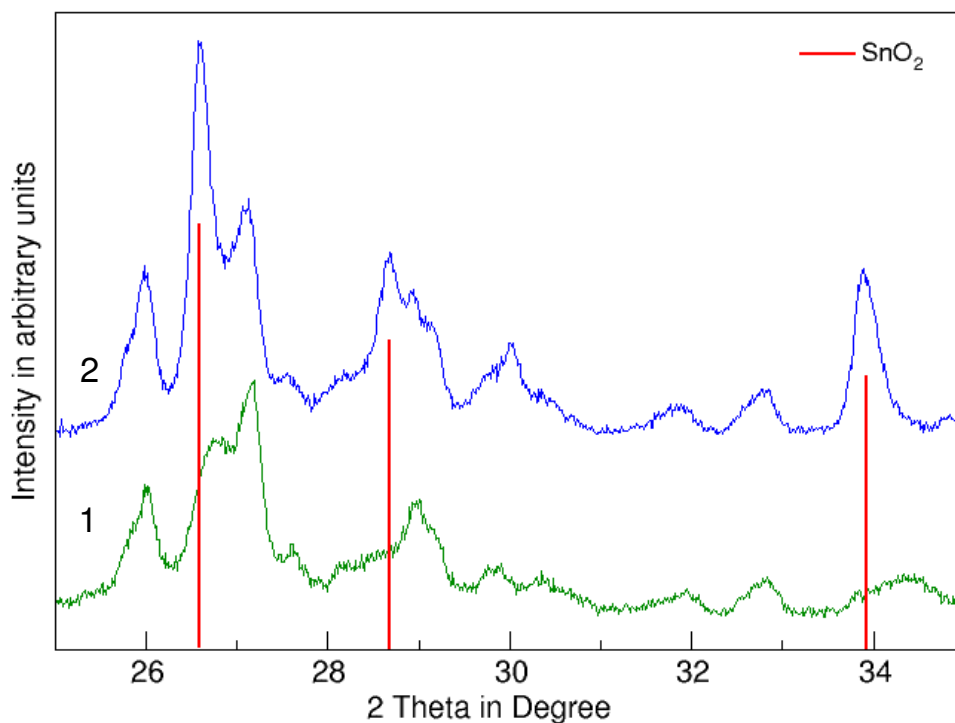


Fig. 5.8.2 Comparison of XRD-patterns of sample M heat treated at: 1. 620 °C for 10 h and 2: 500 °C for 24 h and consequently at 620 °C for 10 h in a narrow 2 Theta interval

The optical properties of the doped SnO₂ nano-crystals have been studied and compared with those of untempered glass. Figure 5.8.4 shows the transmission spectra of glass R52 after quenching, after thermal treatment in air at 620 °C and at 500 °C for 1 and 24 h. The untempered glass possesses a transparency of 90 % in the UV-VIS-NIR range. By comparison, the samples heat treated at 500 °C have notably lower transmittance and the scattering of the light is much higher (see Curves 2 and 3 in Fig. 5.8.4) than in the glass-matrix (Curve 1).

In summary it can be said, that the desired non-transparency in NIR range could be achieved up to now only for In₂O₃ doped with SnO₂.

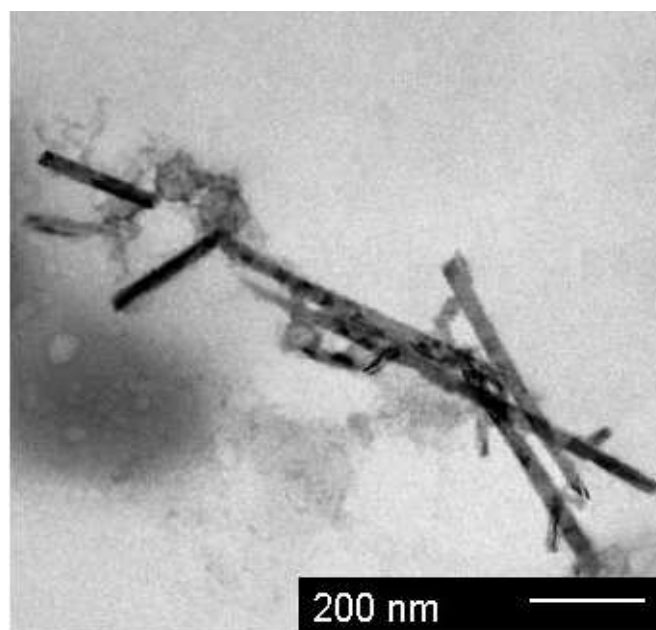


Fig. 5.8.3 TEM micrograph of $\text{SnO}_2\text{:Sb}_2\text{O}_3$ crystals from sample R52 heat treated at 500 °C, 20 h and at 620 °C for 10 h)

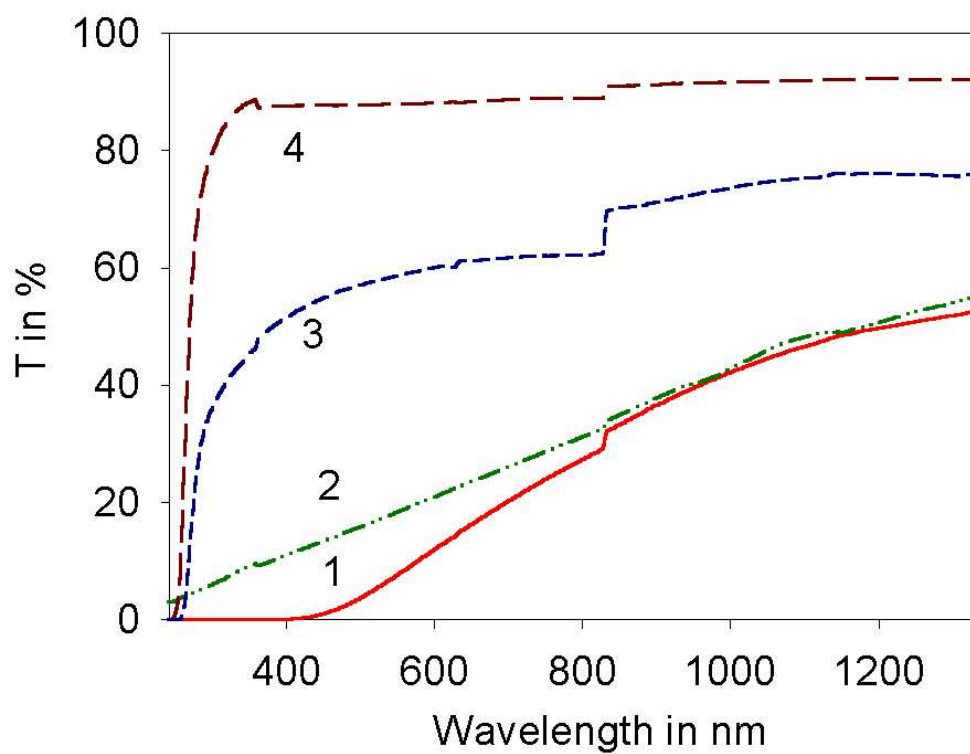


Fig. 5.8.4 Transmission spectra from sample R52, heat treated in air at: 1: 620 °C, 1 h, measured in water suspension against water, 2: 500 °C, 24 h, volume sample; 3: 500 °C, 1h; 4: glass before thermal treatment

6 Discussion

6.1 Discussion for In_2O_3 and $\text{In}_2\text{O}_3\text{:SnO}_2$ -containing glasses, glass-ceramics and nano-powders

Transparent and X-ray amorphous glasses were obtained from the system $\text{Na}_2\text{O}/\text{B}_2\text{O}_3/\text{Al}_2\text{O}_3/\text{In}_2\text{O}_3$. The Na_2O -rich glass compositions ($[\text{Na}_2\text{O}]/[\text{B}_2\text{O}_3] = 1.7$) (sample A) led to spontaneous crystallisation of NaInO_2 during cooling, while in samples with lower Na_2O concentrations ($[\text{Na}_2\text{O}]/[\text{B}_2\text{O}_3] = 0.7$) no In-containing phases crystallised (samples G). At a molar ratio $[\text{Na}_2\text{O}]/[\text{B}_2\text{O}_3] = 1.1$ controlled crystallisation from transparent glasses could be achieved after heat treatment (samples E, G, H and K).

In order to obtain materials, containing relatively high In_2O_3 concentration, sample K (7 mol%, 12 mol% Al_2O_3) has been studied and transparent products have been obtained after quenching. From Al_2O_3 -free glass compositions with molar ratios of 1.1 and 0.9, spontaneous crystallization of In_2O_3 and NaBO_2 occurred (samples B and C) and no indium-containing crystallisation is observed in sample D (5 mol% In_2O_3 , without Al_2O_3). This indicates that the introduction of Al_2O_3 into the glass extends the glass forming range. An Al_2O_3 concentration of 5 mol% is sufficient to suppress the spontaneous crystallization and to induce In_2O_3 crystallization. By further adding alumina to compositions with constant $[\text{Na}_2\text{O}]/[\text{B}_2\text{O}_3]$ -ratio, amorphous samples are obtained up to an Al_2O_3 concentration of 12 mol%. Under the cooling rates supplied a larger concentration of alumina (15 mol% Al_2O_3) resulted in a fully opaque sample (spontaneous In_2O_3 crystallisation). Such compositions are not suitable to form nano-crystalline In_2O_3 . At alumina concentrations in the range from 5 to 12 mol% (samples E, F, H, I and K), the crystallization of In_2O_3 could be achieved at temperatures $> 530^\circ\text{C}$. Increasing temperatures led to decreasing full widths at half maximum of all XRD-lines attributed to cubic In_2O_3 . In principle, two effects may contribute to XRD-line broadening. First,

internal stresses may be responsible and second small crystallites may be the reason. Internal stresses are predominantly formed during cooling at temperatures below T_g due to different thermal expansion coefficients of the crystals formed and the surrounding glass matrix [Esh 57]. These stresses, in the case of spherical particles and cubic crystal phases in a first approximation are isostatic and solely are a function of the thermal expansion coefficients (crystals and glass) and T_g of the glass matrix. Hence, in a first approximation, the size of the particles does not affect the stresses inside the particles. According to TEM micrographs, the XRD-line broadening is in relation with the decrease of the particles size. Therefore, the XRD-line broadening should predominantly be caused by small particle sizes, which enables their calculation using Scherrer's equation. Depending on the tempering conditions, the mean crystallite sizes calculated are in the range from 13 to 53 nm. As shown in Fig. 5.2.7, mean crystallite sizes are generally larger in sample K than in sample H. That means, an increase in the alumina concentration from 10 to 12 mol% increases the crystal growth velocity. An obvious and further increase is observed at an alumina concentration of 15 mol%, where spontaneous crystallisation of In_2O_3 occurs during cooling. In samples H and K, besides the crystallization of In_2O_3 also that of NaBO_2 is observed. Trace quantities of $\text{Na}_2\text{Al}_2\text{B}_2\text{O}_7$ are assumed to be additionally formed. The quantity of NaBO_2 is smaller at alumina oxide concentration of 12 mol% than at 10 mol%. A concentration of 5 mol% In_2O_3 (sample H) is high enough for our studies and its complete dissolution is observed in the melt. A molar ratio $[\text{Na}_2\text{O}]/[\text{B}_2\text{O}_3] = 1.1$ and an Al_2O_3 concentration of 10 mol% suit the crystallisation of nano In_2O_3 crystals. During soaking in dilute acetic acid, the glassy phase and the non In-containing crystalline phases are dissolved. The residual In_2O_3 particles as shown in Fig. 5.3.2 have cubic shape and a size of 20-50 nm (sample H, 700 °C, 1 h). This is in agreement with the mean crystallite size of 35 or 47 nm, calculated using Scherrer's equation for the crystallised glass and the In_2O_3 nano-powder, respectively.

It could be considered that sample H is the appropriate chemical composition for the controlled crystallisation of In_2O_3 nano-crystals from the studied borate glasses.

In order to achieve ITO nano-crystallisation, sample M with a composition similar to sample H, with addition of 1 mol% SnO_2 , has been studied. The sample was transparent and X-ray amorphous (sample M) after quenching the melt. Heat treatment of the sample at 700 °C for 1 h in air, results in nano-crystallisation of In_2O_3 : SnO_2 . A mean crystallite

size of 25 nm is observed (see Fig. 5.6.5). The size of the ITO nano-particles is notably smaller than that of In_2O_3 (47 nm) obtained from sample H at the same heat treatment conditions (see Fig. 5.6.6).

The heat treatment atmosphere has a strong influence on the optical properties of In_2O_3 : SnO_2 -nano-crystals. Heat treatment of sample M (5 mol% In_2O_3 , 1 mol% SnO_2) in forming gas leads to In_2O_3 : SnO_2 powder possessing 90 % transmittance in the visible range and a cut off in the near infrared range (see Fig. 5.6.9). In contrast, sample M and the undoped sample H (5 mol% In_2O_3) heat treated in air as well as sample H tempered in forming gas do not show such an NIR -cut off. This confirms that the combination of SnO_2 doping of In_2O_3 and its reduction leads to a drastic change in the optical properties of the powder, due to oxygen deficiency [Abe 03].

6.2 Discussion for SnO_2 and SnO_2 : Sb_2O_3 -containing glasses, glass-ceramics and nano-powders

The system Na_2O B_2O_3 Al_2O_3 SnO_2 exhibits a fairly large glass forming range. Amorphous products have been obtained if a melt with up to 10 mol% SnO_2 is quenched between copper plates. The SnO_2 raw material is completely dissolved in the melt if fine dispersed SnO_2 raw material and a two step melting procedure is used. Under these conditions, amorphous products without detectable (visually or XRD) crystallisation are obtained at $[\text{Na}_2\text{O}]/[\text{B}_2\text{O}_3]$ - molar ratios in the range from 0.4 to 1.4. After thermal treatment Na_2SnO_3 is precipitated from samples with large $[\text{Na}_2\text{O}]/[\text{B}_2\text{O}_3]$ -ratio (see sample R44 and R30). At smaller $[\text{Na}_2\text{O}]/[\text{B}_2\text{O}_3]$ -ratios, the more Sn-rich phase $\text{Na}_2\text{Sn}_2\text{O}_5$ crystallised (see samples from R33 to R35). SnO_2 crystallisation is achieved from samples with a $[\text{Na}_2\text{O}]/[\text{B}_2\text{O}_3]$ -ratios ≤ 1.1 (see Table 5.7.1). The molar ratio $[\text{Na}_2\text{O}]/[\text{B}_2\text{O}_3] = 1.1$ seems to be a limiting value for the crystallisation of SnO_2 (see sample R35 and R36). At all glasses studied, additionally NaBO_2 and $\text{Na}_2\text{Al}_2\text{B}_2\text{O}_7$ (in the case of samples containing Al_2O_3) crystallise. The XRD-lines attributed to the latter two phases, are not as broadened as those of SnO_2 as shown in Fig. 5.7.9. After dialysis in a cellulose membrane tube, the XRD-lines attributed to borate phases and sodium acetate are no longer detected. Hence, the salts resulting from

the dissolution of the glass and the crystal phases have diffused through the membrane (Figs. 5.4.2 and 5.4.3).

Crystals with needle-like morphology and sizes depending on the heat treatment conditions are obtained. Such crystals with thicknesses in the range from 4 to 7 nm and lengths from 25 to 100 nm are obtained from sample R37 (5 mol% SnO₂), already at a temperature of 600 °C. The aspect ratios (length/ thickness) are hence in the range from 6 to 14. Samples tempered at 700 °C exhibited a smaller aspect ratios, the crystals are up to 2 µm long. Tempering of sample R39 (10 mol% SnO₂) at 650 and 700 °C resulted in approximately the same aspect ratio of around 10. The crystals are notably larger after tempering at 700 °C. The thicknesses of 17 and 40 nm obtained from the micrographs are in agreement with the mean crystallite size determined from XRD-line broadening (Fig. 5.7.10). Thermal treatment of sample R40 (10 mol% SnO₂) at 650 and 820 °C results in crystal thicknesses of 30 and 60 nm respectively. In analogy to sample R39, the crystal thickness after tempering at 650 °C is approximately the same as the mean crystallite size obtained from XRD-line broadening. An increase of the temperature up to 820 °C during tempering results in an increase of the thickness and a decrease of the length of the crystals.

Steady increase in the mean crystalline size (thickness) in sample R39 ([Na₂O]/[B₂O₃] = 1; 10 mol% SnO₂) is observed with increasing temperature from 690 to 710 °C (Fig. 5.7.10). This results in an increase of the mean crystallite size from 30 to 55 nm. By contrast, in sample R40 ([Na₂O]/[B₂O₃] = 0.9; 10 mol% SnO₂), the crystallite size increases strongly if the crystallisation temperature is increased from 650 to 670 °C. Further increasing the temperature to 690 and 820 °C leads only to a slight increase of the crystallite thickness as shown in Figs. 5.7.10 and 5.7.15 b, respectively. The lengths of the crystals decrease with increasing temperature, and the aspect ratio decreases (Fig. 5.7.15 a and 5.7.15 b). This behaviour is quite unusual, the opposite behaviour, i.e. the increase of the aspect ratio due at higher crystallisation temperatures has been reported in the literature [Moi 00], [Höc 01a], [Höc 01b].

This unusual behaviour can be explained as follow: a needle-like morphology is a result from anisometric crystal growth. This anisometric morphology may have different surface tensions in different crystallographic directions. More important, however, are different impingement rates, e.g. caused by screw dislocation along the crystallographic c-axis. This leads to the formation of a thermodynamically less advantageous morphology. As recently

shown in Ref. [Avr 99], in course of an advanced crystallisation stage, the needle-like crystals may decrease in the aspect ratio and hence may transfer to a state with smaller energy. This behaviour is known as “crystallisation pendulum” [Avr 99]. From thickness and length of the crystals (see Fig. 5.7.15 a and b), the volume can roughly be estimated to be $30 \times 30 \times 3000 = 2.7 \times 10^6 \text{ nm}^3$ and $60 \times 60 \times 1000 = 3.6 \times 10^6 \text{ nm}^3$ after tempering at 650 °C and 820 °C, respectively. This shows, that the volume of the respective crystals does not increase notably. In Figures 5.7.16 a and 5.7.16 b the influence of the thermal treatment time at 820 °C on the crystallisation dimensions of SnO₂ crystals from sample R37 (5 mol% SnO₂) is shown. It is observed that initially formed long and thin crystals transform in notably shorter and thicker crystals. It can be assumed that the crystals first grow to needles due to large impingement rates in one crystallographic direction. As a second step, due to the minimization of surface energy, the crystals decrease in length and increase in thickness. This effect is based on a transport, achieved by the SnO₂-concentration gradient. This gradient is formed by the larger solubility at the comparably small face of the crystal. In principle, the driving forces are the same as in the case of “Ostwald ripening”. In our case the transport does not take place from a small crystal to a large one, but from one side of the crystal to the other.

Antimony doped SnO₂ (ATO) nano-crystals have been achieved from R52 (5 mol% SnO₂, 1 mol% Sb₂O₃), which is similar to sample R37 (5 mol% SnO₂). The ATO crystallisation was possible using a two step crystallisation at 500 °C for 24 h and subsequently at 620 °C for 10 h. The sample heat treated at 620 °C for 10 h does not show notable XRD-lines attributed to SnO₂ in comparison to that tempered with the two step crystallisation (Fig. 5.8.1 and 5.8.2). In this way, needle-shape crystals, possessing thicknesses of 50 nm and lengths from 300 to 600 nm are observed by TEM analysis, after dissolution and dialyses of the sample R52.

In order to achieve ATO nano-crystals, possessing NIR-non-transparency, glass sample R52 have been heat treated in air or in reducing atmosphere (forming gas). It is considered, that the reduction atmosphere as well as the Sb-concentration [Zha 04] inhibited the crystallisation of SnO₂ (see Tabl. 5.8.1). As already reported in the literature [Ela 04], the crystallite size of the ATO particles is much larger at lower Sb₂O₃ concentrations than at larger ones (see paragraph 3.4).

7 Summary

The aim of the work was to obtain oxidic nano-crystals (In_2O_3 , $\text{In}_2\text{O}_3\text{:SnO}_2$, SnO_2 , $\text{SnO}_2\text{:Sb}_2\text{O}_3$) through glass-crystallisation and subsequent dissolution of the borate-glass matrix. At the moment, these semiconductive and transparent nano-crystals are predominantly used for fabrication of transparent electrodes for liquid crystal displays and ITO- and ATO-nano-powders might be used also for preparation of thermal barrier nano-composites (polymer and nano-crystals). For this purpose, the crystals should be transparent in the visible and non-transparent in the near infrared range of the optical spectra. According to this, the particles should be much smaller than the wavelengths of the visible light and should have narrow crystal size distribution, because otherwise light scattering will occur.

A preparation method was developed in order to obtain undoped and doped In_2O_3 and SnO_2 nano-powders through controlled crystallisation of borate glasses and subsequent dissolution of the matrix in acetic acid. The nano-powders have been separated from the matrix and the acetates formed, by dissolution of the glassy matrix and subsequent dialysis.

7.1 Summary for In_2O_3 and $\text{In}_2\text{O}_3\text{:SnO}_2$ (ITO)

In_2O_3 cubic shaped crystals were precipitated by thermal treatment at temperatures in the range from 500 °C to 700 °C from glasses in the system $\text{Na}_2\text{O}/\text{B}_2\text{O}_3/\text{Al}_2\text{O}_3/\text{In}_2\text{O}_3$. In the Na_2O -rich glasses with a molar ratio (MR) $[\text{Na}_2\text{O}]/[\text{B}_2\text{O}_3] = 1.4$, NaInO_2 is precipitated (sample A), while in B_2O_3 -rich glasses ($[\text{Na}_2\text{O}]/[\text{B}_2\text{O}_3] \leq 0.7$), the crystallisation of In-containing phases is not observed, after heat treatment (sample D and G). A molar ratio $[\text{Na}_2\text{O}]/[\text{B}_2\text{O}_3] = 1.1$ favours the crystallisation of In_2O_3 and $\text{In}_2\text{O}_3\text{:SnO}_2$ (samples H and K). Another factor, which influences the In_2O_3 crystallisation is the Al_2O_3 concentration in

the glass composition. Controlled crystallisation of In_2O_3 from glass compositions without Al_2O_3 was not possible. In these cases, spontaneous crystallisation of NaInO_2 (sample A with $\text{MR} = 1.4$) or In_2O_3 occurs during cooling the melt (samples B with $\text{MR} = 1$ and C with $\text{MR} = 0.9$) or In-containing phases are not at all crystallised (sample D with $\text{MR} = 0.6$ and G with $\text{MR} = 0.7$). The introduction of Al_2O_3 into the glass gave rise to an extended glass forming range. At Al_2O_3 concentrations from 4.8 to 12 mol % (samples E, F, H, I and K with $\text{MR} = 1.1$), nano crystallisation of In_2O_3 occurred. The mean crystallite sizes of In_2O_3 were in the range from 13 to 53 nm, depending on temperature and soaking times, calculated by Scherrer's equation.

These means that crystalline sizes of 19 nm at 580 °C, 25 nm at 630 °C and 42 nm at 700 °C are in agreement with those observed in TEM images. A narrow crystal size distribution is achieved as it was required (see Figs. 5.4.10, 5.4.11 and 5.4.12). The prevention of nano-particles aggregation after dissolution of the glassy phase is out of the aim of the present work.

The glassy matrix as well as additionally formed phases such as NaBO_2 and $\text{Na}_2\text{Al}_2\text{B}_2\text{O}_7$ can be dissolved in diluted acetic acid in order to obtain nano-crystalline In_2O_3 powders. The peaks of additional crystalline phases are not observed after dissolution in acid, only lines attributed to In_2O_3 are detected through XRD (Fig. 5.4.1). After dissolution of the glass-ceramics in acetic acid and subsequent drying, the formation of CH_3COONa occurred. The separation of In_2O_3 nano-powder from the acetates is possible through dialysis. This was proved with XRD (Fig. 5.4.2) and FTIR (Fig. 5.4.3), where signals due to acetates are not obtained after the salts (acetate solution and nano-particles) have been dialysed.

Through doping of SnO_2 to sample H (5 mol% In_2O_3), glass composition M (5 mol% In_2O_3 and 1 mol% SnO_2) was developed, from which a transparent glass was obtained after cooling the melt. The desired optical NIR non-transparency of the In_2O_3 nano-particles is achieved through combination of doping with SnO_2 and subsequent heat treatment in forming gas in the temperature range from 520 to 700 °C for 1 to 6 h. The ITO nano-crystals possess cubic shape with crystallite sizes of ~ 25 nm. The optical properties of the doped and undoped In_2O_3 have been investigated. Transparency in VIS as well as in NIR region was observed for sample H, heat treated in air and in forming gas. Also transparent at these wavelengths is the nano-powder from SnO_2 doped sample M, thermally treated in

air. Through thermal treatment of SnO₂-doped sample M in forming gas, the desired NIR-non- transparency is achieved.

In summary, In₂O₃ and In₂O₃:SnO₂-nano-powders with predetermined nano-crystal sizes and narrow crystal size distribution were obtained through crystallisation of borate glasses, dissolution of the matrix in acetic acid and subsequent separation of the nano-particles from the salts through dialysis. The desired non-transparency in the NIR range is achieved by In₂O₃:SnO₂ nano-crystallisation in forming gas.

7.2 Summary for SnO₂ and SnO₂:Sb₂O₃ (ATO)

The systems studied to obtain SnO₂ and ATO nano-crystals are similar to those from which In₂O₃ and ITO were prepared: B₂O₃ Na₂O SnO₂ (Al₂O₃) and B₂O₃ Na₂O Al₂O₃ SnO₂ Sb₂O₃. Transparent glasses have been obtained only through using developed technology for the dissolution the SnO₂ raw material in the borate melts. It consists of the preparation of fine dispersed SnO₂ raw material, synthesized by a wet chemical method, and a two step melting procedure, controlling the viscosity of the melt by keeping it long time at lower temperatures. Through these techniques, SnO₂ could be better dissolved in the melt and so, transparent glasses with up to 10 mol% SnO₂ have been prepared. Subsequently, the glasses have been thermally treated in temperature interval from 500 to 820 °C.

Na₂O-rich glass composition R34 (5 mol% SnO₂) similar to sample H, from which successfully In₂O₃ nano-powder was prepared, have been studied first. It was observed that larger Na₂O concentrations, with molar ratios $[\text{Na}_2\text{O}]/[\text{B}_2\text{O}_3] \geq 1.1$, favoured the crystallisation of Na₂SnO₃ or Na₂Sn₂O₅ (samples: R44, R30, R33, R34). A molar ratio $[\text{Na}_2\text{O}]/[\text{B}_2\text{O}_3] = 1.1$ seems to be limiting value between the crystallisation of SnO₂ and Na₂Sn₂O₅ (sample R36 and R35). To avoid the crystallisation of stanates, a large number of glass compositions with different molar ratios have been investigated. It was found that in compositions with molar ratios smaller than 0.3 (sample R49), spontaneous crystallisation of SnO₂ occurs. Therefore, molar ratios $[\text{Na}_2\text{O}]/[\text{B}_2\text{O}_3]$ from 0.5 to 1.0 are preferred for the SnO₂ crystallisation (samples: R47, R39, R40).

The influence of the Al_2O_3 concentration on SnO_2 crystallisation is not such notable as in the case of In_2O_3 crystallisation. This is concluded from the fact that SnO_2 crystallisation is observed from both glasses containing (sample R51 and R45) and which do not contain Al_2O_3 (sample R42).

Generally, the method developed for the preparation of In_2O_3 and ITO nano-powders is also suitable for the synthesis of SnO_2 and ATO nano-powders. So, a similar technology of glass crystallisation, dissolution of the matrix and additional crystalline phases such as NaBO_2 and $\text{Na}_2\text{Al}_2\text{B}_2\text{O}_7$, and the subsequent separation of the obtained SnO_2 or $\text{SnO}_2\text{:Sb}_2\text{O}_3$ nano-particles from the salts formed during dissolution can be used.

Needle like crystals with thicknesses of 4-7 nm and lengths of 25 to 100 nm are observed in sample R37 with 5 mol% SnO_2 tempered at 600 °C for 4 h. With increasing the temperature to 700 °C, the crystal thickness increased to 250 nm and the length was in the range of 1.2 to 2 μm .

A change in the morphology of the SnO_2 crystals is observed during thermal treatment at higher temperatures. During keeping sample R37 at 820 °C, the initially formed thin and long crystals got thicker and shorter with time (from 0.5 to 16 h). These results experimentally confirm the “Crystallisation pendulum theory”, at which the “crystallisation pendulum” is a type of intergranular Ostwald ripening.

Sb_2O_3 doped SnO_2 crystals have been obtained from glasses in the system B_2O_3 Na_2O Al_2O_3 SnO_2 Sb_2O_3 . Transparent and X-ray amorphous glasses were obtained with 5 mol% SnO_2 and with 1 and 0.4 mol% Sb_2O_3 (samples R52 and R55). The two steps thermal treatment enabled nano-crystallisation of needle-like crystals with thicknesses of 50 nm and lengths from 300 to 600 nm.

In summary, a technology for the preparation of SnO_2 and $\text{SnO}_2\text{:Sb}_2\text{O}_3$ nano crystals was developed. The desired optical properties, i.e. NIR non-transparency is achieved up to now only for SnO_2 doped In_2O_3 nano-crystals. Optimisation of the dopant concentration and the thermal treatment conditions, might lead to NIR non-transparent ATO nano-powders.

8 Bibliography

- [Abe 03] K. Abe, Y. Sanada, T. Morimoto, J. Sol-Gel Sci. Tech. 26 (2003) 709
- [Ali 96] A. P. Alivisatos, Science 271 (1996) 933
- [Avr 03] I. Avramov, E. D. Zanotto, M. O. Prado, J. Non-Cryst. Solids 320 (2003) 9
- [Avr 99] I. Avramov, T. Höche, C. Rüssel, J. Chem. Phys. 110 (1999) 8676
- [Bai 02] L. Baia, R. Stefan, W. Kiefer, J. Popp, S. Simon, J. Non-Cryst. Solids 303 (2002) 379
- [Ban 95] G. P. Banfi, V. Degiorgio, D. Fortusini, H. M. Tau, Appl. Phys. Lett. 67 (1995) 1315
- [Bas 98] Sh. A. Bashar, “Study of Indium Tin Oxide (ITO) for Novel Optoelectronics Devices”, PhD thesis, London, 1998
- [Ben 03] D. Benne, M. Menzel, D. Niemeier, K. D. Becker, C. Rüssel, J. Non-Cryst. Solids 318 (2003) 202
- [Bin 96] K. S. Bindra, S. M. Oak, K. C. Rustigi, Opt. Commun. 124 (1996) 452
- [Bla 98] R. Blachnik, “Taschenbuch für Chemiker und Physiker”, Springer, 1998
- [Bom 99] M. J. Van Bommel, W. A. Groen, H. A. M. Van Hal, W. C. Keur, T. N. M. Bernardes, J. Mater. Sci. 34 (1999) 4803
- [Bor 87] N. F. Borelli, D. W. Hall, H. J. Holland, J. W. Smith, J. Appl. Phys. 61 (1987) 5399
- [Bur 02] P. E. Burrows, D. C. Stewart, D. W. Watson, R. Schofield, P. M. Martin, SPIE Conference, Pacific Northwest National Lab, Session 7 (2002) 4800-27

- [Cam 96] A. C. Camargo, J. A. Ignalada, A. Beltran, R. Llusar, E. Longo, J. Andres, Chem. Phys. 212 (1996) 381
- [Cas 98] S. I. Castaneda, F. Rueda, R. Diaz, J. M. Ripalda, I. Montero, J. Appl. Phys. 83 (1998) 1995
- [Chi 01] N. Chiodini, F. Meinardi, F. Morazzoni, J. Padavoni, A. Paleari et. al., J. Mater. Chem. 11 (2001) 926
- [Cho 83] K. L. Chopra, S. Major, D. K. Pandya, Thin Solid Films 102 (1983) 1
- [Ede 03] J. Ederth, P. Johnsson, G. A. Niklasson, A. Hoel, A. Hultaker et. al., Phys. Rev. B 68 (2003) 155410-1
- [Ela 04] E. Elangolan, K. Ramesh, K. Ramamuthi, Solid State Comm. 130 (2004) 523
- [Esh 57] I. D. Eshelby, Proc. R. Soc. (A) 241 (1957) 376
- [Fra 60] G. Frank, E. Kaner, Z. Angew. Phys. 12 (1960) 425
- [Free 00] A. J. Freeman, K. R. Poeppelmeier, T. O. Mason, R. P. H. Chang, T. J. Marks, MRS Bulletin (2000) 45
- [Gie 96] H. Giessen, N. Woggon, B. Fluegel, G. Moks, Y. Z. Hu, S. W. Koch, N. Peyghamba, Opt. Lett. 21 (1996) 1043
- [Goe 94] G. Goerigk, H. G. haubold, C. Klingshirn, A. Uhrig, J. Appl. Cryst. 22 (1994) 907
- [Goeb 00] C. Goebbert, H. Bisht, N. Al-Dahoudi, R. Nonningen, M. A. Aegerter, H. Schmidt, J. Sol-Gel Sci. Technol. 19 (2000) 201
- [Gra 93] C. G. Granqvist, App. Phys. A: Solids Surf. 57 (1993) 19
- [Gri 97] C. Grivas, S. Mailis, L. Bontsikaris, D. Gill, N. A. Vainos, P. J. Chandler, Laser Phys. 8 (1) (1998) 326
- [Gut 95] I. Gutzow, I. Schmelzer, "The Vitreous State: "Thermodynamics, Structure, Rheology, and Crystallization", Springer, Berlin, 1995
- [Ham 86] I. Hamberg, C. G. Granqvist, J. Appl. Phys. 60 (1986) R123

- [Hau 72] A. Haug, theoretical Solid State, Pergamon Press, NY, 1972
- [Het 00] M. S. Hettenback, "SnO₂ (110) and Nano-SnO₂: Characterization by Surface Analytical Techniques", PhD thesis, Eberhard-Karls-University Tübingen, 2000
- [Hir 98] H. Hiramatsu, W. S. Seo, K. Koumoto, Chem. Mater. 10 (1998) 3033
- [Höc 01a] T. Höche, C. Moisescu, I. Avramov, C. Rüssel, W. D. Heerdegen, Chem. Mater. 13(4) (2001) 1312
- [Höc 01b] T. Höche, C. Moisescu, I. Avramov, C. Rüssel, W. D. Heerdegen, C. Jäger, Chem. Mater. 13 (4) (2001) 1320
- [Jia 03] J. K. Jian, X. L. Chen, W. J. Wang, L. Dai, Y. P. Xu, Appl. Phys. A 76 (2003) 291
- [Kas 00] D. Kaschchiev, "Nucleation", Butterworth, Oxford (2000) 140; 380
- [Kei 54] M. L. Keith, R. Roy, Amer. Mineral. 39 (1954) 1
- [Kim 04] H. Kim, A. Pique, Appl. Phys. Lett. 84 (2004) 218
- [Koi 02] R. Koivula, R. Harjula, J. Lehro, Micropor. Mesopor. Mater. 55 (2002) 231
- [Kom 84] T. Komatsu, N. Soga, J. Mater. Sci. 19 (1984) 2353
- [Kri 00] B. R. Krishna, T. K. Subramanyam, B. S. Naidu, S. Uthanna, Ind. J. Eng. Mater. Sci. 7 (2000) 395
- [Kum 92] A. Kumar, S. P. Singh, Glastech. Ber. 65 (1992) 69
- [Läs 01b] C. Löser, C. Rüssel, Glastech. Ber. Glass. Sci. Technol. 74 (2001) 106
- [Lee 96] M. S. Lee, W. C. Choi, E. K. Kim, C. K. Kim, S. K. Min, Thin Solid Films 279 (1996) 1
- [Lei 03] E. R. Leite, T. R. Giralaldi, F. M. Pontes, Acta Microscopica 12 (2003) 325
- [Lev 61] E. M. Levin, R. S. Rroth, J. B. Martin, Amer. Mineral. 46 (1961) 1030
- [Lev 64] E. M. Levin, C. R. Robbins, H. F. McMurdie, "Phase Diagrams for Ceramics", The American ceramic society, Inc., 1964

- [Lim 04] S. J. Limmer, S. V. Cruz, G. Z. Cao, Appl. Phys. A 79 (2004) 421
- [Lös 01a] C. Löser, Ch. Rüssel, J. Non-Cryst. Solids 282 (2001) 228
- [Maz 91] O. V. Mazurin, M. V. Streltsina, T. P. Shvaiko-Schvaikovskaya, "Handbook of glass data", Elsevier, Amsterdam-N. Y-Oxford- Tokyo 15D (1991) 78
- [McMee 00] G. D. McMeeking, www.drgrahammcmeeking.com/latest_publication.htm (2000)
- [Mir 61] L. I. Mirkin," Handbook of Röntgen structural analysis polycrystals", Gosudarstvennoe izdatelstvo fiziko-matematicheskoi literatury, Moscow, (1962) 728 (in Russian)
- [Moh 03] Mohammad-Mehri, Bagheri-Mohaghegni, Mehrdad Shokooh-Saremi, Semicond. Sci. Technol. 18 (2003) 97
- [Moi 00] C. Moisesescu, G. Calr, C. Rüssel, Glastechn. Ber. Glass Sci. Technol. 73 (2000) 187
- [Mül 99a] R. Müsser, R. Hiergeist, H. Steinmetz, J. Magn. Magn. 201 (1999) 34
- [Mül 99b] R. Müller, C. Ulbricht, W. Schüppel, H. Steinmetz, E. Steinbeiß, J. Eur. Ceram. Soc. 19 (1999) 1547
- [Nad 88] Nadaut, J. Sol. State Chem. 135 (1988) 140
- [Nano 03] Nanostructured & Amorphous Materials Inc., Houston, USA www.nanoamor.com/products, 2003
- [Nim 02] Nimai Chand Pramanik, Prasanta Kumar Biswas, Bull. Mater. Sci. 25 (2002) 505
- [Nyg 97] R. A. Nyquist, C. L. Putzig, M. A. Leugers, The Handbook of Infrared and Raman spectra of inorganic and organic salts, Academic Press Inc., San Diego, USA, 1 (1997) 55;57; 209
- [Pet 92] A. Petzold, Anorganisch-Nichtmetallische Werkstoffe: Charakteristik, Eigenschaften, Anwendungsverhalten, Dt. Verl. für Grundstoffindustrie, Leipzig, 1992

- [Pop 01] D. A. Popescu, J. M. Hermann, A. Ensuke, F. B-Verduraz, *Phys. Chem. Chem. Ohys.* 3 (2001) 2522
- [Pot 88] B. G. Potter, J. H. Simmons, *Phys. Rev. B* 37 (1988) 10838
- [Qua 98] M. Quass, C. Eggs, H. Wulff, *Thin Solid Films* 332 (1998) 277
- [Ren 32] C. Renz, *Helv. Chim. Acta* 15 (1932) 839
- [Rez 94] N. Rezlescu, E. Rezlescu, P. Pasnicu, *J. Magn. Magn.* 131 (1994) 273
- [Ris 02] M. Ristic, M. Ivanda, S. Popovic, S. Music, *J. Non-Cryst. Solid* 303 (2002) 270
- [Ris 93] S. H. Risbud, L. C. Liu, J. F. Shackelfold, *Appl. Phys. Lett.* 65 (1993) 1648
- [Saj 93] D. Sajuti, M. Yano, T. Narushima, und Y. Iguchi, *Materials Transaction, JIM* 34 (1993) 1195
- [Sar 90] N. Sarakura, Y. Ishida, T. Yanagawa, H. Nakano, *Appl. Phys. Lett.* (1990) 229
- [Sch 88] H. Scholze, *Glas: Nature, Structure und Eigenschaften*, 3. Edition, Springer, Berlin-Heidelberg, 1988
- [Sch 90] H. Scholze, *Glass: Nature, Structure, and Properties*, Springer, Berlin-Heidelberg, 1990
- [Sch 94] G. Schmid, Ed. *Clusters and Coloids*, VCH Press, NY (1994)
- [Sha 04] K. S. Shamala, L. C. S. Murthy, K. Narasimma Rao, *Bull. Mater. Sci.* 27 (2004) 295
- [Tah 97] R. B. H. Tahar, T. Ban, Y. Ohya, *J. Appl. Phys.* 82 (1997) 865
- [Tha 02] B. Thangarajn, *Thin Solid Films* 402 (2002) 71
- [Val 96] S. V. Vallerien, H.-G. Krohm, E. Wolf, J. von Samson, M. Skoczny et. al., *Sprechsaal* 129 (1996) 35
- [Var 94] A. K. Varshneya, "Fundamentals of Inorganic Glasses", Academic Press, Inc., San Diego, USA, 1994

- [Vas 92] V. Vasu, A. Subrahmanyam, *Semicond. Sci. Technol.* 7 (1992) 1471
- [Wei 66] R. L. Weiher, R. P. Ley, *J. Appl. Phys.* 37 (1966) 299
- [Wel 93] H. Weller, *Angew. Chem., Int. Ed. Engl.* 32 (1993) 41
- [Wog 91a] U. Woggen, M. Müller, V. Lembke, I. Rückmann, J. Cesnulevicius, *Superlatt. Microstruct.* 9 (1991) 224
- [Wog 91b] U. Woggen, I. Rückmann, C. J. Kornack, M. Müller, J. Cesnulevicius et. al., *SPIE Proc.* 1362 (1991) 885
- [Wol 04] S. Woltz, "Herstellung nanoskaliger Magnetit- Teilchen durch Glaskristallisation", PhD Thesis, FSU, Jena, 2004
- [Xia 97] Z. D. Xiang, M. Cabl, *Phys. Chem. Glasses* 38 (1997) 1676
- [Xio 01] X. Li. Xionan, T. Gessert, C. Dettart, T. Barnes, H. Montinho, Y. Yan et. al, Conference Paper, NCPV Programm Review Meeting (2001)
- [Xir 98] C. Xirouchaki, K. Moschovis, E. Chatzitheodoris, G. Kirikidis, P. Morgen, *Appl. Phys. A* 67 (1998) 295
- [Yamada 00] Yamada, Suzuki, Makino, Yoshiba, *J. Vac. Sci. Technol. A* 18 (1999) 83
- [Yan 89] F. Yan, J. M. Parker, *J. Non-Cryst. Solids* 112 (1989) 277
- [Yoo 04] D. H. Yoo, M. W. Shin, Designing, processing and properties of Adv. Mat. 449-4 (2004) 1001
- [Zha 04] J. Zhang, L. Gao, *Inorganic Chem. Comm.* 7 (2004) 91
- [Zho 99] H. Zhou, W. Cai, L. Zhang, *Mater. Res. Bull.* 34 (1999) 845

9 List of Figures

Abbildungsverzeichnis

Fig. 3.1.1 Crystal structure of In_2O_3 [Qua 98] 13

Fig. 3.1.2 Scheme of additional energy level in the Energy band gap:

a) donor levels, b) acceptor levels VB = valence band; CB = conductive band; E_{gap} = energy band gap 14

Fig.3.2.1 Spectral transmittance of double layered (inner layer ITO) coating films quoted from Ref. [Abe 03] 19

Fig.3.2.2 Spectral absorption coefficient from samples annealed for 1 h in air and 1 h in N_2 at different temperatures: sample A (300 °C), B (400 °C), C (500 °C), D (650 °C) and E (800 °C) [Ede 03] 20

Fig. 3.3.1 Crystallite structure of SnO_2 [Cam 96], [Ham 00] 21

Fig.3.4.1 Optical transmission measurements of ATO particle layer on a quartz substrate [Bom 99] 25

Fig. 3.5.1 Optical spectra from glass with the composition

16Na₂O·10CaO·12Al₂O₃·52SiO₂·5In₂O₃·5As₂O₃, tempered at different temperatures, referred from [Lös 01a]. 27

Fig. 3.5.2 Commercial In₂O₃ (Nanostructured & Amorphous Materials, Inc.) [Nano 03] 28

Fig. 3.6.1 Nucleation rate and crystal growth velocity as a function of the temperature [Pet 92] 30

Fig. 3.6.2 Time dependence of crystal size (solid line, left axis) and matrix concentration (dashed line, right axis). The aspect ratio X/R (both line); X: crystal length and R: radius of crystal with cylindrical shape [Avr 99] 31

Fig.4.2.1 Cellulose membranes filled with suspension (dissolved powder from crystallized sample in acid) 37

Fig. 5.1.1 Glass formation range of the system Na₂O·Al₂O₃·B₂O₃ in Mol% [Maz 91] 39

Fig. 5.1.2 Glass formation range of the system Na₂O·In₂O₃·B₂O₃ in Mol% [Maz 91] 39

Fig. 5.1.3 Phase diagram of binary system Na₂O- B₂O₃ [Lev 64] 40

Fig.5.1.4 Phase diagram of binary system In₂O₃- B₂O₃ [Saj 93] 41

Fig. 5.2.1 DTA-profile of sample H 44

Fig. 5.2.2 XRD-patterns of quenched samples B, H, I and K 44

Fig. 5.2.3 XRD-patterns of tempered samples A (700 °C, 3 h), E (700 °C, 1 h), G (580 °C, 20 min), I (580 °C, 20 min) and K (590 °C, 30 min) 45

Fig. 5.2.4 XRD-patterns of sample H after thermal treatment at 630 °C for:
1: 20 min, 2: 40 min, 3: 60 min and 4: 100 min 46

Fig. 5.2.5 XRD-patterns of sample H. 1: without thermal treatment, 2: 500 °C, 20min; 3: 500 °C, 80 min; 4: 530 °C, 80 min; 5: 600 °C, 80 min; 6: 600 °C, 60 min and 7: 700 °C, 60 min

46

Fig. 5.2.6 XRD-patterns of sample K: 1: without thermal treatments; 2: 590 °C, 30 min; 3: 620 °C, 20 min; and 4: 700 °C, 60 min

47

Fig. 5.2.7 Mean crystallite size of In_2O_3 in the samples H and K as a function of the temperature after tempering for 60 min.

48

Fig. 5.3.1 XRD-pattern of the residue obtained after dissolution of the glass-ceramic of sample H (previously tempered at 700 °C for 60 min in air) in water.

49

Fig. 5.3.2 TEM-micrograph of the residue obtained by dissolution the glassy phase of sample H (tempered at 700 °C for 60 min) in water.

50

Fig. 5.3.3 TEM-micrograph of In_2O_3 nano-particles with some residual glass obtained by dissolution of the glassy phase of sample H (tempered at 700 °C) in water and separated by centrifugation.

50

Fig. 5.4.1 XRD-patterns of sample H: 1: without thermal treatment, 2: 580 °C for 1 h, 3: after dissolution in acid

52

Fig. 5.4.2 XRD-patterns of sample H; 1: 580 °C, 1h, 2: after Dialysis

53

Fig. 5.4.3 FTIR-Spectra from sample H; 1: without heat treatment, 2: 580 °C, 1 h, air 3: after dissolution the sample in acid, 4: after dialysis

54

Fig. 5.4.4 TEM -micrograms from In₂O₃ nano-crystals from sample H (580 °C, 1 h, in air) after Dialysis; a) single crystals, b) distribution of the nano-crystals. 55

Fig. 5.4.5 Measurement of the crystalline size from In₂O₃ nano-particles from TEM-image, Sample H (580 °C, 1 h, in air) with “Optimas 6.2” software 55

Fig. 5.4.6 TEM-image of sample H, thermal treated at 630 °C for 1 h in air 56

Fig. 5.4.7 TEM-image of sample H, thermal treated at 700 °C for 1 h in air 56

Fig. 5.4.8 Characteristic particle size histogram from TEM image of sample H (580 °C, 1 h) 56

Fig. 5.4.9 Characteristic particle size histogram from TEM image of sample H (630 °C, 1 h) 57

Fig. 5.4.10 Characteristic particle size histogram from TEM image of sample H (700 °C, 1 h) 57

Fig. 5.5.1 Optical spectra from In₂O₃ nano-powder of sample H (580 °C, 1 h, air) in different matrices: 1: in molten polystyrene against air, 2: in paraffin oil against reference paraffin oil, 3: in polystyrene dissolved in chloroform against reference chloroform 59

Fig. 5.6.1 Sample M heat treated at 560 °C for 6 h:
1: in air, 2: in forming gas 62

Fig. 5.6.2 Powders from sample M

(560 °C for 6 h) dispersed in 0,6N CH₃COOH: 1: in air, 2: in forming gas 62

Fig. 5.6.3 XRD patterns of samples heat treated at 700 °C for 1 h in air 1: In₂O₃:SnO₂ from sample M and 2: In₂O₃ nano-powder from H 63

Fig. 5.6.4 XRD peak [222] of undoped and SnO₂ doped Indium oxide from samples heat treated at 700 °C for 1 h in air 1: In₂O₃:SnO₂ from sample M and 2: In₂O₃ nano-powder from H 63

a) b)

Fig 5.6.5 TEM-images of crystals from samples heat treated at 700°C, 1h in forming gas: a) sample H and b) sample M. 64

Fig. 5.6.6 TEM-images of crystals from samples heat treated at 700 °C, 1 h in air a) In₂O₃ nano-crystals from sample H. and b) In₂O₃:SnO₂ nano-crystals from sample M 65

Fig. 5.6.7 EDX analysis of nano-crystal from sample M (700 °C, 1 h, forming gas) 66

Fig. 5.6.8 Transmission spectra from sample: heat treated at 700 °C, 1 h, acetic acid solution: 1: powder from sample M (in forming gas); 2: powder from sample M (air); 3: powder from sample H (in forming gas); 4: powder from sample H (air) 67

Fig. 5.6.9 UV-VIS Spectra: 1: industrial sample with In₂O₃- nano-crystals in polystyrene, 2: In₂O₃:SnO₂- nano-crystals in water (dialysed sample M, 540 °C, 6 h in forming gas) 68

Fig. 5.7.1 SEM-images from the residual SnO₂ crystals in glass sample R40: a) distribution of the crystals in the sample, b) SnO₂ crystals 70

Fig. 5.7.2 SEM-images from the residue of SnO₂ crystals in sample R40, after heat treatment: a) distribution of the crystals in the sample, b) SnO₂ crystals 71

Fig. 5.7.3 XRD patterns from products of the wet chemical synthesis: 1 after drying at 40 °C, 2: after thermal treatment at 500 °C for 1 h, 3: SnO₂ commercial raw material 72

Fig. 5.7.4 TEM – micrographs of SnO₂-crystals prepared by wet chemical synthesis 73

Fig. 5.7.5 XRD-patterns of sample R34: 1: without thermal treatment, 2: after thermal treatment at 700 °C for 2 h 75

Fig 5.7.6 XRD-patterns of samples: 1: sample R30, 2: sample R35 (650 °C, 60 min), 3: sample R39 (650 °C, 60 min) 76

Fig. 5.7.7 XRD-patterns of sample R40; 1: without thermal treatment, 2: after thermal treatment at 650 °C for 60 min and 3: at 670 °C for 80 min. 76

Fig. 5.7.8 XRD-patterns of sample R42; 1: without thermal treatment, 2: 580 °C, 4 h and 3: 650 °C, 4 h 77

Fig. 5.7.9 XRD-patterns of samples thermal treated at 650 °C for 1 h: 1: R40 and 2: R42 78

Fig. 5.7.10 SnO₂ crystallite size calculated from XRD-line broadening of samples after thermal treatment at temperatures in the range from 650 to 710 °C for 1 h 79

Fig. 5.7.11 XRD-patterns of sample R40: 1: without thermal treatment; 2: after thermal treatment at 670 °C for 80 min; 3: after dissolution in acetic acid 80

Fig. 5.7.12 XRD-patterns of sample R40 tempered at 670 °C for 80 min: 1. after dissolution in acetic acid, 2: after dialysis 81

Fig. 5.7.13 TEM- micrographs of SnO₂ crystals from sample R37, tempered at

a) 600 °C for 4 h and b) 700 °C for 18 h 82

Fig. 5.7.14 TEM- micrographs of SnO₂ crystals from sample R39, tempered at a) 650 °C for

1 h and b) 700 °C for 1 h 83

Fig. 5.7.15 TEM- micrographs of sample R40, tempered at: a) 650°C for 1 h and b) 820 °C

for 1.5 h 83

Fig. 5.7.16 TEM- micrographs of sample R37, tempered at 820 °C for:

a) 0.5 h and b) 8 h 84

Fig. 5.7.17 XRD-patterns of sample R37 thermally treated at 820 °C for: 1: 0.5 h, 2: 2 h, 3: 8 h

and 4: 16 h 85

Fig. 5.7.18 XRD-patterns of the SnO₂ peak [110], obtained from sample R37 thermally

treated at 820 °C for: 1: 0.5 h and 2: 16 h. 85

Fig. 5.7.19 Aspect ration versus time of crystals from sample R37 thermal treated at 820 °C

86

Fig. 5.8.1 XRD-patterns of sample M heat treated at : 1. 620 °C for 10 h and 2. 500 °C for 24

h and subsequently at 620 °C for 10 h 88

Fig. 5.8.2 Comparison of XRD-patterns of sample M heat treated at: 1. 620 °C for 10 h and

2: 500 °C for 24 h and consequently at 620 °C for 10 h in a narrow 2 Theta interval 89

Fig. 5.8.3 TEM micrograph of SnO₂:Sb₂O₃ crystals from sample R52 heat treated at 500 °C,

20 h and at 620 °C for 10 h) 90

Fig. 5.8.4 Transmission spectra from sample R52, heat treated in air at: 1: 620 °C, 1 h,

measured in water suspension against water, 2: 500 °C, 24 h, volume sample; 3: 500 °C, 1h; 4:
glass before thermal treatment 90

List of Abbreviations:

TCOs	Transparent Conducting Oxides
INO	Indium Oxide
ITO	SnO ₂ doped Indium Oxide
TO	Tin Oxide
ATO	Sb ₂ O ₃ doped Tin Oxide
LCD	Liquid Crystal Displays
OLED	Organic Light Emitting Diodes
CVD	Chemical Vapour Deposition
PLD	Pulsed Laser Deposition
UV	Ultraviolet
VIS	Visible
IR	Infrared
NIR	Near Infrared
VB	Valence Band
CB	Conductive Band
Egap	Energy band gap
LPCVD	Low Pressure Chemical-Vapour Deposition
TMT	Tetramethyltin
FTIR	Fourier-Transform-Infrared Spectrometry
XRD	X-ray diffractometry
FWHM	Full Width at Half Maximum
SEM	Scanning Electron Microscopy
TEM	Transmission Electron Microscopy
EDX	Energy Dispersive X-ray analysis

DTA	Differential Thermal Analyse
GFRs	Glassformation Ranges
JCPDS	Joint Committee on Powder Diffraction Standards
MR	Molar Ratio

Danksagung

Mein herzlicher Dank gilt Prof. Dr. Christian Rüssel für die Möglichkeit der Promotion, sowie der äußerst interessanten Themenstellung und die sehr gute Betreuung.

Prof. Dr. Dörte Stachel möchte ich für die Bereitschaft, ein Gutachten für diese Dissertation zu erstellen, danken.

Prof. Biserka Samuneva und Prof. Janko Dimitriev (UCTM, Sofia, Bulgarien) danke ich für die moralische Unterstützung bei meiner Arbeit.

Mein besonderer Dank gilt Herr Dr. Ivailo Gugov für die gute Zusammenarbeit und sein Hilfsbereitschaft, für die Interesse an der Arbeit und die fachlichen Diskussionen.

Für die Durchführung der FTIR-Spektroskopischen Messungen bedanke ich mich sehr bei Dr. Thomas Mayerhöfer und Frau Inge Weber (Institut für Physicalischechemie FSU-Jena).

Frau Elke Wagner und Steffi Ebbinghaus danke ich für die zahlreichen Messungen am Röntgendiffraktometer, sowie Frau Hartmann für die UV-VIS-NIR Mesungen.

Für die vielen rasterelektronenmikroskopischen und TEM Aufnahmen bedanke ich mich an Herr Dr. Völksch und Frau Claudia Hertig.

Frau Lindner danke ich für die durchgeführte chemische Analyse, Frau Lösche für die DTA-Messungen und Frau Gabi Möller für die sorgfältige Durchführung von Oberflächen-Bearbeitungen meiner Proben.

Auch allen anderen Angestellten des Instituts möchte ich für ihre Unterstützung meiner Arbeit meinen Dank aussprechen, vor allem Herr Dr. Bürger für die angenehme Arbeitsatmosphäre, Herrn Thomas Kittel für die Auswertung der TEM-Aufnahmen, sowie Dr. Ralf Keding für die Hilfe bei diversen technischen und Computer Problemen.

Mein besonderer Dank gilt Herrn Dr. Achim Wiedenroth für die sprachliche Korrektur meiner Arbeit.

Meinen Laborkollegen Anja Hunger, Diana Tauch, Luciana Maia und Wen Liang möchte ich für die angenehme Arbeitsatmosphäre meinen Dank aussprechen.

Außerdem gilt mein Dank allen Mitarbeiterinnen und Mitarbeitern des Otto-Schott-Institutes für das sehr angenehme und freundlichen Arbeitsklima und die vielfältige Unterstützung bei der Durchführung dieser Arbeit.

Meinen Mann Torsten bin ich sehr dankbar für die Geduld und Unterstützung, Hilfsbereitschaft bei Sprachproblemen und für die jederzeit gegebene Kraft während meiner gesamten Promotionszeit.

Bei meiner Familie will ich mich ebenfalls bedanken für die Unterstützung und Ermutigung jederzeit während meiner Promotion.

Ilona und Werner Mudra danke ich für die Herzlichkeit und Hilfsbereitschaft.

Dem Deutsche Akademische Auslands Dienst (DAAD) danke ich für die Finanzierung dieser Arbeit.

Selbständigkeitserklärung

Ich erkläre, daß ich die vorliegende Arbeit selbständig und nur unter Verwendung der angegebenen Hilfsmittel und Literatur angefertigt habe.

Jena, den

Lebenslauf

Name: Rosenow
Vorname: Ralitsa
Vatersname: Peteva
geborene Garkova
Staatsbürgerschaft: Bulgarien
Familienstand: verheiratet
Geburtsdatum und -ort: 22.03.1977, Sofia, Bulgarien

1984-1991	Grundschule, Sofia, Bulgarien
1991 - 1996	Fremdsprachengymnasium, Sofia, Bulgarien
1996	Diplom über Oberschulabschluss (allg. Hochschulreife)
1996-2001	Studium der Technologie der Werkstoffe und Werkstoffkunde mit Spezialisierung: Silikatwerkstoffe an der Universität für Chemische Technologie und Metallurgie-Sofia, Bulgarien
06.2001 -10.2001	Stipendiatin Socrates/Erasmus für Masterarbeit am Otto-Schott-Institut, FSU-Jena
10.2001	Abschluß: Diplom Ingenieurchemiker an der Universität für Chemische Technologie und Metallurgie, Sofia, Bulgarien
1999-2001	Weiterbildung: Wirtschaftsinformatik an der Universität für Chemische Technologie und Metallurgie, Sofia, Bulgarien mit Abschluss Staatsexamen (10.2001)
seit 15.11.2001	Promotion mit DAAD Stipendium der Fachrichtung Glaschemie, Otto- Schott-Institut, FSU-Jena,

Unterschrift:
/Ralitsa Rosenow/

Jena, den 17.05.2005